Neuronal Activity Propagation in the Brain: From Neuronal Avalanches to Synfire Chains and Gamma Oscillations

Gerald Hahn

Thèse pour l'obtention du grade de

Docteur de l'Ecole Polytechnique

Presentée par

Gerald Hahn

Sujet

Neuronal Activity Propagation in the Brain: From Neuronal Avalanches to Synfire Chains and Gamma Oscillations

Propagation de l'activité neuronale dans le cerveau: des avalanches neuronales aux chaînes synfire et oscillations gamma

Soutenu le 15 juillet devant le Jury composé de

Khashayar PAKDAMAN	Président du Jury
Gustavo DECO	Rapporteur
Matthias MUNK	Rapporteur
Arvind KUMAR	Examinateur
Danko NIKOLIC	Examinateur
Yves FREGNAC	Directeur de thèse

Unité de Neurosciences, Information et Complexité (UNIC, UPR-3293), Centre National de la Recherche Scientifique (CNRS), 1, Avenue de la Terrasse, 91198 Gif-sur-Yvette, France

Contents

Preface

The brain is an organ that has sparked interest for more than 4000 years. Since the discovery and translation of the Smith papyrus (Breasted, 1930), it became clear that already the Egyptians realized that brain injuries can cause symptoms like paralysis. It was the Greek physician Hippocrates, who for the first time speculated that human behavior, experience and mental diseases are rooted in the brain. In his book 'On the sacred disease' he writes: "*Men ought to know that from nothing else but the brain come joys, delights, laughter and sports, and sorrows, griefs, despondency, and lamentations...And by the same organ we become mad and delirious, and fears and terrors assail us...In these ways I am of the opinion that the brain excercises the greatest power in man. This is the interpreter to us of those things which emanate from the air, when the brain happens to be in a sound state.*"

For the 2000 years to come after Hippocrates, fundamental advances in the understanding of the brain were mainly provided by outstanding anatomists like Galen and Vesalius, who investigated the principal structure of the human central nervous system. An important conceptual breakthrough came only at the beginning of the 19th century, when the Austrian physician Franz Joseph Gall (Gall and Spurzheim, 1810-1819) suggested the existence of distinct brain area that represent different mental functions and personality traits. The notion of localized brain function was later experimentally supported by the discovery of brain regions that are specialized for speech (Broca, 1863), motor action (Fritsch and Hitzig, 1870; Ferrier, 1875) and vision (Munk, 1879). The tradition of cortical localization initiated by these pioneers is carried on by a large number of contemporary neuroscientist, who attempt to delineate functionally different regions in the cortex through advanced imaging techniques like fMRI.

Despite the appeal of localization theory, several scientists already argued at the end of the 19th century that brain function is in general distributed across the cortex and only motor and sensory functions are localized in distinct cortical areas. They opposed the view that intellectual function reside in association cortices and rather believed that interactions between different brain areas (Munk, 1890) and the brain as a whole (Loeb, 1902) generate intelligence and associative memory. This holistic approach was extended by the Gestalt movement (Ehrenfels, 1890), which emphasized the premise of the whole (the "Gestalt") over its parts in mental and brain function (Goldstein, 1942). In the meantime, neuroscience had established the existence of neurons (Ramon y Cajal, 1906) and electrical signals in the form of action potentials as the basic currency of communication in neuronal networks (Du Bois-Reymond, 1848-1884). Both concepts were combined by Donald Hebb (1949) to develop a novel framework for distributed cortical functioning and communication based on groups of neurons ("cell assemblies"),

Statue of Episteme ("knowledge"), Celsus library, Ephesus (Turkey).

which cascade through brain as "phase sequences". The notion of cell assemblies pervades neuroscience up to today and has found expression in many theories of brain communication like synfire chains (Abeles, 1991), gamma oscillations (Fries, 2005) and neuronal avalanches (Plenz and Thiagarayan, 2007).

During my PhD, I came across all these theories and developed a fascination for the concept of cascading activity as the main agent of cortical processing. While I was studying the existence of neuronal avalanches in cortical activity of living animals, I made it a habit to think about brain activity as a collection of many avalanches spreading through cortical areas and more importantly interacting. I started to think about basic rules of cascade formation based on excitation and inhibition and believed that the secret to brain function lies in the principles that govern the interaction between avalanches. This in mind, I wondered how different theories of brain communication may be understood by avalanches and their interactions and pondered about a common framework. The results of this thinking process together with experimental findings and modeling studies are presented in this thesis. Throughout these years of my doctoral work, I recognized that neuroscience has acquired an enormous body of knowledge about the brain during the past decades. However, despite these efforts, I came to realize that general principles that organize all this knowledge into an intuitive framework of brain function are still missing, just like the head of the statue of knowledge in the ancient library of Celsus in Ephesus (Turkey). Finding these principles will remain a challenge for future generations of neuroscientists.

Acknowledgement

Ever since the beginning of my scientific studies, it was my conviction that advancing in science requires knowledge of various fields and disciplines. This applies even more to the neurosciences which are composed of a large number of subfield ranging from physics, mathematics and computer science to biochemistry, biology and philosophy. Thus, my aim not only consisted in acquiring sufficient knowledge from a variety of disciplines, but also finding laboratories, in which my credo of interdisciplinary research was shared by others. I was lucky enough to join the lab of Yves Frégnac (UNIC), who personifies like few others in neuroscience the combination of experimental and theoretical research. Under his liberal supervision, I was able to develop my own ideas about neuronal communication and test them experimentally as well as in modeling studies. He created an atmosphere that encouraged me to look beyond current ways of thinking in my field of research and put my ideas into a broader context through various discussions.

Thanks to Yves, I also applied to the FACETS-ITN PhD program, which I am highly indebted to. It not only provided generous financing for my PhD project, but also put interdisciplinary training and research as its highest priority. It allowed me to participate in a large number of courses in different areas of neuroscience research and gave me the opportunity to meet and befriend other students from various countries with a mindset similar to mine. It is important to mention that two of my research projects in this thesis were done in collaboration with students and labs within the FACETS-ITN consortium, which facilitated my studies. I need to highlight the role of Giacomo Benvenuti in Marseille, who kindly offered his own data and lots of philosophical discussions. Furthermore, without the help of Alejandro Bujan and Arvind Kumar in Freiburg, my ideas on synfire chains and gamma oscillations would not have found expression in a computational model. I would also like to thank Karlheinz Meier and especially Bjoern Kindler, the coordinator of this PhD program, for assisting in various administrative issues during the course of my studies and answer every question in detail and with patience. In the same vein, I wish to acknowledge Kirsty Grant, who provided invaluable help with all sorts of matters concerning FACETS-ITN and administrative question arising at UNIC.

Naturally, my research would not have been possible without the interaction and help of my colleagues at UNIC. First and foremost, I need to thank Cyril Monier, who introduced me to the art of animal experimentation and helped performing all the experiment in our lab. Moreover, he always had time and an open ear for any question about my research, which he always tried to answer patiently. He often helped to put my thought into a different perspective by offering alternative and challenging views. I

also need to say thank you to Aurelie Dauret for preparing the experiments and making each of them a pleasant experience through her cheerful nature. I am also obliged to all the other lab members and especially my fellow PhD students in the lab with whom I shared many interesting discussions about science and life as a doctoral student. My gratitude also goes to Alain Destexhe and Nima Dehghani, who helped me to develop a critical mind and look at my own research from a different angle. Discussions with Claude Bédard and Michelle Rudolph also fostered my ability to view things from a more philosophical and unconventional side.

My scientific education started already before my joining the lab of Yves, at the Max Planck Institute for brain research in Frankfurt/Main (Germany) and the National Institute for Health (Bethesda, USA). Parts of the research presented in this thesis were performed in both institutes. I wish to thank Prof. Wolf Singer for hosting me at his institute and creating an ideal environment to learn the craft of a scientist. My special thanks are addressed to Danko Nikolic, who was of unique importance for introducing me to the scientific world. He was not only eager to teach me a lesson, wherever possible, but also gave me personal guidance, which tremendously aided in developing my scientific thinking. Especially his tendency to look at the big picture of things had an important influence on me. Moreover, I also want to express my gratitude to Dietmar Plenz at NIH, who let me join his lab for two months and gave me deeper insights into the field of self-organized criticality during years of collaboration. In this respect I also need to thank my coworkers at the MPI and NIH, whose efforts was instrumental in obtaining some of the results in this thesis.

Finally, I am highly indebted to my family, both in Austria and in France, who supported me in various matters throughout my PhD. Claire was a continuous source of inspiration and provided the emotional environment, in which my scientific mind was able to thrive.

Summary

The brain is thought to be a highly complex and adaptive system that transforms sensory input into meaningful behavior. Processing of environmental information takes place in a highly distributed network of specialized areas that are believed to coordinate their dynamics into coherent spatiotemporal patterns of activity. This coordination requires efficient communication between brain areas and has been hypothesized to be accomplished by different mechanisms. In this doctoral work, we experimentally test in detail the presence of neuronal avalanches, a candidate mechanism for communication, in cortical activity of anesthetized and awake animals. Moreover, we suggest a novel theoretical framework to bridge the conceptual gap between synfire chains and gamma oscillations, two other putative hypotheses for neuronal communication, and test its validity in numerical simulations of neuronal networks.

In a first study, we recorded spontaneous activity with multi-electrode arrays (16 electrodes) in the primary visual cortex of (halothane) anesthetized cats and searched for power laws and long-range correlations in local-field potentials (LFP) as well as spiking activity. These two statistics can be a signature of critical dynamics, which is referred to as neuronal avalanches in neural networks. In spiking activity, we found power laws in avalanche size distributions in four out of seven recordings and a consistent power law exponent of -1.8. In the same recordings, lifetime distributions and inter-spike interval distribution of population spike trains were better fit by a power law than an exponential distribution. In the other three datasets, these distributions were rather curved and were equally well described by power law and exponential statistics. Average correlation as measured by average pairwise cross-correlation across all units was stronger and extended over a longer period of time in datasets with power laws than in those where power laws were absent. Finally, we sub-sampled the spiking data by randomly removing spikes and thereby transformed power laws into curved distributions. Surprisingly, power laws were present in the LFP in six out of seven datasets, even though the underlying spiking activity did not show evidence for power law scaling. In summary, we showed that spiking activity can sometimes have features of critical dynamics, while at other times evidence for neuronal avalanches is absent. Our sub-sampling analysis demonstrated that insufficient recording of spikes can indeed destroy power law statistics. However, we alternatively propose the existence of different cortical states with a varying correlation structure as a potential cause for critical statistics in some, but not in other recordings.

In a second study, we further pursued the cortical state hypothesis and recorded multi-electrode array data from the primary visual cortex of (isoflurane) anesthetized cats (32 electrodes) and one awake monkey (96 electrodes) in the dark. We developed a novel

method to separate different cortical states within short time windows based on LFP power spectra using principal component analysis and k-means clustering. We thus identified up to five different states with different spectral profiles. In spiking activity, these states showed marked differences in their collective dynamics with synchronized states displaying population bursts followed by periods of silence and desynchronized states exhibiting continuous and asynchronous population activity. Neuronal avalanche analysis of these different spiking dynamics indeed revealed that desynchronized activity is associated with more curved distribution, while synchronized activity shifts avalanche distributions closer to power laws, as measured by higher values of the scale parameter of fitted lognormal distributions. The same result was found for inter-spike interval statistics of the population spike train. In contrast, neuronal avalanche analysis of the LFP always approached power law distributions, even though the size of the tail was slightly modulated by the cortical state. In addition, we showed that correlations between electrodes in the LFP recordings were much higher than in spiking activity. Finally, these results were similar across different datasets within a species and did not differ between the anesthetized and awake recordings. An important difference was an increase of population firing rate in monkey recordings with desynchronization as opposed to a decrease in the anesthetized cat cortex during desynchronized states. In conclusion, we demonstrated a modulation of tails in neuronal avalanche statistics by the cortical state in spiking activity of both anesthetized and awake preparations. These findings suggest the presence of both critical and non-critical fluctuation regimes in neuronal network. The modulation of tails was in general much weaker for LFP, which was on average more correlated than unit activity. The origin of this high correlation in the LFP is unclear and might be partly due to volume conduction. Sub-sampling may not explain the absence of power law in the monkey recordings, as the firing rate increases with further desynchronization of population spiking activity.

In a third study, we study two other prominent theoretical frameworks for neuronal communication, the synfire chain model and the communication through coherence (CTC) hypothesis. In these models, communication between remote brain areas is established through two different types of synchrony, which have hitherto believed to be distinct from each other. In the synfire chain, synchrony is generated through common drive from previously firing neurons, while synchrony in the CTC model is generated through oscillations of local neuronal populations. In this work, we suggest a novel framework, in which coherent oscillation are a manifestation of synchrony spreading across a diluted synfire chain architecture which does not have strong enough connections to transmit synchrony across its layers. These weak connections are compensated for by amplification and synchronization of excitation during repeated cycles of an oscillation. The amplification is caused by progressive synchronization of inhibition within the oscillation, which in turn increases the gain of excitatory input. We introduce the concept of oscillation chains which represents the spread of a coherent oscillation across layers of a

weakly connected synfire chain. We hypothesize that these oscillations trigger synaptic potentiation and transform the oscillation chain into a synfire chain, once the synaptic weights are sufficiently strong. Synfire chains may thus be regarded as a special case of oscillation chains. We tested this framework in layered networks of integrate and fire neurons and indeed found the presence of oscillation chains that supported the spread of synchrony with connections, whose strength was insufficient for synfire chain transmission. Further analysis revealed that oscillation chains can be converted to synfire chains by increasing synaptic weights and the emergence of oscillation chains depends on resonance properties of the network. Taken together, these results propose a new interpretation of communication through synchrony in neuronal networks and link coherent oscillations with synfire chains and synaptic plasticity.

In summary, we used experimental techniques and modeling to study different modes of communication in neuronal networks. Experimentally, we found that neuronal networks display both critically synchronized population activity and desynchronized dynamics indicating that communication based on criticality may change as a function of cortical state. Furthermore, we show in a modeling study that synchrony created in synfire chains may be equivalent to synchronization created within coherent oscillations. Each of these two modes of communication is used for different strengths of synaptic weights and synaptic plasticity may be the key to convert oscillation dynamics into synfire chains.

Resumé

Le cerveau est un système complexe, qui transforme les signaux d'entrée sensoriels en un comportement. Le traitement de l'information issue de l'environnement se distribue au niveau cortical dans un réseau d'aires spécialisées qui coordonnent leurs dynamiques à travers une activité neuronale spatio-temporelle cohérente. Cette coordination requiert une communication efficace entre les aires du cerveau et plusieurs hypothèses théoriques, souvent présentées comme alternatives, ont été proposées. Dans cette thèse, nous testons expérimentalement la présence d'avalanches neuronales, un mécanisme potentiel pour contrôler la communication neuronale, dans l'activité corticale des animaux anesthésiés et éveillés. A partir de ces observations expérimentales, nous proposons un nouveau cadre théorique qui réunit le concept de chaîne de synchronie ("synfire chain") et des oscillations gamma, deux autres hypothèses élémentaires dans la propagation de l'activité neuronale. Des simulations numériques sont présentées pour tester la validité du modèle présenté.

Dans une première étude, nous avons enregistré de l'activité spontanée avec un peigne d'électrodes (16 électrodes) dans le cortex visuel primaire des chats anesthésiés (halothane) et recherché des lois de puissance et des corrélations à longue distance dans les potentiels de champs (LFP) ainsi que les potentiels d'action. Ces deux mesures peuvent être considérées comme une signature de la criticalité de la dynamique de l'activité neuronale, et caractérisent le processus d'avalanche dans les réseaux neuronaux.

L'analyse des patterns de potentiels d'action, a permis d'extraire des lois de puissance dans les distributions d'avalanches - dans quatre des sept enregistrements - avec un exposant fractal de -1,8. Dans les mêmes enregistrements, les distributions de durée des avalanches ont été mieux expliquées par une loi de puissance que par une distribution exponentielle. Dans les trois autres expériences, ces distributions ont présenté une asymétrie ("skewness") expliquée par une loi de puissance et de distribution exponentielle. La corrélation moyenne a été plus forte et longue dans l'ensemble de données avec des lois de puissance que dans celles ou la loi de puissance a été absente.

Étonnamment, à un niveau plus mésoscopique, des lois de puissance étaient présentes dans le LFP de six des sept enregistrements, même si des lois de puissance étaient absentes dans l'activité des potentiels d'action. En résumé, nous avons montré que l'activité de potentiels d'action peut parfois avoir des caractéristiques d'un état critique, tandis qu'à d'autres instants ou pour d'autres assemblées, le comportement d'avalanche était absent. Nous discutons la possibilité que le sous-échantillonnage puisse expliquer l'absence des lois puissance, mais nous proposons une autre hypothèse selon laquelle l'hétérogénéité des états dynamiques corticaux et la diversité des corrélations observées rendent chacun des comportements (critique vs non critique) à leur tour plus dominant.

Dans une deuxième étude, nous avons poursuivi notre étude de la dynamique spontanée corticale et enregistré des données avec des peignes d'électrodes dans le cortex visuel primaire (32 électrodes chez le chat anesthésié avec de l'isofluorane, et 96 électrodes chez le singe éveillé) en l'absence de stimulations visuelles. Nous avons développé une nouvelle méthode permettant de séparer les différents états corticaux basés sur les spectres de puissance LFP. Nous avons donc identifié jusqu'à cinq états différents. Dans l'activité des potentiels d'action, ces états ont montré des différences dans leur dynamique collective avec des états synchronisés et désynchronisés. Une analyse d'avalanche neuronale a révélé que l'activité désynchronisée est associée avec une distribution plus asymétrique ("skewed"), tandis que l'activité synchronisée montre des distributions d'avalanche proches d'une loi de puissance. Le même résultat a été trouvé pour les statistiques établies à partir des intervalles entre potentiels d'actions. Par contre, les distributions dans le LFP ont été toujours proches d'une loi de puissance, même si la taille de la queue des distributions était légèrement modulée par l'état cortical. En outre, nous avons montré que les corrélations entre les électrodes pour le LFP étaient beaucoup plus élevées que dans l'activité des potentiels d'action. Enfin, ces résultats étaient similaires entre les différentes espèces et ne différait pas entre les enregistrements anesthésiés et éveillés.

En conclusion, nous avons montré chez les animaux anesthésiés et éveillés que les statistiques dans l'activité des potentiels d'action peuvent révéler des avalanches neuronales conditionnelles de l'état cortical. Ces conclusions suggèrent la coexistence de dynamiques à la fois critiques et non critiques dans le cortex. La modulation des distributions est en général beaucoup plus faible pour le LFP, qui est en moyenne plus corrélé et tend à révéler un régime dynamique proche de la criticalité. L'origine de cette forte corrélation nest pas complètement élucidée, mais la conduction de volume pourrait jouer un rôle.

Dans une troisième étude, nous étudions deux autres cadres théoriques pour la communication neuronale, l'un s'appuyant sur l'existence de chaînes de propagation de synchronie ("synfire chain") et l'autre s'appuyant sur le rôle des oscillations dans la cohérence d'activité au sein des réseaux corticaux (CCT). Dans la chaîne de synchronie, la synchronisation est générée grâce à un entraînement des autres neurones, tandis que la synchronisation dans CCT est creée par des oscillations neuronales. Dans ce travail, nous proposons un nouveau cadre réunificateur, dans laquelle les oscillations cohérentes sont une manifestation de la synchronisation dans une chaîne synchronie dont la propagation directe ("feedforward") n'est pas de force initiale suffisante pour transmettre de l'activité synchronisée. Ces connections faibles sont compensées par l'amplification et la synchronisation de l'excitation s'établissant au cours des cycles successifs d'une oscillation résonnante. Nous introduisons le concept de chaînes d'oscillation, ce qui représente la propagation d'une oscillation cohérente au travers d'une hiérarchie de couches faiblement connectées soumise au bombardement direct d'une chaîne de syn-

chronie. Nous introduisons l'hypothèse supplémentaire d'un processus de plasticité synaptique dépendant des oscillations. Ce processus adaptatif permet de transformer le processus oscillatoire en une chaine de synchronie, une fois que les poids synaptiques excitateurs ont dépassé une efficacité seuil. Notre théorie propose donc que les chaînes de synchronie peuvent être vues comme un cas particulier de chaînes oscillatoires. Cette hypothèse a été testée par des simulations numériques des réseaux neuronaux faiblement connectés, qui permettent de détecter la présence de chaînes d'oscillation liées à la propagation de la synchronisation. Les simulations montrent que les chaînes d'oscillation peuvent être converties en chaînes de synchronie en augmentant les poids synaptiques et que l'émergence de chaînes d'oscillation dépend des propriétés de résonance du réseau neuronal. Ces résultats proposent une nouvelle interprétation de la communication à travers la synchronisation dans les réseaux neuronaux et établissent un lien original entre les oscillations cohérentes, les chaînes de synchronie et la plasticité synaptique associative.

En résumé, nous avons utilisé des techniques expérimentales et de modélisation pour étudier différents modes de communication dans les réseaux neuronaux. Expérimentalement, nous avons montré que les réseaux neuronaux affichent à la fois une dynamique désynchronisée et une activité synchronisée avec des signes d'un état critique, indiquant que l'expression de "criticalité" dans la dynamique corticale peut changer en fonction de l'état collectif du réseau. Nous montrons par ailleurs par une approche théorique que les chaines de synchronisation pourraient provenir d'un renforcement adaptatif de la synchronisation crée dans les oscillations cohérentes. Chacun de ces deux modes de communication est utilisé pour différents valeurs de poids synaptiques et la plasticité synaptique associative peut être la clé pour transformer la dynamique des oscillations en des chaines de synchronie.

Part I

Introduction

1 Complexity and Criticality

1.1 The Science of Complexity

What is complexity? At the moment, there is no unanimous answer to this question and an exact definition of complexity is still under debate (Ziemelis, 2001). In general, complexity is a feature of a system, a concept that evolved out of thermodynamics of steam engines in the 19th century (Carnot, 1824) and was later formalized in general systems theory (Bertalanffy, 1968) and by the cybernetics movement (Wiener, 1948). All systems are composed of a number of elements or components with connections between them. These connections enable the components to interact with each other and separate a system from its environment by boundaries. A system is closed, if the interactions are restricted to the components within the system or open, if elements of a system interact with its environment. The brain can be considered as an open system, since it receives energy and information from its surroundings and the body through sensory organs and transfers energy and information back to the environment through behavior and to the body through chemical and neuronal signals.

Traditionally, science attempted to reduce systems to its elementary components and understand a systems' behavior in terms of component properties and their interactions. The reigning paradigm was an additive approach which claimed that adding up the features of individual components can explain and predict macroscopic variables of a system. Failure to predict behavior was regarded as a problem of measurement through insufficient knowledge of system parameters or components and not a fundamental property of nature (Nicolis and Nicolis, 2007). Classical physics was indeed very successful in mathematically capturing and predicting the macroscopic behavior of simple mechanic (Newtons laws of motion) and thermodynamical systems (Boltzmann equation) by this reductionist approach. A similar strategy was adopted in biology, where it was attempted to explain the behavior of biological systems by lower level rules established by molecular biology.

However, it was later realized that a certain class of systems cannot be successfully understood by this reductionist paradigm. These systems are not additive in the sense that understanding the properties of individual components cannot explain the systems macroscopic dynamics. This lack of applicability of the linear superposition principle and predictability is an important property of complex systems and has been summarized in the concept of emergence ("The sum is more than its parts", Simon, 1981). Nonlinear interactions between non-linear components of a system are indeed regarded as essential for complexity (Frégnac et al., 2006; Chialvo, 2010). Moreover, as pointed

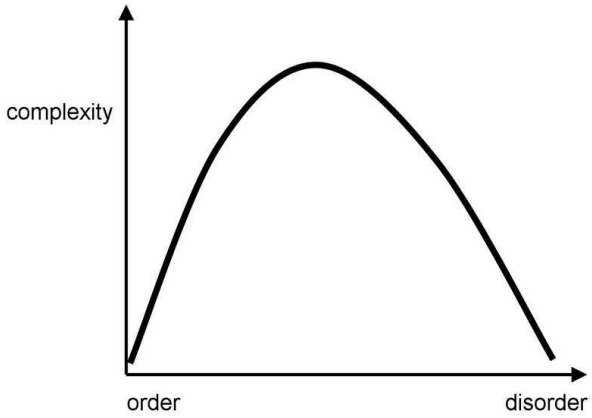

Figure 1.1: Complex systems lie in between order and disorder. Taken from Sporns (2007).

out by Hermann Haken (2004), these interactions endow complex systems with a peculiar circular causation. In one direction, interactions of local components cause novel dynamics at the macroscopic level. In the other direction, cooperative dynamics and emerging macroscopic variables (i.e. the system as a whole) influence and constrain the interactions of components through downward causation. The cybernetics movement also pointed out that complex systems often include feedback loops between components with highly recurrent interactions (Ashby, 1947). Moreover, there is a balance between positive and negative feedback which allows for development and stabilization of the system. As a consequence of these interactions, complex systems generate coherent spatiotemporal patterns and move away from thermodynamical equilibrium, thereby reducing statistical entropy. Ilya Prigogine referred to these patterns as dissipative structures (Prigogine and Nicolis, 1967). This emergence of order puts complex systems in between random, disordered (e.g. gases) and highly ordered systems (e.g. crystals) at equilibrium (see Fig. 1.1). Complex systems are also said to be metastable and at the edge of chaos, as they generate a large number of patterns in response to external perturbation and yet remain stable (Kauffman, 1993). This variety of patterns also makes complex systems adaptive, i.e. they are able to react to perturbations and act on their environment. Finally, systems with complex properties often display a hierarchical organization with nested subsystems and different levels of order and structure (Simon, 1962).

1.2 Measures of Complexity

Apart from defining complexity qualitatively, attempts have been made during the last decades to quantify complexity in order to compare the behavior of different systems

(Sporns, 2007). In general, there is no generally accepted metric and several different approaches have been employed depending on the studied system.

1.2.1 Complexity as Randomness

In a first approach, complexity was equated with randomness and systems with the most random behavior were considered as the most complex. Kolmogorov (1965) defined complexity as the length of the shortest description necessary to specify a string of symbols. Accordingly, random strings display the highest degree of complexity. The logical depth concept of Bennet (1988) regards the time needed for an algorithm to compute a string as indication of complexity. Another metric views complexity as the information contained in the history of a thermodynamical process before it reaches its final state (thermodynamical depth; Lloyd and Pagels, 1988; Crutchfield and Shalizi, 1999).

1.2.2 Complexity as Spatiotemporal Order

In another approach, complexity is seen as the amount of spatiotemporal structure and information expressed by a system. These measures separate structured parts of a system from random elements and attempt to quantify this structure. One example is effective complexity (Gell-Mann, 1995) which uses the minimal length of description analogous to algorithmic complexity (see above) in order to quantify only ordered features of a system. Another measure quantifies the overlap between the symbol sequence of a system and the sequence of its environment through Kolmogorov complexity (physical complexity; Adami and Cerf, 2000).

1.2.3 Complexity as Correlations

A third approach looks at complexity from the perspective of correlations. These correlations are expressed in different measures and are a result of the formation of large-scale spatiotemporal patterns after external perturbation of a system. Typically, complex systems display long-range correlations that can span the entire system and the correlation length diverges (Chialvo, 2010). A consequence of these long-range correlations is the presence of power laws in a variety of measures, which is a hallmark of complex systems (Nicolis and Nicolis, 2007). Power laws are mathematically defined as $P(s) = s^{\alpha}$, where α is the exponent of the power law. When the logarithm is taken on both sides, the power law relationship turns into the equation for a straight line with slope α. This is the reason, why power laws appear as straight lines in a double logarithmic plot.

1.3 Complexity and Fractals

1.3.1 Definition of a Fractal

Power laws have been reported in statistics collected from a variety of natural and man-made systems. In addition, they are found in static as well as dynamical systems. Mandelbrot coined the term fractal to describe geometrical structures that show power laws and self-similarity (1982). Self-similarity refers to the fact that fractals contain copies of themselves, when the scale of observation is changed. This means that a structure viewed from a smaller scale is similar to the pattern observed at larger scales. This self-similarity is quantitatively captured by power laws and their exponent which is also called the fractal dimension. An example is shown in Figure 1.2A which illustrates the coastline of Norway with its numerous fjords and smaller copies of fjords embedded within larger ones. The length of the coast as a function of the box size used to measure it follows a power law with fractal dimension D (Fig. 1.2B). Even though initially regarded as purely mathematical constructs (e.g. Cantor set, Koch curve), Mandelbrot made the observation that many structures in nature are fractal. Natural objects like clouds, river networks, mountain ranges, snowflakes, blood and pulmonary vessels have fractal features. He used simple iterative equations and computer simulations to generate patterns with a self-similar structure. Fractals are not restricted to static structures, but also occur in time. This phenomenon is sometimes referred to as 1/f noise, as the power spectrum of this dynamics decays as a power law (Ward and Greenwood, 2007).

1.3.2 Examples of Fractals

Fractals are found in many scientific fields including physics (Feder, 1988; Sornette, 2004), geology (Turcotte, 1997), biology (Havlin et al., 1995) and behavior (Werner, 2010). In addition, the frequency of words used in books (Zipf, 1949), stock market fluctuations (Mandelbrot and Hudson, 2006), water level fluctuations of the river Nile (Hurst, 1951) and solar flares (Lu and Hamilton, 1991) have fractal power law statistics (for more examples see Newman, 2006). It is also noteworthy that many physical laws like Newton's law of gravitation and the Coulomb law for electrostatic potentials are power laws. In these cases the power law takes on the form $\frac{1}{r^2}$with an exponent $\alpha = 2$. Fractals are also abundant in the brain and include the morphology of dendritic branching patterns of neurons (Kniffki et al., 1994), dynamics of ion channel opening and closing (Liebovitch et al., 2001), secretion of neurotransmitters (Lowen et al., 1997), spike trains of individual neurons in the auditory nerve (Teich et al., 1990) as well as the visual cortex of the cat (Teich et al., 1997) and awake monkeys (Baddeley et al., 1997), and the power spectrum of membrane potential fluctuation in neurons of the

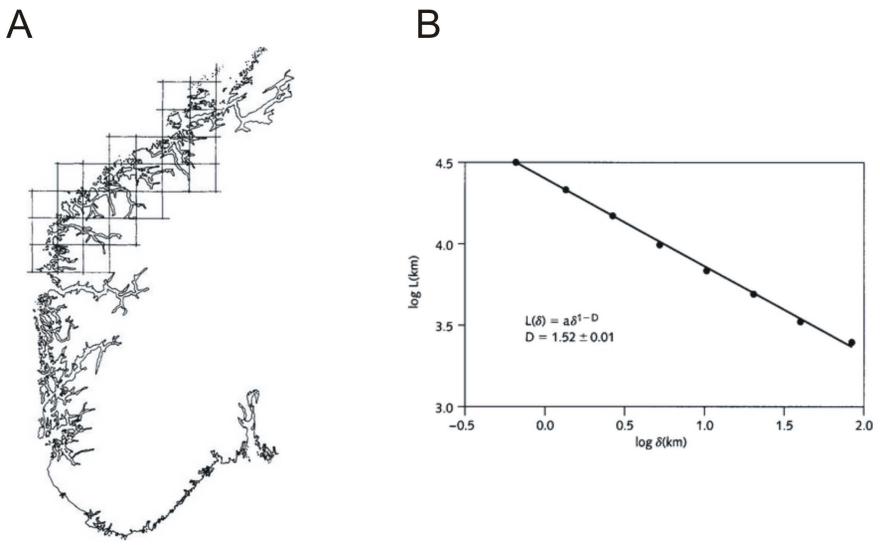

Figure 1.2: A: Coast of Norway with fractal geometry. B: The length of the coast measured by covering the coast with boxes, like the ones shown in A, of various lengths 8. The straight line indicates that the coast is a fractal. The slope of the line yields the "fractal dimension" of the coast of Norway, D = 1.52. Taken from Bak (1996).

cat visual cortex (El Boustani et al., 2009). Fractals and power law at the neuronal network level will be reviewed below.

1.3.3 Features of Natural Fractals

Unlike mathematical fractals, natural fractals are limited to minimum and maximum values. A coast cannot be larger than a country or smaller than a grain of sand. These power laws show upper and lower cut offs as a consequence of the confined size of natural objects. In addition, the restricted resolution of measurement devices imposes cut offs to the range of fractal features. Moreover, several fractals with different exponents α may occur at different scales, which is called a multifractal (Sornette, 2004). The presence of only one power law is referred to as monofractal (Lowen and Teich, 2005). Fractals can be deterministic, i.e. smaller copies fit the whole exactly, while in random fractals structure at smaller scales resembles the whole only in a statistical sense.

1.4 Mechanism of Complexity

The definitions of complexity and examples of fractal structures given so far are phenomenological and agnostic about the mechanisms creating complex structures and behavior in nature. The question to be answered is how interactions between components render a system complex.

1.4.1 Complexity and Second-Order Phase Transitions

First evidence for a candidate mechanism that can create complexity came out of statistical physics. In 1822, the French engineer Charles Cagniard de la Tour studied phase transitions between liquid and gas phases in his cannon barrel experiments (see Berche et al., 2009). He discovered that at a certain temperature a distinction between gas and liquid phase cannot be made anymore, as parts of the substance continuously fluctuate between both phases. This phenomenon was further studied by the Irish physicist Thomas Andrews (1869), who introduced the terms critical temperature and critical pressure. Later, Paul Ehrenfest (see Jaeger, 1998) summarized all types of phase transitions with critical parameters as second order (or continuous). It was observed that this type of phase transition is characterized by infinite correlation length and power law statistics near the critical point (Beggs and Timme, 2012). Importantly, criticality and complex behavior in these thermodynamical systems are achieved through fine tuning of parameters.

1.4.2 Ising Model

A classic example of a second-order phase transition is the ferromagnetic phase transition which has been elegantly explained by the Ising model (see Brush, 1967) (Fig. 1.3). This mathematical model contains a lattice of iron, in which each square is filled by an electron. Each electron has a spin which can assume two different directions and influence the spin of its nearest neighbor. The temperature T of the iron can be modified externally by adding heat and the behavior of the spins can be examined as a function of T. At low temperature, all the spins are aligned in one direction due to local interactions resulting in magnetization of the iron. In contrast, at high temperature the additional energy applied to the system prevents effective spin interaction and spins remain aligned randomly with no net magnetization. However, at the critical temperature, where the system undergoes a phase transition between order and disorder, local groups of electrons with the same spin orientation and different sizes emerge at varying locations of the lattice, while electron spins in other parts of the system remain randomly aligned. The system is a mixed state of order and disorder. The macroscopic variable that describes the order in the Ising model is generally called the order parameter. It is zero for complete disorder and approaches a maximum value for complete order. For the Ising model the order parameter would be the magnetization of the system. The variable that controls the order in a system is denoted the control variable. In the Ising framework, temperature regulates the net magnetization and thus serves as the control parameter. The amplitude of the order parameter fluctuations grows with increasing control parameter until it reaches a maximum at the critical point.

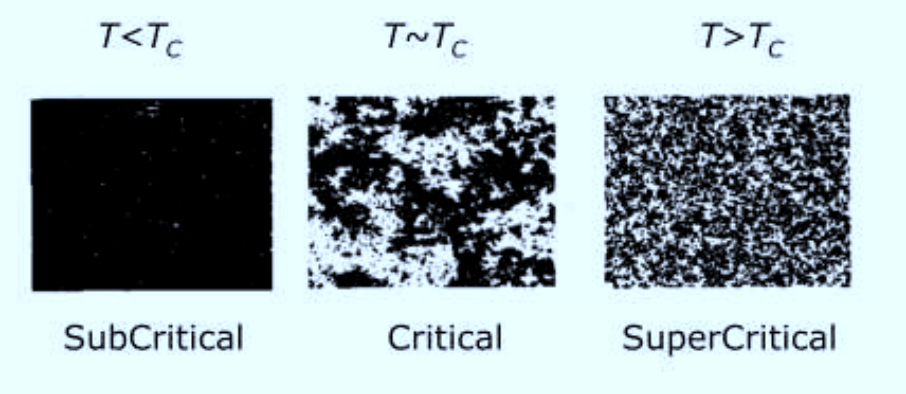

Figure 1.3: Ising model. Three snapshots of the spin configurations at one moment in time for three temperatures (subcritical, critical and supercritical) from numerical simulations of the Ising model. Only at the critical temperature systems exhibiting a second-order phase transition show the highly heterogeneous correlated domains commonly seen as complex, while both sub- and supercritical conditions result in homogeneous states. Taken from Chialvo (2010).

1.4.3 Self-Organized Criticality

As illustrated in the Ising model, tuning of a control parameter to a critical value is crucial to establish criticality and complex fluctuations of order parameters. However, as pointed out by Bak (1996), nature in general exhibits complex dynamics and behavior without precise fine tuning of parameters. He and his colleagues proposed a different mechanism that is employed by nature to reach criticality. According to their view, self-organization without external influence is at work in many natural and man-made systems and drives these systems to the critical point (Bak et al., 1987). The theory of self-organized criticality combines the concepts of self-organization, criticality and complexity into one common framework to explain the widespread existence of fractals and 1/f noise in nature. Self-organized systems consist of a number of components which interact through internal interaction forces. In addition, the system is subject to an external driving force serving as the principle source of self-organization. After a sufficient amount of time the system will be driven to a critical point through the slow input, at which the accumulated energy dissipates through the fast internal forces by way of cascading dynamics. Bak illustrated the working principles of self-organized criticality in his well-known sandpile model (Bak et al., 1987; see Bak et al., 1996 for a historic account; Turcotte, 1999). In this model, sand is continuously added to an initially small pile of sand corresponding to an externally applied slow driving force. As the sandpile grows, small avalanches start to slide down the slopes of the pile caused by fast interactions between sand grains (Fig. 1.4). Importantly, the sandpile will eventually reach a maximum height, at which the average number of grains added is on average equal to the amount of sand leaving the pile through sand slides. As

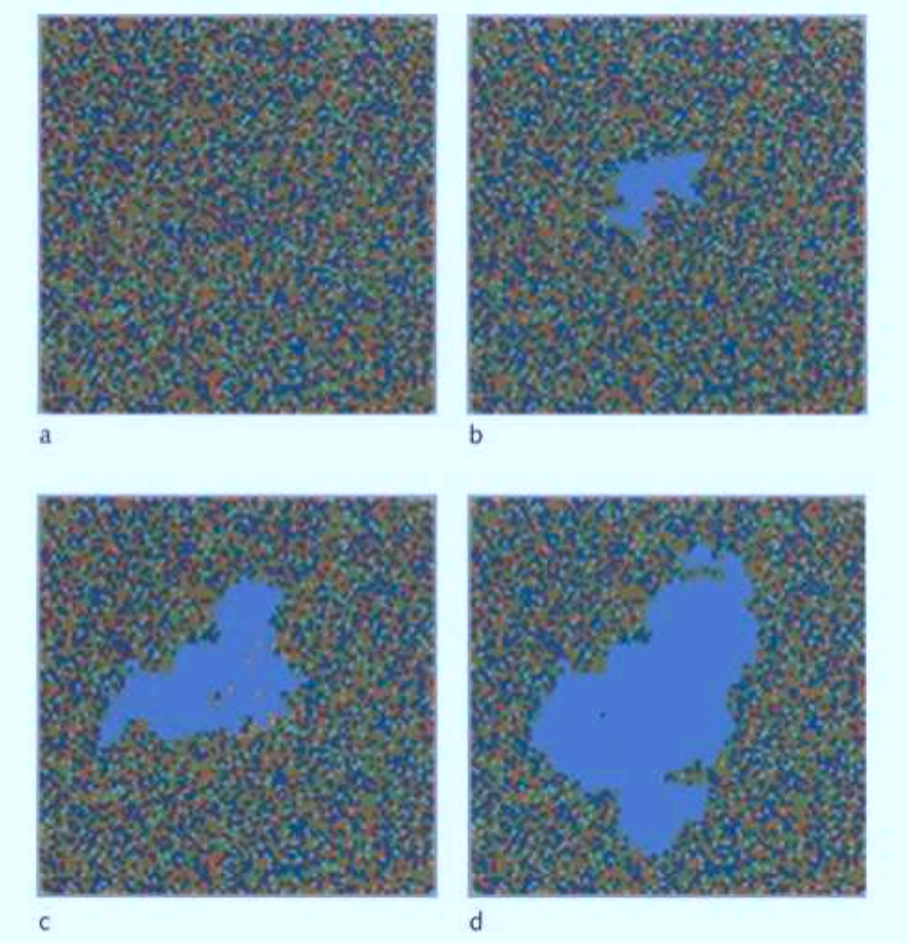

Figure 1.4: Self-organized criticality in sandpile avalanches. Snapshot of propagating avalanche in the sandpile model. The colors gray, green, blue and red indicate heights of 0,1,2, and 3, respectively. The light blue show the columns that have toppled at least once. As the avalanche grows, the light blue area increases. Taken from Bak (1996).

shown in Bak's model (1987), this steady state is critical with long-range spatiotemporal correlations (Jensen, 1998) and avalanche sizes following power law distribution. Self-organized criticality has been regarded as "Newton's law of complexity" (Bak, 1996) and provided a mechanism that could generate complex global behavior through simple local interaction. This concept has been used to satisfactorily explain a variety of complex phenomena such as forest fires (Drossel and and Schwabl, 1992), earthquakes (Bak and Tang, 1989), landslides (Malamud and Turcotte, 1999), solar flares (Lu and Hamilton, 1991), evolution of species (Bak and Sneppen, 1993), and epidemics (Gisiger, 2001).

1.5 Critical Brain Dynamics

Alain Turing was the first to suggest that the brain might be critical in order to overcome the highly correlated subcritical and supercritical states which are detrimental for all information processing (Turing, 1950). After Bak's seminal discovery of self-organized criticality (1987), a number of studies addressed the question of SOC in neuronal networks (Chen et al., 1995; Corral et al., 1995; Herz and Hopfield, 1995). Later, Bak devoted a whole chapter to the brain in his famous book 'how nature works' (1996) and sparked further interest among physicists and neuroscientists about critical brain dynamics. He argued that criticality in neuronal networks is necessary for neuronal communication allowing input to sensory areas to easily access remote brain areas. This is in contrast to subcritical dynamics which remain local and supercritical activity which activates the entire brain. Furthermore, he suggested that criticality allows the brain to switch quickly between different patterns reflecting the representation and processing of different stimuli. More modeling studies followed trying to implement critical dynamics in neuronal networks and test Bak's original ideas about the brain (Chialvo and Bak, 1999; Bak and Chialvo, 2001).

1.5.1 The Discovery of Neuronal Avalanches

It was not until the landmark paper by Beggs and Plenz (2003) that experimental brain research picked up the criticality hypothesis and tested its validity in neuronal networks of the brain. The authors recorded local field potentials (LFP) from organotypic cultures and acute slices of rat somatosensory cortex with 60 channel electrode arrays. These preparations were spontaneously active after appropriate treatment with neuroactive substances (NMDA and dopamin agonists). This spontaneous activity was characterized by intermittent bursts of neuronal activity (~100-200ms) that were interrupted by periods of silence (~several seconds) (Fig. 1.5A). The new conceptual step forward in this study was to consider these burst as cascades of neuronal activity analogous to the sand avalanches in Bak's sand pile model. If the activity in the cortical preparation was indeed critical, it should display power laws and long range correlations as predicted from theory. In order to analyze the data, the authors converted the continuous LFP signal into a point process by applying a threshold and defining discrete events (so called nLFPs), whenever the signal crossed this threshold. To search for signs of criticality the authors counted the number of events from all electrodes in each burst and defined the sum of event counts as the size of a neuronal avalanche. First, this study showed that the extracted events indeed show long-range correlations as predicted by criticality (Fig. 1.5B). More importantly, however, was the finding that the avalanche size distributions decayed as a power law with exponent -1.5 (Fig. 1.5C), closely matching theoretical predictions (Eurich et al., 2002). In addition, the initial

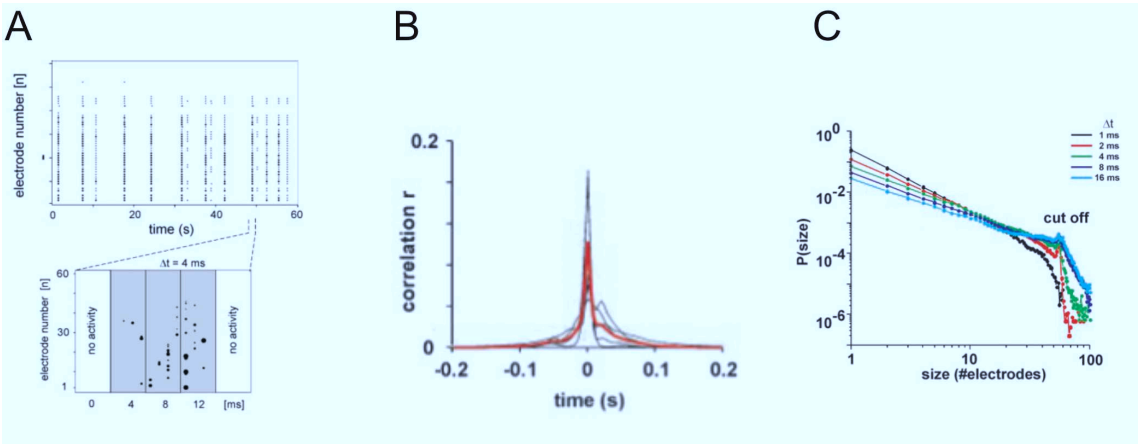

Figure 1.5: Activity within synchronized periods in neuronal cultures is composed of neuronal avalanches. A: Raster of spontaneous activity (top) shows correlated periods containing spatiotemporal patterns (middle) and an avalanche of three frames in the original coordinates of the multielectrode array (bottom). Avalanches were defined as sequences of continuous activity that were preceded and terminated by a bin width of t with no activity. B: Population cross-correlograms shows correlation falls to zero within +- 100-200 msec. red, average; black, individual cultures. C: Probability distribution of avalanche sizes (number of electrodes activated) in loglog coordinates at different t (average for n = 7 cultures). The linear part of each function indicates power law. Cutoff given by maximal number of electrodes. Adapted from Beggs and Plenz (2003).

part of avalanche lifetime distributions displayed power laws with exponent -2. Moreover, changing the spatial arrangement of the electrode array did not alter the power law properties of the data, but only shifted the power law cut-off to different values. This property, also known as finite size scaling in critical systems (Bak, 1996; Klaus et al., 2011), provided further support for critical dynamics in these preparations. These results were further corroborated by the application of disinhibiting GABAa antagonists, which destroyed the power laws and rendered the avalanche size distributions bimodal, as expected from a supercritical state. The study concluded that critical dynamics in the form of neuronal avalanches represent a different mode of neuronal network activity distinct from oscillations and wave-like propagation of neuronal activity.

1.5.2 Neuronal Avalanches as a Critical Branching Process

The specific exponents found for avalanche size and lifetime distributions by Beggs and Plenz (2003) lead to the hypothesis that a critical branching process is the underlying principle of neuronal dynamics in their in vitro preparations. Branching processes were studied in detail by Harris (1963) and describe cascading dynamics, in which a unit active at time t causes a number of other units (sigma) to be active at time t+t. This

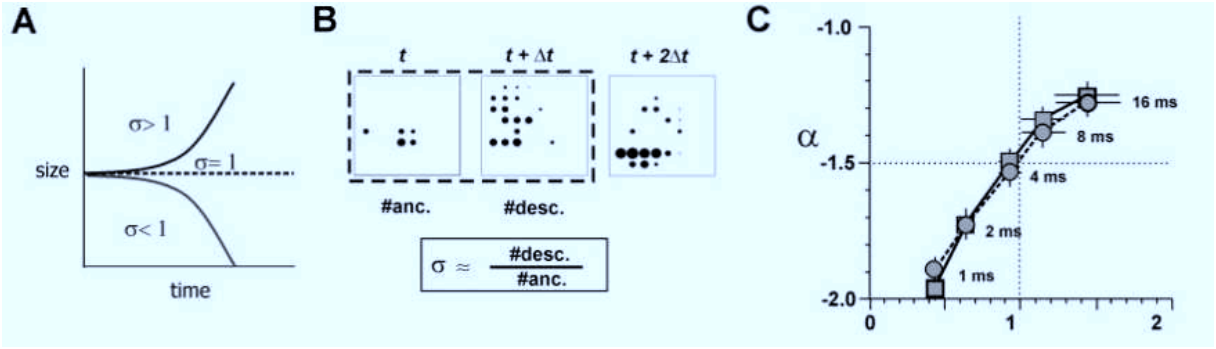

Figure 1.6: A: Network dynamics in cultured networks are characterized by a critical branching sigma = 1, suggesting a state of optimal information transmission. A: Estimate of branching parameter sigma from individual avalanches. Sigma = the ratio of descendant electrodes to ancestor electrodes. B: Sketch depicting the critical behavior of a branching process over time. If sigma = 1, the size of the avalanche will grow over time, taking over the network (epilepsy), whereas at sigma = 1, the avalanche will diminish quickly in size. Only at sigma = 1 (critical) can avalanches persist at all scales. C: Phase plot of (sigma, alpha) as a function of t. Note that the trajectory passes through critical point (1,-1.5) at the average population IEI of 4.2 msec. Adapted from Beggs and Plenz (2003).

number is denoted as branching parameter and can be intuitively understood as the ratio between descendants (# of active units at time t+t) and ancestors (# active units at time) in a branching process. Importantly, the value of sigma determines the behavior of the network and constrains the network dynamics to three different states. When sigma<1, the dynamics is subcritical and generates mainly small cascades that fade away quickly. At sigma>1, activity becomes supercritical and leads to cascade explosion. Only with sigma precisely tuned to a value of 1, each unit activates on average one other unit and the dynamics has critical properties with cascade sizes that decay according to a power law. Figure 1.6A illustrates the branching properties of cascades with different values of sigma. Critical branching processes were investigated in models of neuronal networks (Haldeman and Beggs, 2005) and produced exponents that matched those found by Beggs and Plenz (Zapperi et al., 1995). Notably, Beggs and Plenz also estimated the branching parameter of their *in vitro* networks based on the thresholded events (Fig. 1.6B) and found a value of sigma close to 1 as predicted from a critical branching process (Fig. 1.6C).

1.5.3 Further Evidence for Neuronal Avalanches *In Vitro* and *In Vivo*

After the seminal study of Beggs and Plenz (2003), the same authors published another report (2004), in which they show that the previously discovered neuronal avalanches embed a large number of spatiotemporal patterns which repeatedly recur during 10

hours of recording from organotypic cultures of rat somatsosensory cortex. These patterns were organized as distinct families and occurred with millisecond precision. Another study (Stewart and Plenz, 2006) investigated the role of dopamine in the formation of neuronal avalanches in acute prefrontal slices of adult rats. It found that the slope of the power law is a function of dopamine concentration and peaks at medium dopamine levels with a value of -1.5. Higher or lower dopamine levels reduced the slope and spatial correlation in the recorded nLFP activity, thereby defining an optimal dopamine concentration for occurrence of critical dynamics. Another important finding was that neuronal avalanches appear mainly in superficial layers. Stewart and Plenz (2008) also demonstrated that neuronal avalanche with a slope of -1.5 and a branching parameter of 1 characterize the dynamics of the maturing cortex of newborn rats despite large changes in neuronal activity levels during development. Plenz and Chialvo (2009) uncovered more features of cortical slice activity that are consistent with critical dynamics. They found that power laws were independent of slow external drive to the slices, avalanche distributions remained stationary over time, avalanche distributions before and after large avalanches were described by Omori's law for earthquakes and decayed as a power law, and the spatial patterns of avalanches were fractal.

In parallel to *in vitro* studies of neuronal avalanches in LFP, attempts were made to also show their existence in intact animals. Gireesh and Plenz (2008) recorded spontaneous LFP in the somatosensory cortex of urethane anesthetized rats during cortical development. They showed that neuronal dynamics during development evolves into a state of nested oscillations in the theta, beta and gamma range that are coherent across electrodes. Notably, neuronal avalanche analysis of these coherent oscillations revealed a power law with slope -1.5. The authors applied a range of substances to pharmacologically characterize the origin of the power law. They found that neuronal avalanche formation in the immature rat cortex is dependent on GABAa and NMDA mediated synaptic transmission and does not require AMPA receptors. In 2009, Petermann et al. recorded LFPs in the primary and premotor cortex of quietly sitting monkeys and reported the presence of power laws and long-range correlations demonstrating that neuronal avalanches are not only confined to anesthetized preparations (Fig. 1.7). Moreover, Yu et al. (2011) demonstrated that power laws in the LFP rely on higher order statistics and cannot be explained by pairwise correlations.

Several studies also extended the search for neuronal avalanche from LFP to spiking activity. Mazzoni et al. (2007) recorded spikes from dissociated cultures of hippocampal rat neurons and intact leech ganglia. Their preparations exhibited population burst behavior similar to the study of Beggs and Plenz (2003) with spike correlations lasting up to several 100 milliseconds. Burst sizes and lifetimes followed a power law, suggesting critical dynamics even when spikes were used as an indicator of neuronal activity. Importantly, neuronal avalanche statistics were destroyed by either blocking NMDA or GABAa receptors. Similar results were obtained in dissociated cultures of embry-

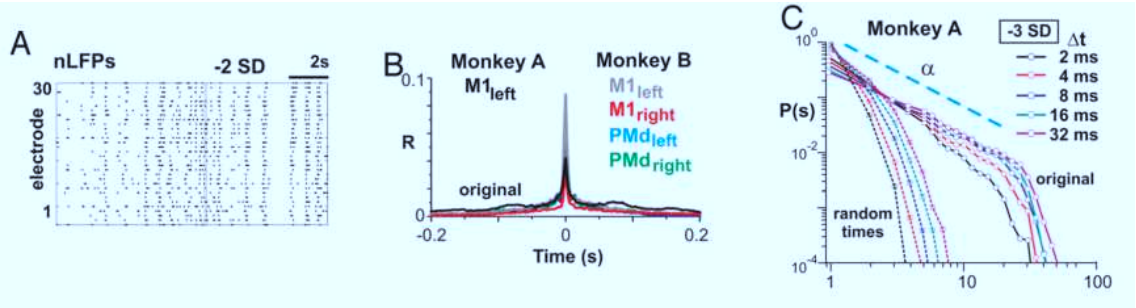

Figure 1.7: nLFP peaks cluster as neuronal avalanches that are invariant to temporal scale. A: Raster of nLFP peak occurrences (dots) extracted at -2SD (M1left; monkey A) B: Mean cross-correlation function for nLFPs between electrodes (t = 2 ms). Peak at around time 0 reveals strong correlation between simultaneous and successive nLFPs. (C) Cluster sizes distribute according to a power law (straight line in log-log coordinates) up to a cut-off determined by the total number of electrodes. Slope varies systematically with t. Broken lines, squares: Exponentially decaying size distributions from corresponding time-shuffled rasters (R=0.999). Adapted from Petermann et al. (2009).

onic rat brain with population burst dynamics and power laws in neuronal avalanche distributions (Pasquale et al., 2008). An important additional finding was the loss of power law and a shift towards subcritical distributions and desynchronized activity after application of the neuromodulator acetylcholine. Friedman et al. (2012) reported not only power laws in avalanche sizes and duration in cultured neuronal networks, but also a single scaling function for the temporal characteristics of avalanches and scaling relationships between different exponents providing further evidence of critical network dynamics in *in vitro* preparations. Reports on power laws in recordings of spiking activity *in vivo* are rare. Ribeiro et al. (2010) described power laws in population burst dynamics in various cortical areas of anesthetized rats (ketamin and xylazin). These power laws were replaced by subcritical lognormal distribution in the awake and sleep condition. Notably, despite the absence of power law, the activity was still governed by a universal scaling function in the temporal domain. This finding lead to the conclusion that a lack of power laws is not sufficient to disprove critical dynamics. Petermann et al. (2009) found heavy-tailed distributions instead of power laws in neuronal firing statistics of awake monkeys, when analysis was restricted to activity epochs with locally synchronized spiking activity.

1.5.4 Evidence against Neuronal Avalanches

Despite the growing evidence for critical brain dynamics, a number of experimental studies cast doubt on the applicability of criticality theory to neuronal network activity. First data arguing against criticality were published by Bédard et al. (2006), who

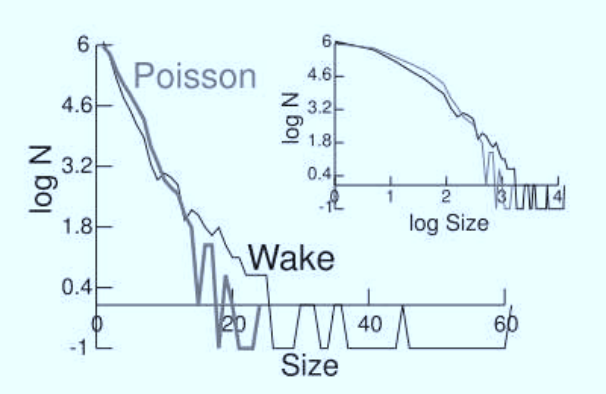

Figure 1.8: Avalanche analysis realized by taking into account the statistics from all simultaneously-recorded cells in Wake. The distribution of avalanche sizes scales exponentially (black curves), similar to the same analysis performed on a Poisson process with same statistics (gray curves). Taken from Bédard et al. (2006).

recorded spikes from parietal cortex of awake and sleeping cats and found strongly curved avalanche size and inter-spike interval distributions (Fig. 1.8). Priesemann et al. (2010) analyzed LFP data from awake monkey prefrontal cortex and reported either curved distributions or distributions with clear peaks. As mentioned above, Ribeiro et al. (2010) found curved statistics in spiking activity of awake and sleeping rats. Touboul and Destexhe (2010) found power law like distributions in the LFP of the same recordings as in Bédard et al. (2006), but discarded the power law hypothesis by using sophisticated statistical tests. An extensive neuronal avalanche study based on LFP and spiking data from humans, monkeys and cats did not find evidence for power laws, when the same tests were applied (Dehghani et al., 2012).

1.5.5 The Sub-Sampling Hypothesis

The presence of distributions different from power laws in neuronal data sparked a debate on whether the brain is truly critical. While some studies rejected the criticality hypothesis altogether (Bédard et al., 2006; Touboul and Destexhe, 2010; Dehghani al., 2012), attempts were made to reconcile the apparently negative results with critical brain activity. The main approach was first put forward by Priesemann et al. (2009) and became subsequently known as the sub-sampling hypothesis of critical dynamics. The principal idea was that neuronal activity recorded with current micro-electrode technology is fundamentally sub-sampled as each electrode picks up the signal of a few neurons only, while the majority of neuronal activity remains undetected. Consequently, avalanches and concomitant correlations are insufficiently captured to be reflected as power law distributions in the data. In models of critical dynamics, it was indeed shown that power law statistics are lost, when only a subset of the activity was used for analy-

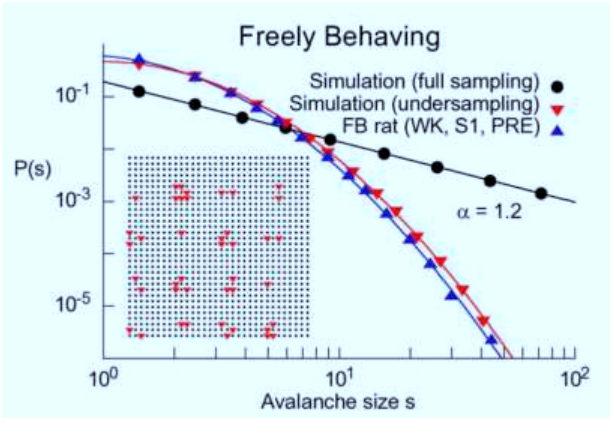

Figure 1.9: Size distributions for model (red triangles: undersampling; circles: full sampling) and data from freely behaving animals (blue triangles). Lines are lognormal and power law fits. Inset: model lattice (black dots) and sampled sub-lattice that mimics the configuration of the neurons recorded by the multi-electrode array (red triangles). Adapted from Ribeiro et al. (2010).

sis, mimicking sparse sampling by electrode arrays (Priesemann et al., 2009; Ribeiro et al., 2010) (Fig. 1.9). As the LFP samples larger populations of neurons, it was argued that sub-sampling mainly affects power law distributions in spiking activity and critical properties are more readily found in LFP recordings (Plenz and Thiagarayan, 2007). However, as pointed out by Dehghani et al. (2012), the LFP may also contain artifacts due to volume conduction and measure spurious correlations along with those produced by the underlying neuronal network dynamics.

1.6 Putative Functions of Critical Neuronal Network Dynamics

Already in 1950, Alain Turing speculated that the brain may exhibit critical behavior to avoid highly correlated subcritical activity and supercritical explosions. Bak (1996) also believed in a critical brain as its complexity may be ideal to process the abundance of complex structures and dynamics in its environment. Many neuronal network models and also experimental studies followed to demonstrate how brain functions are optimized during critical neuronal activity (see Beggs (2008) and Shew and Plenz (2012) for comprehensive reviews).

The first function found to be optimized in neuronal networks tuned to criticality was information transmission. Beggs and Plenz (2003) simulated a feedforward network and found that input to the first layer was best decoded at output layers (i.e. the mutual information between input and output was maximal), when the branching parameter between the layers was close to one, indicating criticality (Fig. 1.10A). Likewise, it was

shown that learning rules that maximize mutual information between neurons lead to dynamics with critical features (Tanaka et al., 2009). These theoretical claims were recently tested by Shew et al. (2011) in slice cultures of rat cortex. In this study, the balance of excitation and inhibition was altered by administering drugs that either decreased inhibition by blocking GABAa receptors or reduced excitation through NMDA and AMPA antagonists. The authors found that these pharmacological manipulations either lead to supercritical or subcritical dynamics. Electric pulses with different current amplitudes were applied at one site of the recording area and responses in LFPs were recorded with multi-electrode arrays. It was subsequently shown that the mutual information between a set of electric inputs and output patterns was maximized, when the neuronal network was tuned to criticality and decreased during pharmacologically induced super- and subcritical states.

Another theoretical prediction was made by Haldeman and Beggs (2005), who proposed that the capacity to store information in neuronal networks is optimized during critical activity. This means that critical networks can generate a large number of complex spatiotemporal patterns that can be used to represent and store information. In a study by Stewart and Plenz (2006) the number of patterns generated in LFP signals of acute cortical slices was the highest, when the dopamine concentration was at a level that favored criticality. Shew et al (2011) quantified the information content of LFP patterns in cortical cultures using entropy and again found peak entropy values during critical dynamics and reduced values after pharmacological intervention.

Another notable theoretical finding was that the dynamical range of input responses is maximized at criticality (Kinouchi and Copelli, 2006). Dynamical range is referred to as a network's ability to create distinct responses for both small and large inputs. In this study, the firing rate of an external drive to a neural network was consistently varied and the network's response to varying input rates was studied. The authors found that the range of input rates at which responses were still distinguishable was highest, when the network was tuned to criticality (Fig. 1.10B). In a subcritical state, small stimuli were not separable anymore, while supercritical states were not sensitive to large stimuli due to response saturation. The validity of these modeling results was tested by Shew et al. (2009), who measured the response amplitude of LFPs recorded by multi-electrode arrays in neuronal cultures during electric stimulation with varying current amplitude and various pharmacological manipulations (Fig. 1.10C). As predicted theoretically, the dynamical range of network responses was maximized during critical states and lower for pharmacologically induced super- and subcritical dynamics (Fig. 1.10D).

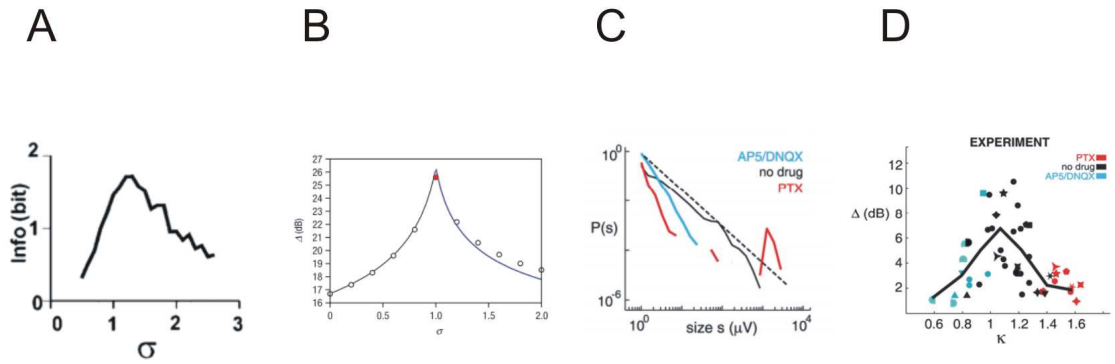

Figure 1.10: A: Transmitted information (Info) peaks near sigma=1. Adapted from Beggs and Plenz (2003). B: Dynamic range versus branching ratio is optimized at the critical point =1. Taken from Kinouchi and Copelli (2006). C: PDFs of spontaneous cluster sizes for normal (no-drug, black), disinhibited (PTX,red), and hypoexcitable(AP5/DNQX, blue) cultures. Broken line, 3/2 power law. Cluster sizes is the sum of nLFP peak amplitudes within the cluster; P(s) is the probability of observing a cluster of sizes. D: Network tuning curve for dynamic range near criticality. C and D taken from Shew et al. (2009).

1.7 Conclusion

In summary, the joint effort of theoretical and experimental studies provided evidence that criticality may be an ideal dynamical substrate for implementing a variety of functions relating to processing of external stimuli and transmission of neuronal activity. In addition, these studies clearly demonstrated the importance of an excitatory-inhibitory balance for criticality suggesting that neuronal networks are tuned to a critical point.

2 Cortical States

Ever since the work of Adrian (1928), neurophysiology was concerned with measuring the response of neurons to external input and attempted to extract information about the environment from neuronal activity. This approach successfully attributed firing rate changes of neurons to stimulus features (e.g. Hubel and Wiesel, 1959; Barlow, 1972) or argued that synchronization between different neurons is pivotal in the processing of stimuli (von der Malsburg, 1981; Singer, 1999). However, it recently became clear that the brain is highly active even in the absence of stimuli and spontaneous activity is an important variable in shaping cortical responses to external input. This spontaneous activity changes its characteristics depending on the phase of the sleep-wake cycle.

2.1 Synchronous vs. Desynchronized Cortical States

Classically, EEG signals recorded during slow wave sleep display slow and large amplitude fluctuations which are caused by strong synchronization of the underlying activity. Accordingly, this dynamics has been termed as 'synchronized' state. In contrast, the same type of signals recorded during waking and rapid-eye movement (REM) sleep are fundamentally different showing fast and low amplitude deflections. This phenomenon has been referred to as the 'desynchronized' state. Recent studies point to a more complicated scenario, in which the traditional synchronized and desynchronized states are just the extremes of a continuum with a number of states having intermediate degrees of synchronization in between them (see Harris and Thiele, 2011, for review) (Fig. 2.1). Cortical state in these studies was assessed by the amount of fluctuations shared by multiple recorded neurons as measured by for instance the mean pairwise correlation coefficient across the neuronal population. Alternatively, cortical state was defined by the slow frequency power in local field potentials (LFP). Synchronized states are characterized by up phases, in which neurons fire, followed by down phases, where neurons are silent. These phases can last up to several 100ms, in cortical slices even up to several seconds. Thus, during the synchronized state, neuronal firing is clustered in time, which is quantified as positive mean correlation coefficient (Renart et al., 2010) between neurons and the rhythmic nature of these events at a timescale of a few 100ms gives rise to an increase in low frequency power (1-5 Hz) of the LFP. Strong membrane potential fluctuations that are in phase with the LFP can also be seen in intracellular recordings during synchronized population activity (Okun et al., 2010). Moreover, synchronized states have been associated with intermittent traveling waves that can be observed in a variety of cortical areas in the LFP (Nauhaus et al., 2009) and voltage-sensitive dye (VSD) signals (Ferezou et al., 2006). In desynchronized states, fluctuations in the LFP and intracellular signals are largely reduced, which is reflected in much smaller low

frequency power. Spiking activity lacks the typical bursting character of the synchronized state and rather displays continuous and irregular firing of individual neurons without synchronization at the population level. As a consequence, mean correlation of the population spiking activity is close to zero, even though individual pairs can show significant positive or negative correlations (Renart et al., 2010). Moreover, desynchronization has been linked to an increase of LFP power in the gamma frequency range (Niell et al., 2010), especially during active stimulation of subcortical structures (Munk et al., 1996) and attention (Fries et al., 2001). However, recent studies show that the inverse may also be true and decorrelation reduces gamma power (Chalk et al., 2010; Puig et al., 2010). Aside from the discovery that cortical activity moves along a continuum between the two ends of synchronized and desynchronized states (Curto et al., 2009), evidence has been found that synchronized states are not only present during slow wave sleep and certain types of anesthesia (Clement et al., 2008; Renart et al. 2010, Ribeiro et al., 2010), but are also expressed during waking which has been traditionally associated with desynchronization. More specifically, desynchronization is seen in active, behaving rodents (Okun et al., 2010; Poulet et al., 2012), while immobility and quiescence favor synchronized cortical activity (Crochet et al., 2006; Poulet and Petersen, 2008), albeit with smaller amplitude than during slow wave sleep.

2.2 Mechanism for Cortical Synchronization and Decorrelation

A number of theoretical studies have investigated the mechanisms underlying synchronization and decorrelation in different cortical states and the transition between them. As shown by Reyes (2003), feedforward networks with divergent-convergent connections, similar to those observed in the brain (Braitenberg and Schütz, 1998), quickly synchronize neuronal activity while propagating across the network. Thus, it was concluded that synchronization is an inherent property of neuronal network dynamics due to shared presynaptic input and common drive. However, mechanisms that counteract synchrony and enforce decorrelated dynamics were discovered recently (Renart et al., 2010; Tetzlaff et al., 2012). It was shown that sufficiently strong and fast inhibitory feedback can effectively prevent the building up of synchronous excitation. As a consequence, neuronal population activity remains decorrelated and the mean pairwise correlation coefficient in these networks is close to zero. The dominance of inhibition in decorrelated cortical activity was also noted in an experimental study by Rudolph et al. (2007), in which excitation was only predominant during synchronized cortical activity. In order to prevent runaway excitation during synchronized states, the cortex employs a number of strategies (see Harris and Thiele, 2011 for review). In general, while excitatory activity builds up and spreads like a wave across the cortex, neuronal adaptation mechanisms start to act in order to confine excitation (e.g. synaptic depression, ATP

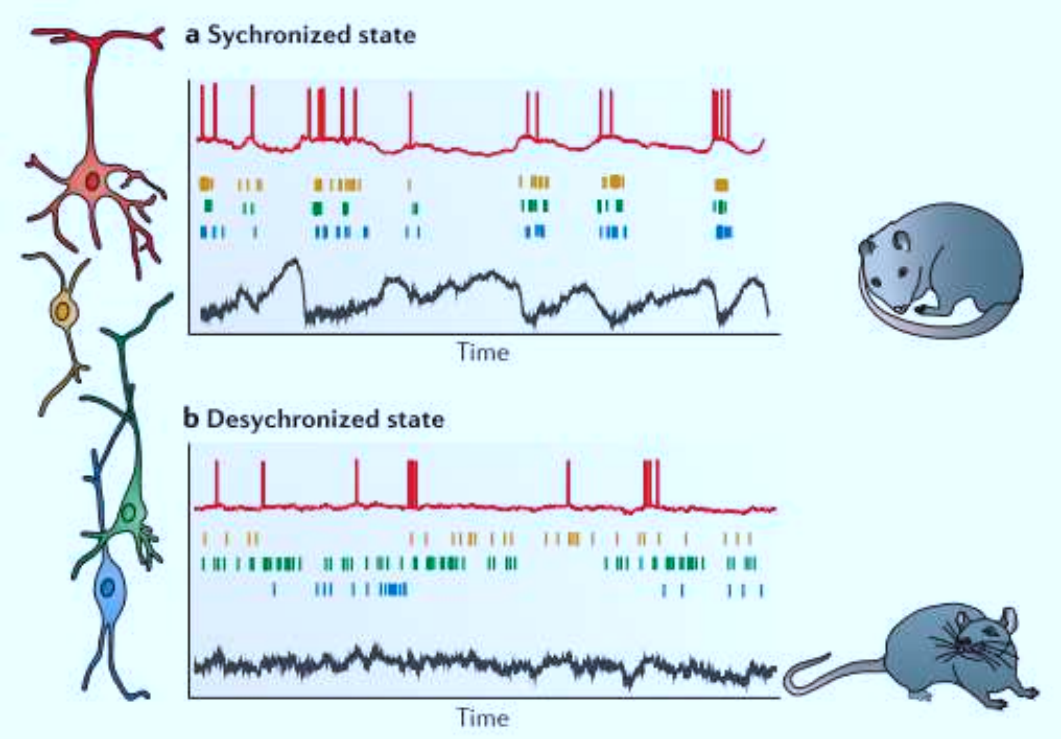

Figure 2.1: Population activity patterns vary with cortical state. Illustrations of two extremes of a continuum of states seen in awake rodents. A: In synchronized states, cortical populations show spontaneous common fluctuations in firing rate. During the up phase, all neuronal classes show a propensity to fire (shown by the colored raster plots), whereas during the down phase spiking is reduced or absent. These phases are accompanied by corresponding depolarization and hyperpolarization in intracellular potentials (shown by the red trace). The deep-layer cortical local field potential (LFP) (shown by the black trace) shows slow negative waves accompanied by high-frequency activity in the up phase and smooth dome-shaped positive waves in the down phase. This type of activity is seen in drowsy or quiescent animals. B: In the desynchronized state, coordinated slow fluctuations in population activity are not seen, and low-frequency fluctuations in the LFP and membrane potentials are suppressed. This type of activity is seen in actively behaving, alert animals. Note that this figure does not show actual recordings from the neurons whose morphology is illustrated to the left, but is a drawing integrating the results of multiple studies. Taken from Harris and Thiele (2011).

depletion, and increase in K+ conductance with hyperpolarization). As a result, neuronal activity fades away completely and is followed by a period of silence, during which the network is not excitable enough to sustain excitation. When the network recovers from adaptation, the process starts again, thereby creating a sequence of alternating up (activity) and down (silence) phases which can appear as a regular oscillation especially in reduced and anesthetized preparations. A new up-state may be spontaneously generated by miniature EPSPs as a result of spontaneous transmitter vesicle release (Bazhenov et al., 2002) or originate in layer 5 pyramidal neurons (Sanchez-Vives and McCormick, 2000; Sakata and Harris, 2009). The role of these mechanisms in creating this up-down dynamics has been also confirmed in computational studies (Bazhenov et al., 2002; Compte et al., 2003). In contrast, during desynchronized cortical states, adaptation is less strong and neurons display more continuous firing without the bursting behavior typically seen in synchronized states. In addition, tonic glutamatergic input from subcortical structures like the thalamus may also drive the cortex into a more desynchronized regime as suggested by a recent study (Poulet et al., 2012). Transitions between synchronized and desynchronized cortical dynamics are mediated by a variety of neuromodulators including acetylcholine, noradrenaline and serotonine, which affect neuronal adaptation and excitability (see Harris and Thiele, 2011).

2.3 Response Modulation by Cortical States

Neuromodulation allows the cortex to swiftly switch between different cortical states and modulate the processing of incoming stimuli, which has been shown to be highly influenced by the cortical state (Harris and Thiele, 2011). However, this modulation is a function of stimulus properties and has been studied mostly in rodents for simple and brief stimuli as well as longer lasting and more realistic natural stimuli. For point stimuli like a whisker deflection, the initial response (<50ms) is typically stronger during quiescence displaying synchronized activity than in actively behaving animals with desynchronized cortical dynamics (Fanselow and Nicolelis, 1999; Castro-Alamancos, 2004). In the later phase of the response (>50ms), there are more profound differences across states. Stimuli presented during the synchronized can evoke a long lasting spread of activity (Ferezou et al., 2006; Haider et al., 2013), while responses during the desynchronized state remain more localized and are accompanied by strong inhibition (Haider et al., 2013). The coding of natural scenes in the rat visual cortex is enhanced during cortical desynchronization following basal forebrain stimulation and resulting release of acetycholine (Goard and Dan, 2009). In addition, natural stimuli desynchronize cortical activity and evoke sparse and temporally precise spiking activity (Haider et al., 2010).

2.4 Conclusion

The cortex can assume different dynamical states ranging from synchronized to desynchronized activity and has evolved mechanisms to dynamically control these states according to the computational needs for the representation and processing of external stimuli.

3 Synfire Chains

A synfire chain is a type of neuronal network model, in which excitatory neurons are grouped in distinct pools. The neurons of each pool are connected to neurons of a subsequent pool in a feedforward fashion through divergent/convergent connections such that multiple pools form an anatomical chain of interconnected groups of neurons. From a dynamical point of view, these chains support the stable propagation of synchronous ("synfire") activity across the different pools and thus have attracted widespread attention as a substrate for reliable information transmission in the brain. A synfire chain is characterized by its width (w) which indicates the number of neurons per pool, and the multiplicity (m) denoting the average number of synapses that a neuron receives from a previous pool. A scheme of a synfire chain is shown in Figure 3.1. The synfire chain concept was introduced by Moshe Abeles (1982; 1991) and later studied extensively in numerical simulations as soon as the required computer technology was available. Some experimentalists also adopted the synfire chain hypothesis and searched for their signature in neuronal data with limited success.

3.1 The Synfire Chain Concept

The origins of the synfire chain hypothesis rooted in the necessity to explain peculiar experimental findings reported by Abeles (1982). While studying the timing relationship of three neurons through cross-correlation histograms, he found that the firing of these neurons followed characteristic sequences. First, neuron A would fire and after some delay T1 neuron B would respond with a discharge. After a further delay T2, neuron C would eventually fire, thereby creating a repeatable sequence of discharge patterns between these three neurons. Importantly, these firing delays could reach up to 450ms. To explain these results, Abeles introduced the concept of a synfire chain, which generates precise spatiotemporal firing relationships between different neurons. In a synfire chain neuronal activity cascades across different pools of neurons, which are connected in a feedforward fashion through divergent-convergent connections. He hypothesized that these pools either reside in cortical columns and layers or are spatially distributed across the cortex. Importantly, when neurons within each pool fire synchronously (synchronous mode), activity can spread reliably across the chain, while asynchronous activation through increasing the firing rate (asynchronous mode) alone does not generate reliable propagation. In the synchronous mode, neurons of different pools fire sequentially as activity spreads along the chain and thus produces precise spatiotemporal firing sequences with firing delays between neurons being dependent on the transmission delays between different pools. The proper functioning of a synfire chain is a function of w, m and also the synaptic strength of neuronal connections between pools.

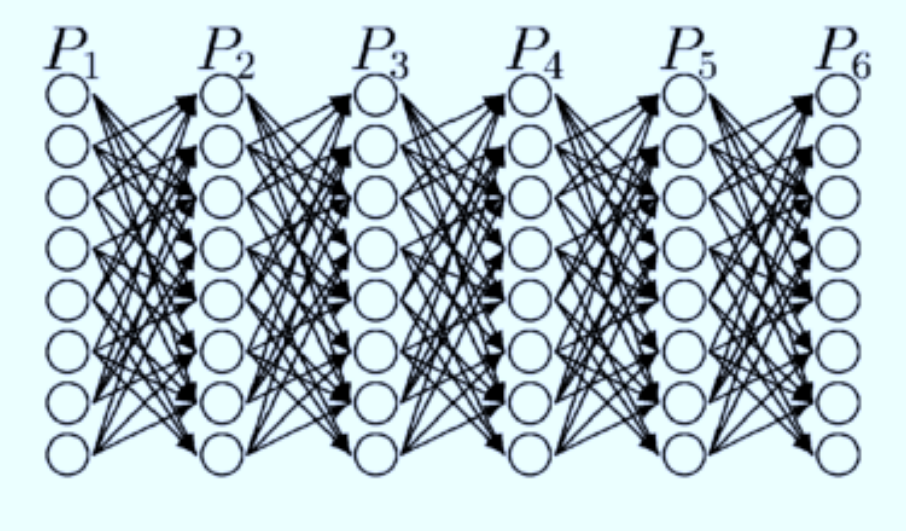

Figure 3.1: Schematic view of a synfire chain: Every neuron in pool i projects to m neurons in pool i + 1. The width of the chain is the number of neurons in a pool (eight in this example), and the multiplicity (m) of a chain is the average number of cells in pool Pi+1 to which a cell in pool Pi is connected (four in this example). Taken from Abeles et al. (2004).

In general, complete chains (Griffith, 1963) with fully connected pools require only a small number of neurons per pool to operate in the synchronous mode, if the synaptic weights are sufficiently strong. In contrast, w needs to be higher in not fully connected chains with weaker synapses to enable reliable synchronous transmission. Thus, synfire chains only occur, when the strength and density of inter-pool connections as well as the number of neurons per pool crosses a threshold above which synchronous neuronal activity is transmitted faithfully through a number of pools. Abeles put forward the idea that the sequential neuronal activation in synfire chains may be the dynamical backbone of information transmission and processing through successive steps. Quantitative analysis revealed that even random networks can implement a large number of synfire chains given that synaptic weights are sufficiently strong.

3.2 Computational Studies

After the publication of Abeles' ideas, the synfire chain hypothesis was extended, extensively studied in computer simulations and tested in experiments. First, it was realized that the time delays between neurons of different pools do not need to be equal as long as neuronal discharges arrive synchronously at a subset of neurons in the next pool. This insight led to the concepts of synfire braids (Bienenstock, 1994) and polychrony (Izhikievich, 2006). Next, a number of models tested relevant parameters for the propagation of synchrony in isolated synfire chains driven by external Poisson noise and chains

that were embedded in a background network. Aertsen et al. (1996) simulated synfire chains and studied the propagation of synchronous activity (pulse packets) as a function of the input to the first layer of a chain. To this end they stimulated their network with synchronous activity, whose properties where determined by the number of spikes (alpha) and their temporal dispersion (sigma) which indicates the degree of synchrony between the input spikes. This approach was used by subsequent studies (Diesmann et al., 1999; Gewaltig et al., 2001) to comprehensively investigate the propagation of an input pulse packet with varying alpha and sigma along the chain network (Fig. 3.2A). They found that the evolution of a pulse packet was characterized by a dynamical attractor. If alpha of the input pulse packet was sufficiently high and sigma sufficiently small, the number of spikes and their dispersion ended up in a fixed point leading to stable transmission of activity along the chain. However, when these two dynamical variables were outside the basin of attraction, the number of spikes generated in each layer and spike time precision rapidly decreased resulting in pulse packet transmission failure. These two dynamical regimes were delineated by a so called separatrix in the alpha-sigma state space which was defined by the mean propagation behavior of a pulse packet (Diesmann et al., 1999) (Fig. 3.2B). As shown by Gewaltig et al. (2001), trial to trial variability of pulse packet transmission can be very high due to synaptic background noise and blurs the separatrix. Cateau and Fukai (2001) modeled pulse packets with the Fokker Planck formalism and were able to reproduce the results of Diesmann et al. (1999). Further studies examined biologically more realistic scenarios, in which synfire chains were embedded in a background network displaying asynchronous irregular (AI) activity and replacing the previously applied stationary Poisson drive. The results were discouraging as the synchronous activity generated by the synfire chain strongly interfered with the background such that the AI activity was replaced by an oscillation synchronized across the whole network (Mehring et al., 2003). This scenario was called a synfire explosion as the pulse packet did not remain confined to the synfire chain, but also spread to the surrounding network, in contrast to predictions by Abeles (1991). Another study (Aviel et al., 2003) tried to solve this problem by introducing lateral inhibition to the network. In this case, the spread of a pulse packet not only activated excitatory neurons, but also recruited inhibition which was fed back into the background network. As a consequence, the background activity remained stable and synchrony only spread along the synfire chain. A different solution was provided by another study (Kumar, 2008) which realized that the synaptic model used in previous simulations is responsible for synfire explosions. According to this paper, biologically unrealistic current-based synapses produce very large compound EPSPs in response to synchronous input and are thus prone to destabilize the surrounding activity. However, when biologically plausible conductance-based synapses were used for the simulations, joint EPSPs generated by a pulse packet remained small and allowed for selective synfire chain dynamics without the aid of lateral inhibition. Thus, this paper was the first to show the general possibility of synfire chains in a biologically realistic setting.

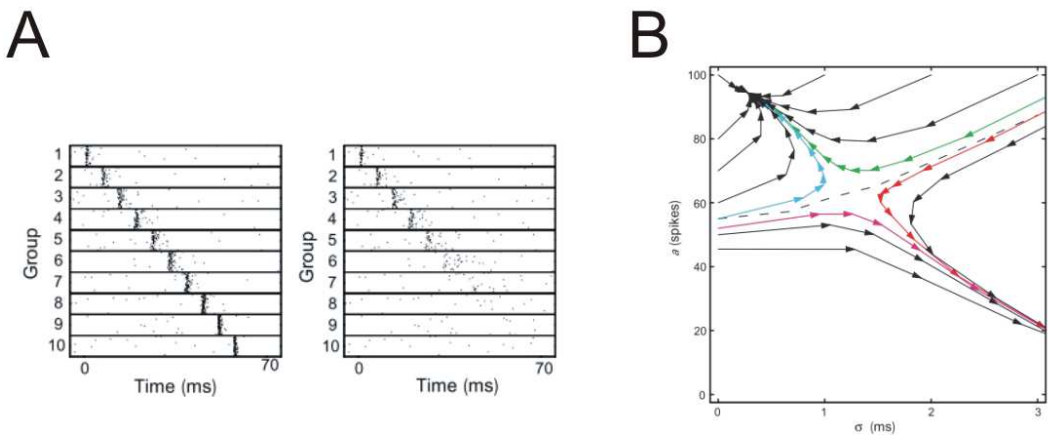

Figure 3.2: A: Raster displays of propagating spike volley along fully connected synfire chain. Panels show the spikes in 10 successive groups of 100 neurons each (synaptic delays arbitrarily set to 5ms). Initial spike volley (not shown) was fully synchronized (sigma=0ms), containing a = 50 (left) or a = 48 (right) spikes; background activity identical in both cases. B: State space portrait of dynamic variables a and sigma. The stable (upper) and unstable (lower) regimes are separated by the separatrix. Colored curves, evolution of a synchronous spike volley along a synfire chain for different input configuration. Arrows, group to group transformation. Adapted from Diesmann et al. (1999).

A number of other studies investigated the asynchronous propagation of firing rates along the synfire chain network (van Rossum et al., 2002; Litvak et al., 2003; Vogels and Abbott, 2005; Kumar et al., 2008). They showed that feedforward networks with synfire chain architecture can in principle support this mode of propagation. However, firing rates are only faithfully transmitted, when the connections between pools are sparse and strong, as denser connectivity creates more shared input, which in turn synchronizes activity and shifts propagation towards the synchronous mode (Kumar et al., 2010). Finally, it should be noted that networks other than synfire chains can produce precise spatiotemporal firing patterns (Abeles, 2009). Attractor networks (Hopfield, 1982; Amit, 1989; Wills et al., 2005) have sparked widespread theoretical attention as a mechanism for pattern generation and completion in neuronal networks. In addition, liquid state machines (Maass et al., 2002) generate spatiotemporal patterns in neuronal activity. Also, a recent study pointed out the importance of input statistics and similarity between input patterns and patterns of ongoing activity for the transmission of neuronal activity (Marre et al., 2009).

3.3 Synfire Chains and Cortical Computations

Synfire chains have been considered as a potential candidate for information transmission and precise communication between brain areas (Vogels and al., 2005; Kumar et

al., 2010), but may also be used for computational purposes (Abeles, 2009; Kumar et al., 2010). More specifically, the interaction and gating between several synfire chains can be used to construct compositional systems and solve the binding problem (Bienenstock, 1995; Frégnac and Bienenstock, 1998). Synfire chains can be routed flexibly through different brain areas depending on the presence of other chains, thereby implementing basic computational operations. In the context of the binding problem, each synfire chain may represent different features of an input which can be bound together by dynamically linking separate synfire chains into a larger chain. This chain then would represent a whole object composed of several distinct features. It has indeed been shown in modeling studies that several chains can interact and synchronize their activity such that larger and more stable synfire chains emerge (Arnoldi and Brauer, 1996; Abeles et al., 2004; Hayon et al., 2005; Kumar et al., 2008). In addition, inhibition may play a pivotal role in gating synfire chains (Kremkov et al., 2010) and implement a winner-take-all mechanism for competing chains (Chang and Jin, 2009). Taken together, these studies suggest the principal possibility of computing and binding with synfire chains. Other applications of synfire chains include pattern recognition (Arnoldi et al., 1999; Jin, 2004), language processing (Pulvermüller, 2002; Wennekers et al., 2006), the representation of internal clocks to build a time frame for external events (Kitano et al., 2003; Hass et al., 2008), bird song generation (Hahnloser et al., 2002; Jin, 2007; 2009) and the execution of complex motor plans (Schrader et al., 2011; Hanuschkin et al., 2011).

3.4 Learning Synfire Chains

Even though synfire connectivity may exist in abundance even in random networks (Abeles, 1991; 2009), the connection strength may be too small to reliably transmit synchrony across the network. This raised the question how synfire chains can be learned in a neuronal network through neuronal plasticity mechanisms. In 1981, von der Malsburg already proposed that mental objects are represented in the correlated firing of groups of neurons and are stabilized through Hebbian type plasticity. In his PhD thesis, Doursat obtained spatiotemporal activity patterns and synfire chains in an initially random network by implementing rules for (Hebbian) plasticity and competition to stabilize global network activity (Doursat, 1991). Hertz and Prügel-Bennett (1996) used a Hebbian learning rule to learn synfire chains in networks with sustained chaotic activity. However, the resulting synfire chains were typically short and had a tendency to build closed loops. A study using spike-time dependent plasticity (STDP) found similar results (Levy et al., 2001). Izhikievich (2006) simulated a random network and applied an STDP rule. The result was the emergence of gamma oscillations, in which polychronous groups (see above) were embedded. Kunkel et al. (2011) argued that previous studies on learning synfire chains were based on too simplified network

models and unrealistic assumptions. In contrast, this study showed that large random networks do not support the implementation of feedforward structures through STDP. The authors suggest that synfire chains may still emerge in non-randomly connected networks, using realistic neuron models, different input statistics and more sophisticated STDP rules. Indeed, subsequent studies demonstrated that synfire chains can be successfully embedded with biologically plausible conductance based neurons (Trengove et al., 2011) or triphasic STDP rules (Waddington et al., 2012). Finally, experimental results from cultured neuronal networks showed that temporal correlations due to well-timed transmission delays in networks with divergent-convergent connections play an important role in inducing LTP or LTD (Bi and Poo, 1999), and change the efficacy of neuronal pathways and information flow through neuronal networks.

3.5 Experimental Evidence

In parallel to theoretical studies, a number of experiments have been conducted to find evidence for synfire chains in living neuronal networks. Most studies concentrated on finding precise spatiotemporal firing sequences of neurons as predicted from the sequential activation of neurons within a synfire wave. Abeles et al. (1993) recorded from up to 10 neurons in parallel from the frontal cortex in behaving monkeys and interpreted the existence of firing patterns within the spike trains of single units and between two single units as evidence of reverberating synfire chains. A subsequent study (Prut et al., 1998) also found precise firing sequences in spike triplets in the prefrontal and premotor cortex of awake and behaving monkeys. Spikes within these triplets were on average 200ms apart. Notably, it was shown that different clusters of spike patterns were associated with different tasks, suggesting a link between precise spike timing and behavior. Two following papers (Oram et al., 1999; Baker and Lemon, 2000) reported spike patterns in the LGN and V1 as well as primary and supplementary motor cortex of monkeys. However, the authors disputed the significance of these patterns with novel statistical measures and explained their task dependence as a consequence of firing rate modulations. Yet, Shmiel et al. (2005, 2006) defined a new null hypothesis for detecting precise firing sequences and indeed found statistically significant patterns between spikes from one or two neurons. Despite the presence of firing patterns in a number of other reports from evoked and spontaneous activity (see Luszak and Maclean, 2012 for review), it was argued that precise firing statistics are not sufficient to prove the existence of synfire chains as other mechanisms may also generate spatiotemporal spike patterns (Shmiel et al., 2006; Abeles, 2009; Gerstein et al., 2012). To further establish the presence of synfire chains in neuronal data, novel methods were developed that go beyond the classical search for spike patterns (Schrader et al., 2008; Gerstein et al., 2012). These methods rely on the recent advent of massively parallel recording techniques and require activity from more than 100 neurons in parallel to detect synfire

chains. However, these new statistics did not yet reveal any evidence for synfire chains in large scale spiking data despite the presence of spatiotemporal firing patterns (Gerstein et al., 2012). Another approach to find synfire chains was pioneered by Ikegaya et al. (2004), who looked at motives in the membrane potential and calcium transients obtained through intracellular and calcium imaging *in vitro* as well as *in vivo*. Indeed, this study found repeating activity patterns, which were organized in even larger motives, and interpreted these findings as caused by spreading synfire chains. Similar to the spiking data before (see above), these results were questioned by a follow-up study which disputed the statistical significance of these patterns (Mokeichev et al., 2007). Ikeagaya et al. (2008) reanalyzed the data with new statistical test and concluded that the results remain statistically significant. Another study fitted a Poisson process generated by the activity of an unconnected neuronal network to the same data and was able to explain most of the found patterns by uncorrelated neuronal activity without the presence of synfire chains. Only a small subset of the patterns could be explained by neuronal interactions after incorporating connections in the network (Roxin et al., 2008).

3.6 Conclusion

In summary, the synfire chain hypothesis represents a simple and attractive model for neuronal processing and communication, and was studied in detail theoretically and in numerical simulations. So far unresolved problems comprise learning of synfire chains and finding the right criteria to detect their presence in neuronal data.

4 Gamma Oscillations

Ever since the discovery of the alpha rhythm in the EEG of humans (Berger, 1929), it was realized that brain activity can display a variety of different rhythms. Oscillations with different frequencies are observed at different levels of neuronal organization (Buszaki, 2006), from macroscopic recordings (EEG, MEG) down to the level of local neuronal populations (LFP) and single cell activity. Typically, neuronal oscillations do not resemble classical harmonic oscillators as extensively studied in physics, but are rather defined as periodic changes in neuronal excitability with time-varying amplitude and frequency (Traub and Whittington, 2010; Nikolic et al., 2013) as a function of cortical state (Harris and Thiele, 2011) and stimulus properties (Feng et al., 2010).

4.1 Types of Thalamocortical Oscillations

Oscillations in different frequency bands have been associated with different behavioral states (Bazhenov and Timofeev, 2006) and found to be altered during mental diseases like schizophrenia (Uhlhass and Singer, 2010), autism (Uhlhaas and Singer, 2006; 2012) and anxiety disorders (Sohal, 2012). Slow oscillations (0.3-1 Hz, Steriade et al., 1993) and delta oscillations (1-4 Hz, Ball et al., 1977; McCormick and Pape, 1990) occur during anesthesia and are typically observed during slow-wave sleep, where they may help to consolidate plastic changes of neuronal connections acquired during wakefulness (Steriade and Timofeev, 2003). Recent studies revealed that delta activity can also occur in awake animals during drowsiness and immobility (Harris and Thiele, 2011). Theta rhythms in the hippocampus are linked to memory functions (Hasselmo, 2005) and locomotion in rodents (Vanderwolf, 1969), while the role of cortical theta is less well understood. Oscillations in the alpha band (8-12Hz) are mainly found during relaxed wakefulness and closed eyes in the occipital cortex of humans (or as mu rhythm in the motor cortex) and have been either regarded as idling cortical activity or as playing an important role in neuronal communication (Palva and Palva, 2007). Fast oscillations in the beta range (15-30 Hz) have been implicated in cognitive processes that require working memory and occur in motor cortex during the preparation of movements (Engel and Fries, 2010). Much attention has been paid to gamma oscillations (30-70 Hz), as synchronization in this frequency band between neurons across different brain areas has been hypothesized to serve the formation of large-scale cell assemblies and thus a variety of cognitive functions (Singer, 1999; Varela et al., 2001).

Precise timing relationships and synchronization between neurons were first proposed by von der Malsburg (1981) to serve as a neuronal mechanism for the representation of mental objects. More specifically, the main hypothesis was that this synchronization

may be the physiological solution to functionally bind different components of a perceptual scene into an integrated whole (also known as the binding problem) and thus allow the perception of Gestalt. It was subsequently suggested that synchronization and binding may be implemented by phase locking of oscillations (von der Malsburg and Schneider, 1986; Stryker, 1989). This framework received increased attention with the discovery of synchronized gamma oscillations in the cat visual cortex (see below) and was later summarized in the binding by synchrony hypothesis (BBS; Singer, 1999; Engel and Singer, 2001). Later, synchronization of gamma oscillations has been described in more general and mechanistic terms as a means of neuronal communication between different brain areas, a concept, which has become known as the communication through coherence hypothesis (CTC; Fries, 2005; 2009). This hypothesis states that synchronization is an efficient way to communicate neuronal information to downstream neurons and communication is optimized, when separate neuronal groups transmit synchrony through coherent oscillations (Fig. 4.1). Experimental and theoretical evidence indeed suggest that transmission of information between two groups of neurons is highest when they oscillate coherently such that the output of one group arrives at the other group during the susceptible phase of the oscillation cycle (Womelsdorf et al., 2007; Buehlmann et al., 2010; Deco et al., 2011). Thus, information can be flexibly routed across the cortex by synchronizing locally oscillating populations of neurons in different brain areas.

4.2 Phenomenology of Gamma Oscillations

First evidence for the existence of gamma oscillations and their role in synchronizing the activity of local neuronal population came from two studies published almost simultaneously (Eckhorn et al., 1988; Gray and Singer, 1989). These studies in the visual cortex of anesthetized cats not only reported that neurons increase their firing rate during stimulation with a moving bar, but also start to oscillate and synchronize at frequencies in the gamma frequency range. This oscillation was seen both in the spiking activity and in the local field potentials. Importantly, these oscillations were not phase locked to the stimulus and occurred with latencies between 10 and several 100ms ('induced oscillations'). Synchronized oscillatory responses were later also found during the awake state in cats (Gray and Viana di Prisco, 1997) and monkeys (Kreiter and Singer, 1996; Frien et al., 2000), showing that the initial results are not restricted to anesthetized animals. An important ingredient of the BBS or CTC hypotheses is the presence of not only local synchronization of neuronal activity but also longer-range phase-locking of induced oscillations. Indeed, Gray et al. (1989) demonstrated synchronization between neurons recorded from different cortical columns in the visual cortex of anesthetized cats, when a long and continuous bar was presented. However, when the bar's center piece was left out (i.e. two smaller and separate bars were shown

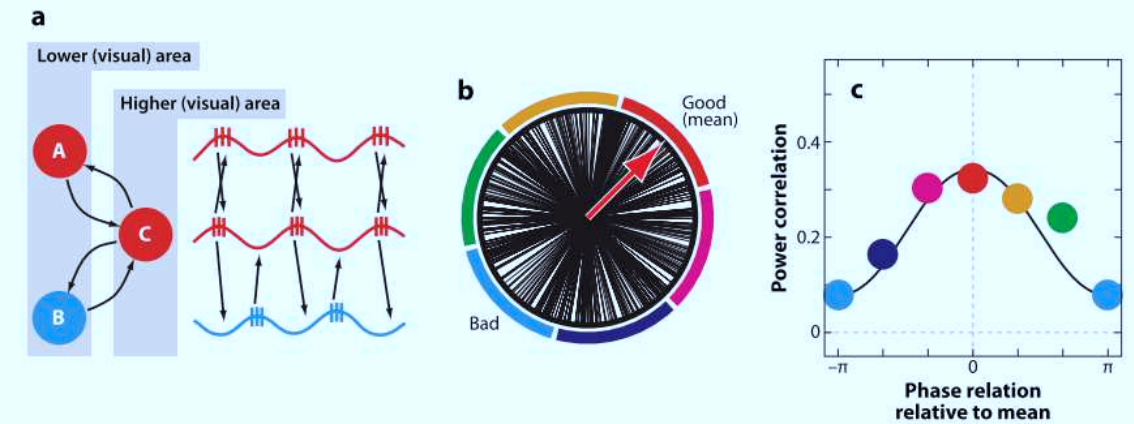

Figure 4.1: The communication-through-coherence concept and direct physiological evidence for it. a: Three neuronal groups (A, B, and C). The neurons inside group A are rhythmically synchronized as indicated by the undulating lines with spikes around the peaks. The same holds for the neurons inside groups B and C. However, C is in-phase synchronized exclusively to A and not to B. b: Each vector corresponds to the relative gamma-band phase in a 250-ms-long epoch between gamma-band rhythms in two separate neuronal groups recorded in awake cat visual cortex (Womelsdorf et al. 2007). The thick red arrow indicates the mean relative phase across all epochs. The outer ring segments illustrate the sorting of epochs according to their relative phases. c: After epochs have been sorted into six bins, each bin contains many epochs of a defined relative phase among gamma rhythms. For each relative gamma-phase bin, the interaction strength between neuronal groups was then estimated by calculating the correlation of gamma-band power between groups and across epochs in the respective bin. Taken from Fries (2009).

to the animal) synchronization between the two different recording sites was considerably reduced. Synchronization was also found between the same areas in two different hemispheres (Engel et al., 1991), and was abolished, when corticocortical connections were cut in the corpus callosum. A similar synchronization was seen between widely distributed brain areas (Engel et al., 1991; Roelfsema et al., 1997; Brecht et al., 1998). Another study (Yu et al., 2008) reconstructed functional networks based on neuronal synchronization in the gamma range and found small world properties in the uncovered networks indicating cortical optimization for local (feature detection) and global computation (binding). Moreover, gamma oscillations were also seen in the retina and the LGN (Neuenschwander and Singer, 1996; Neuenschwander et al., 1999), and can be synchronized with the primary visual cortex (Castelo-Branco et al., 1998). Even though oscillatory synchronization has been initially thought to have on average zero-phase lag (Gray et al., 1989; Roelfsema et al., 1997), later studies reported variable phase delays (Schneider et al., 2006) and stimulus dependent sequences of neuronal firing within oscillation cycles (Havenith et al., 2011). A similar long-range synchronization and coherence in the gamma range has been observed in studies using EEG (Rodriguez et al., 1999) and ECoG (Tallon-Baudry et al., 2003), However, despite the evidence for the role of synchrony in binding of perceptual components, contradictory results have also been reported (Lamme and Spekreijse, 1998; Stoner and Thiele, 2003; Roelfsema et al., 2004; Lima et al., 2010) doubting the role of synchronization in Gestalt grouping within visual scenes.

4.3 Cellular Mechanisms of Gamma Oscillations

In parallel to studying the phenomenology and functions of gamma oscillations, mechanisms of oscillatory activity and its synchronization across widespread brain areas were also investigated theoretically and experimentally. In general, two different scenarios were considered to be responsible for the generation of gamma oscillations. First, it was believed that pacemaker cells, which intrinsically generate gamma frequency discharges, can entrain other cells to fire at the same frequency. The discovery of so called chattering cells (fast rhythmic bursting cells) *in vitro* (Llinas et al., 1991) and *in vivo* (Gray and McCormick, 1996), which exhibit rhythmic gamma bursts in response to tonic depolarization, supported this hypothesis. The alternative view postulated that gamma rhythms arise from network mechanism as a consequence of synaptic interaction between neurons. Intracellular studies *in vivo* (Frégnac et al., 1994; Bringuier et al., 1997) provided evidence for a synaptic origin of cortical gamma oscillations and questioned the importance of chattering cells for the generation of gamma oscillations (Cardin et al., 2005). The detailed cellular mechanisms of gamma oscillations have been mostly studied in hippocampal and neocortical slices by either tetanic electrical stimulation (Traub et al., 1996; Whittington et al., 1997) or application of chemicals

like carbachol or kainate (Buhl et al., 1998; Fisahn et al., 1998). While electrical currents induce transient epochs of gamma oscillations (lasting hundreds of milliseconds) similar to the *in vivo* condition, drug application leads to persistent gamma activity with a duration of up to several hours (Traub and Whittington, 2010). These studies pointed to a pivotal role of inhibitory neurons for the generation of gamma oscillations (Whittington et al., 2000). In particular, locally connected inhibitory basket cells were thought to be responsible for oscillatory activity in the gamma range (see Bartos et al., 2007; Buzsaki and Wang, 2012 for review), a hypothesis that was confirmed by recent optogenetic studies *in vivo* (Cardin et al., 2009; Sohal et al., 2009). Furthermore, it was shown that even interneuron network in isolation without the presence of excitatory neurons can sustain gamma oscillations (Traub, 1995; Wang and Buzsaki, 1996). Theoretical studies further identified the necessary cellular mechanisms for oscillations in the gamma range (see Wang, 2010 for review) and described a number of different scenarios. As shown by *in vitro* experiments, simulations of reciprocally coupled inhibitory neurons driven by sufficiently strong external input display synchronized oscillations whose frequency is determined by the time constant of GABAa currents (Brunel and Hakim, 1999; Brunel, 2000). This mechanism has been denoted as ING (inhibitory neuron gamma), as it is independent of excitatory neurons. The other mechanism is based on the interaction between excitatory neurons and inhibitory neurons in a local network and has been called PING (pyramidal interneuron gamma). In this scenario, inhibitory neurons are driven by excitatory neurons and in turn temporarily shut down the excitatory neuronal population. After the decay of inhibition, pyramidal cells become excitable again and the whole cycle restarts. As a consequence, the local network undergoes rhythmic changes of excitability with neuronal firing occurring only during the phase with reduced inhibition (Wilson and Cowan, 1972; Freeman, 1975; Brunel and Wang, 2003). Very recently, another mechanism that can promote gamma oscillations was described (Moca et al., 2012). It emphasizes the role of resonance properties of inhibitory neurons to create stable oscillations in the gamma range and was called resonance induced gamma (RING). Moreover, it became clear that cortical gamma oscillations are different from classical (Huygens) oscillations, where oscillators fire at each cycle of the oscillations. While interneurons fire quite regularly at each cycle, pyramidal neurons usually skip cycles and fire only irregularly and stochastically without showing signs of an oscillation, when measured individually. Thus, oscillations in the cortex are visible only at the population level (e.g. when multi-unit or LFP activity is analyzed) and this phenomenon has been summarized in the framework of sparsely synchronized oscillations (Brunel and Hakim, 2008; Wang, 2010). Finally, gamma oscillation seem to be primarily associated with superficial layers 2/3 (Buhl et al., 1998; Roopun et al., 2006) in the cortex, while slower rhythms in the alpha/beta range dominate in deeper layers (Roopun et al., 2006; Buffalo et al., 2011).

4.4 Long-Range Synchronization in the Gamma Band

Another field of research concerned the mechanisms by which locally oscillating groups of neurons can synchronize their activity across large distances. A prominent candidate is the spike-doublet mechanism (Kopell et al., 2000), through which long-range axon collaterals of pyramidal cells reset the inhibitory neurons of distant neuronal networks. This leads to a characteristic doublet firing of inhibitory neurons, as observed experimentally in hippocampal slices (Traub et al., 1996). However, synchronization in the gamma range is restricted to short conduction delays and synchronization across more distant areas can only be achieved by reducing the oscillation frequency to the beta range. Moreover, long-range interneurons were proposed to synchronize spatially separated oscillators (Buzsaki et al., 2004). A third candidate mechanism involves synchronization of two cortical areas through reciprocal thalamocortical connections (Llinas and Pare, 1998), a hypothesis that was later supported by a theoretical study (Vicente et al., 2008).

4.5 Gamma Oscillations and Cortical State

Another line of research examined the link between the occurrence of gamma oscillations and the level of cortical activation. It was shown that gamma oscillation responses to visual stimuli were preferentially seen during the activated cortical state with little power in low frequency ranges of EEG recordings. This effect was mediated by artificial stimulation of cholinergic brainstem structures through muscarinic receptors (Munk et al., 1996; Herculano-Houzel, 1999; Rodriguez et al., 2010). These results lead to the hypothesis that attention may enhance gamma band synchronization during the awake state, an idea that was supported by experiments on awake monkeys (Fries et al., 2001; Jensen et al., 2007; Lima et al., 2011). The role of gamma band synchronization was pushed even further and hypothesized to be the neuronal correlate of conscious perception. Studies using binocular rivalry (Fries et al., 1997) and masked stimuli (Melloni et al., 2007) found evidence for this idea.

4.6 Gamma beyond the Visual System

Finally, gamma oscillations have not only been reported in the visual system, but were also discovered in the auditory cortex in response to auditory stimuli (Palva et al., 2002), the somatosensory system after median nerve stimulation (Chen and Herrmann, 2001), the olfactory system (Freemann, 1975; Laurent, 2002) and the hippocampus (Buzsaki, 2006). They also occur in the motor cortex during movement execution (see

van Wijk et al., 2012 for review). In addition, gamma oscillations were observed in a number of non-cortical structures like the amygdala (Halgren et al., 1977), the striatum (Berke et al., 2004), the thalamus (Pinault and Deschénes, 1992) and the cerebellum (Middleton et al., 2008).

4.7 Conclusion

Gamma oscillations are a ubiquitous phenomenon in brain activity and are associated with a variety of cognitive processes. Their intrinsic ability to synchronize activity has been proposed to serve as a tag for relations between different aspects of sensory inputs and bind these aspects into an integrated whole. Moreover, local and long-range synchronization in the gamma band may be suitable for effective communication between spatially separated brain areas. However, the detailed mechanisms of the generation of gamma oscillations and their long-range synchronization remain elusive.

5 Electrophysiological Measurement Techniques

Neurons generate electromagnetic signals and use them to process and transmit information to other neurons. Electrophysiology studies the origin of these signals and attempts to understand their role in the overall functioning of individual neurons, neuronal networks and the entire brain. To this end, electrophysiologists have devised a variety of tools to measure electromagnetic signals of single neurons and neuronal populations which allow investigating neurons at work during controlled external stimulation, behavior or spontaneous activity. In general, electric signals are picked up by electrodes placed in the vicinity of neurons (extracellular recording) or inserted into individual cells (intracellular recording). These methods allow the recording of spiking activity of individual neurons and in the case of intracellular recordings also membrane potential fluctuations. Extracellular recording methods are also sensitive to the activity of neuronal populations, which is reflected by the synchronous input to a group of neurons near the electrode and referred to as local field potential (LFP). Non-invasive extracellular techniques like EEG or ECoG solely record this type of signal or its magnetic counterpart (MEG).

5.1 Spiking Activity

5.1.1 Recording of Spike Signals

Neurons integrate synaptic activity coming from the dendrites and generate an all-or none signal, the action potential or spike which propagates along the axon and triggers neurotransmitter release at synaptic contacts with other neurons. The key mechanism for spike generation is the successive opening and closing of sodium and potassium channels, which produces transmembrane currents and characteristic changes of the membrane potential with a depolarization, repolarization and hyperpolarization phase. These voltage changes affect the extracellular medium in the vicinity of a cell and also create currents in electrodes placed near the neuron (Buszaki, 2004). These currents are then amplified and further processed by specialized recording devices. Electrode types comprise single microwires, stereotrodes, tetrodes, and multi-electrode arrays with a variety of different shapes and number of electrodes (up to several 100). Prominent examples include the silicon probes (Neuronexus Technologies, Ann Arbor, USA) and the Utah array (Blackrock Microsystems, Salt Lake City, UT, USA) (Fig. 5.1). As spikes are very fast processes with a duration in the millisecond range, the recorded signal is high-pass filtered between 500 and 5 kHz to extract spiking activity. However, the filtered signal not only contains spikes from closeby neurons, but also a considerable amount of (thermal) noise. Thus, as a next step a threshold is applied to separate

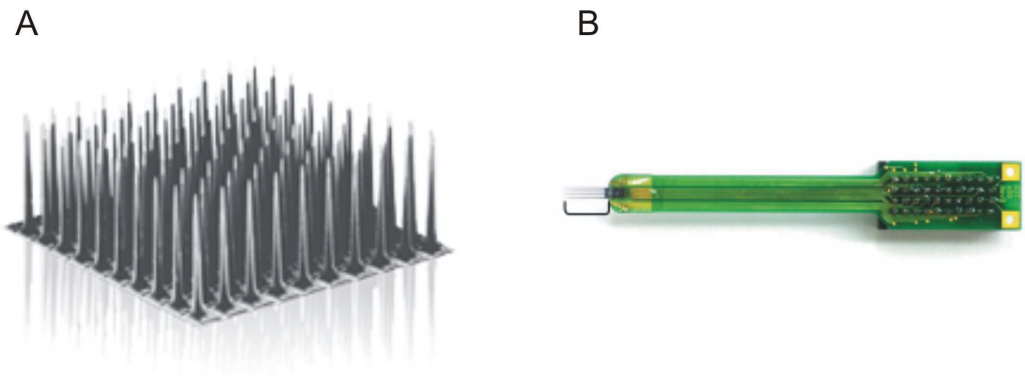

Figure 5.1: Multi-electrode arrays. A: Utah array with 96 electrodes. B: Example of a silicon probe (Michigan array) with four shanks and 32 electrode contacts.

spikes with large amplitude from lower amplitude noise fluctuations. As a result, a large number of waveforms are obtained which usually stem form a number of different neurons. This mixture of activity from different neuronal sources is dubbed multi-unit activity (MUA).

5.1.2 Spike Sorting

Even though MUA contains useful information about the local neuronal population, further processing steps are necessary to assign each waveform to its putative neuron of origin (single-unit activity, SUA) (Lewicki, 1998; Quiroga, 2007). This assignment is based on the principle that different neurons have different waveforms, as each recorded neuron has a specific position with respect to the electrode and hence the shape of the signal is also neuron specific. This is especially true for neurons close to the electrode, while waveforms of different cells become more similar with larger distance from the electrode. In addition, as long as the electrode position does not change, the waveform for each neuron remains the same. Based on these principles, a number of approaches have been developed to extract features from waveforms according to which neurons can be successfully distinguished. A first approach regarded simple properties like waveform amplitude or width as sufficient separation criteria. However, more advanced strategies based on principal component analysis or wavelet transformation reduce waveforms to its first two or three principal components or characterize them by wavelet coefficients. After feature extraction, waveforms with similar properties are grouped and each group ideally contains only the spikes of one neuron. A variety of clustering algorithm has been used to accomplish this grouping. However, so far no algorithm achieves an ideal separation of waveforms and is subject to spike sorting errors due to overlapping clusters. As a final step, a timestamp (usually with 0.1 - 1ms resolution) is assigned to each waveform and the spiking activity of each cluster is represented by a spike train.

These spike trains are then analyzed with various methods based on the theory of point processes.

5.2 Local Field Potentials

The local field potential is a slow signal and is obtained by low-pass filtering of the recorded signal between 1 and several 100 Hz. The local field potential mainly reflects the synaptic activity of the local population and samples the summed input to the neuronal network. The sources of the LFP largely stem from transmembrane currents caused by neurotransmitters at synaptic sites, which give rise to excitatory (EPSP) and inhibitory postsynaptic potentials (IPSP). However, other types of neuronal activity like action potentials, calcium spikes, intrinsic currents and a variety of other sources contribute to the generation of the LFP (see Buszaki et al., 2012 for review). Sophisticated numerical tools exist to model the LFP based on these mechanisms and the shape of neurons which also plays an important role in the generation of the LFP (LFPy, http://compneuro.umb.no/LFPy). Since postsynaptic potentials are relatively small, a large number of the same potentials need to be integrated to have an effect on the LFP. Thus it is thought that local field potentials are associated with synchronous synaptic activation of the underlying neuronal population (Buszaki, 2006). However, the size of the local population recorded in the LFP is still under debate, since the local currents generate electric fields that can spread across the extracellular medium by way of volume conduction and contaminate the LFP measured by distant electrodes (Buszaki et al., 2012). Thus, the spatial extend of the LFP found in experiments ranges between several 100 micrometer (Katzner et al., 2009; Xing et al., 2009) and several millimeter (Kajigawa and Schroeder, 2011).

Part II

Studies

6 Thesis Overview

The ability of the brain to process information from the environment and perform a variety of cognitive functions requires communication and coordination between different specialized brain areas. Signals processed in one brain areas must be reliably sent to other areas for further processing. This insight lead to a number of hypotheses how brain communication and neuronal signal propagation is implemented in neuronal networks (Vogels et al., 2005; Kumar et al., 2010). As reviewed in the introduction, there are three main approaches to the problem of neuronal communication. The neuronal avalanche hypothesis (Beggs and Plenz, 2003; Plenz and Thiagarayan, 2007) posits that neuronal networks can assume a dynamical state, in which neuronal populations can generate complex spatiotemporal activity patterns that can easily travel across the entire network. This critical state thus implements long-distance communication in contrast to a subcritical state, where activity spreads only locally, and supercritical dynamics, in which activity unselectively fills out the entire network. Even though the theory of neuronal avalanches is an attractive model to understand the general conditions under which neuronal communication is optimized, it does not explain how the brain selectively routes activity along specific neuronal pathways. This issue is addressed in two other concepts of neuronal communication, the synfire chain (Abeles, 1982; 1991) and communication through coherence (CTC; Fries, 2005; 2009) hypotheses. In both frameworks, precise and selective synchronization plays a key role in the transmission of neuronal activity, as synchronous spike input is known to effectively drive postsynaptic targets (Salinas and Sejnowski, 2000). In the synfire chain framework, synchronous activity propagates along a chain of individual local networks (layers), which are linked by precisely timed divergent-convergent connections with sufficiently strong synaptic weights. These connections enable synchrony generated in one layer to be faithfully transmitted to subsequent layers. The main ingredient for the CTC hypothesis is oscillations in the beta-gamma range, which are generated locally by the interaction between excitatory and specialized inhibitory neurons and have the ability to synchronize neuronal activity. The main idea is that distant populations of neurons exchange information by synchronizing their oscillations and establishing a consistent phase relationship between them. Notably, synchrony in the synfire chain and CTC framework has been viewed as originating from two different sources. According to this view, synchronization in synfire chains is driven by common input as a consequence of shared connections from previous layers (Kumar et al., 2010), while synchronization created by oscillations is a consequence of the interplay between excitatory and inhibitory neurons (Wang, 2010).

In this thesis, we use a combined experimental and theoretical approach to study all three models of neuronal communication. In a first study, we will address the question, whether cortical activity in the primary visual cortex of anesthetized cats displays

the characteristics of neuronal avalanches and criticality. To this end we will test the presence of power laws and long-range correlations in spontaneous spiking activity and local field potentials recorded by 16 channel silicon probes, as predicted by criticality theory (Bak et al., 1987). In a second study, we will extend our findings from the first study and examine the existence of different cortical states in recordings of spontaneous spiking activity and local field potentials from the primary visual cortex of anesthetized cats (32 channel silicon probes) and awake monkeys (Utah array). We then search for signs of neuronal avalanches in the separated cortical states and quantify how close each state comes to criticality. In a third study, we will ask the question how the seemingly different concepts of synchrony in synfire chains and the communication through coherence hypothesis can be brought together in a common framework. We will question the assumption that synfire chain and gamma oscillation synchrony are fundamentally different and develop new ideas that view both synchronization types as the manifestation of only mode of synchrony. We will argue that synfire and gamma activity are two complementary means of neuronal communication and their expression is dependent on the synaptic strength of the underlying network. The role of synaptic plasticity in shaping communication will also be discussed. Finally, we will implement and test the novel theoretical framework in a neuronal network model using the NEST simulation software.

7 Neuronal Avalanches in Spiking Activity and Local Field Potentials In Vivo

7.1 Introduction

It is a widespread belief that the brain produces complex spatiotemporal activity to represent and process the complexity inherent to stimuli from its environment. Currently, the mechanisms that allow neuronal networks to generate complexity are unknown, but recent discoveries in physics suggest that self-organized criticality might be a potential candidate operating in the brain (Bak et al., 1987; Bak, 1996). This hypothesis was backed up by recent findings in neurobiological experiments that reported power laws and long-range correlation, the signature of critical dynamics, in preparations ranging from acute cortical slices and cultures (Beggs and Plenz, 2003; Pasquale et al., 2008) to anesthetized rats (Gireesh and Plenz, 2008) and awake monkeys (Petermann et al., 2009). However, opposite results were also reported with absence of power laws in sleeping and awake cats (Bédard et al., 2006) arguing that the brain does not always show critical features. Determining the presence of criticality in brain activity is of important functional relevance, as theoretical studies indicate that critical neuronal networks can optimize a variety of functions comprising information processing (Bertschinger and Natschläger, 2004), memory storage (Haldemann and Beggs, 2005), maximum dynamical range of stimulus responses (Kinouchi and Copelli, 2006) and transmission of information (Beggs and Plenz, 2003). In this study, we explore the criticality hypothesis in recordings of spontaneous spiking activity and local field potentials (LFP) from anesthetized cat primary visual cortex. We study cluster size and lifetime distributions based on the original analysis by Beggs and Plenz (2003), inter-spike intervals and the correlation structure of spiking activity with respect to power laws and long-range correlations.

J Neurophysiol 104: 3312–3322, 2010.
First published July 14, 2010; doi:10.1152/jn.00953.2009.

Neuronal Avalanches in Spontaneous Activity In Vivo

Gerald Hahn,[1,2] Thomas Petermann,[3] Martha N. Havenith,[1] Shan Yu,[1,3] Wolf Singer,[1,4] Dietmar Plenz,[3] and Danko Nikolić[1,4]

[1]*Department of Neurophysiology, Max-Planck Institute for Brain Research, Frankfurt, Germany;* [2]*Unité de Neuroscience, Information et Complexité, Centre National de la Recherche Scientifique, Gif-sur-Yvette, France;* [3]*Section on Critical Brain Dynamics, Porter Neuroscience Research Center, National Institute of Mental Health, Bethesda, Maryland; and* [4]*Frankfurt Institute for Advanced Studies, Frankfurt, Germany*

Submitted 28 October 2009; accepted in final form 9 July 2010

Hahn G, Petermann T, Havenith MN, Yu S, Singer W, Plenz D, Nikolić D. Neuronal avalanches in spontaneous activity in vivo. *J Neurophysiol* 104: 3312–3322, 2010. First published July 14, 2010; doi:10.1152/jn.00953.2009. Many complex systems give rise to events that are clustered in space and time, thereby establishing a correlation structure that is governed by power law statistics. In the cortex, such clusters of activity, called "neuronal avalanches," were recently found in local field potentials (LFPs) of spontaneous activity in acute cortex slices, slice cultures, the developing cortex of the anesthetized rat, and premotor and motor cortex of awake monkeys. At present, it is unclear whether neuronal avalanches also exist in the spontaneous LFPs and spike activity in vivo in sensory areas of the mature brain. To address this question, we recorded spontaneous LFPs and extracellular spiking activity with multiple 4×4 microelectrode arrays (Michigan Probes) in area 17 of adult cats under anesthesia. A cluster of events was defined as a consecutive sequence of time bins Δt (1–32 ms), each containing at least one LFP event or spike anywhere on the array. LFP cluster sizes consistently distributed according to a power law with a slope largely above –1.5. In two thirds of the corresponding experiments, spike clusters also displayed a power law that displayed a slightly steeper slope of -1.8 and was destroyed by subsampling operations. The power law in spike clusters was accompanied with stronger temporal correlations between spiking activities of neurons that spanned longer time periods compared with spike clusters lacking power law statistics. The results suggest that spontaneous activity of the visual cortex under anesthesia has the properties of neuronal avalanches.

INTRODUCTION

Neurons in primary sensory cortices display firing even in the absence of sensory stimulation. Previously, this spontaneous activity was considered to be noise, discharges of single neurons being stochastic and uncorrelated (Shadlen and Newsome 1998). Recently, this view was challenged by several studies using voltage-sensitive dye imaging (Arieli et al. 1995) and intracellular recordings (Bringuier et al. 1999), suggesting that spontaneous neuronal activity is coherent and correlated within a large cortical area. Activity in different brain areas is linked through a cascade of synaptic inputs that propagates in a wave-like fashion from one cortical site to another (see Wu et al. 2008 for a review). Such activity propagation was shown in both anesthetized and awake animals (Ferezou et al. 2007; Petersen et al. 2003; Xu et al. 2007) Notably, these waves exhibit different sizes (Petersen et al. 2003) and organize in diverse spatiotemporal patterns (Tsodyks et al. 1999), which resemble underlying functional maps (Kenet et al. 2003). It was also shown that these spontaneous waves influence the response to sensory inputs (Ferezou et al. 2007; Petersen et al. 2003) and can account for the variability of evoked activity (Arieli et al. 1996), indicating a pivotal role of spontaneous activity in processing sensory information.

Recently, another type of correlated spontaneous neuronal activity was described in cortical tissue. Beggs and Plenz (2003) found that negative deflections in local field potential signals (nLFP) can propagate in neuronal cultures and acute cortical slices in a nonwave (i.e., noncontiguous) fashion. These cascades of nLFPs, dubbed neuronal avalanches, form spatiotemporal clusters of synchronized activity interrupted by periods of silence and, as shown later in vivo (Gireesh and Plenz 2008), can coexist with theta and beta/gamma oscillations. Furthermore, nLFPs can propagate across many millimeters of the cortex and display long-range temporal correlations, thereby establishing complex spatiotemporal patterns (Beggs and Plenz 2004). Neuronal avalanches emerge during the earliest time of the development of superficial layers in cortex (Gireesh and Plenz 2008; Stewart and Plenz 2008), and their emergence requires a balance of excitatory and inhibitory transmission as well as the presence of the neuromodulator dopamine (Beggs and Plenz 2003; Gireesh and Plenz 2008; Stewart and Plenz 2006). Most importantly, the sizes of neuronal avalanches distribute typically according to a power law with slope -1.5 and show long-range temporal correlations (Beggs and Plenz 2003; Plenz and Thiagarajan 2007). The recent discovery of a power law and long-range temporal correlations in the motor cortex of awake and resting monkeys indicates that neuronal avalanches are not restricted to in vitro and anesthetized in vivo preparations (Petermann et al. 2009). These findings bring the occurrence of avalanches in neural tissue close to the theory of self-organized criticality (SOC), which links power law statistics of events sizes with cascading systems (Bak et al. 1988). Recently, in vitro experiments showed that neuronal networks poised at the critical state display a maximal dynamic range of responses, which disappears when the balance of excitation and inhibition is altered (Shew et al. 2009). This provided first experimental evidence for a possible functional role of critical dynamics such as found in SOC in living neuronal networks.

The LFP signals used in the previous avalanche studies lump together activity of many neurons (mainly synaptic) within a large field of integration. Therefore attempts have been made to extend the investigation of neuronal avalanches to spiking events, and previous studies indeed reported a power law

Address for reprint requests and other correspondence: D. Nikolić, Dept. of Neurophysiology, Max Planck Inst. for Brain Research, Deutschordenstr. 46, 60528 Frankfurt/Main, Germany (E-mail: danko.nikolic@gmail.com).

organization similar to that obtained from the earlier LFP studies in vitro (Mazzoni et al. 2007; Pasquale et al. 2008). However, another recent attempt to detect avalanches in the spiking activity in cat parietal cortex in vivo during either awake state or slow wave sleep failed when using small electrode arrays (8 electrodes, aligned linearly) and a large interelectrode distance (1 mm between neighboring electrodes; Bédard et al. 2006). In this study, we made highly parallel recordings of spontaneous spiking activity and LFPs in the visual cortex (area 17) of four anesthetized cats by using 16 or 32 electrodes simultaneously (4 × 4 arrays) with small interelectrode distances (200 μm between neighboring electrodes). This allowed us to test for evidence of neuronal avalanches in LFP events and spikes simultaneously. Our results suggest that spontaneous activity of the visual cortex under anesthesia has statistical properties similar to the neuronal avalanches that were initially described by Beggs and Plenz (2003) and thus may impact the processing of sensory information in a way similar to that of waves of synaptic activity.

METHODS

Preparation

Four cats were initially anesthetized with ketamine (Ketanest, Parke-Davis, 10 mg/kg, im) and xylazine (Rompun, Bayer, 2 mg/kg), and the anesthesia was maintained with a mixture of 70% N_2O-30% O_2 and halothane (1.0%). Tracheotomy was applied, and the animal was fixated in a stereotactic frame. The animals were artificially ventilated, and after craniotomy, the skull was connected to a metal rod, and the halothane level was reduced to 0.5–0.6%. After ascertaining stability of anesthesia to prevent vegetative reactions to somatic stimulation, pancuronium bromide (Pancuronium, Organon, 0.15 mg/kg/h) was applied to obtain paralysis. Glucose and electrolytes were provided by a gastric catheter, and the end tidal CO_2 and rectal temperature were maintained between 3 and 4% and 37 and 38°C, respectively. The value of 0.5–0.6% halothane was held constant throughout the experiment except for potentially painful procedures (e.g., intramuscular injection of antibiotic). In this case, we increased the level of halothane to 1.2% 10 min before the procedure and returned immediately back to 0.5–0.6%, which was followed by a period of ≥20 min without new recordings. The nictitating membrane was prepared with neosynephrine, the pupils were dilated with atropine, and the eyes were covered by contact lenses with artificial pupils for protection from desiccation. All procedures abided to the German law for the protection of animals and were supervised by a veterinarian.

Recordings

We recorded spontaneous activity in area 17 with one or two 16-channel silicon-based microelectrode arrays (Neuronexus Technologies) (Fig. 1). Each array consisted of four 3 mm long shanks, with a profile of 100 × 10 μm at its widest point. Each shank had four electrode contacts. The separation between the neighboring contacts was 200 μm in both directions, i.e., along and across the shanks. This symmetric 4 × 4 arrangement allowed for the maximum distance spanned by the centers of the contacts to equal 600 μm along each dimension and 850 μm diagonally. Thus the recording area of one array spanned ~0.6 × 0.6 mm^2. This array spacing is similar to that used by Beggs and Plenz (2003). Each electrode contact covered an area of 1,250 μm^2 and had impedance of 0.3–0.5 MΩ at 1,000 Hz. The arrays were inserted into the cortex always in the same hemisphere such that they penetrated the surface approximately perpendicularly. We recorded mostly the activity from superficial layers;

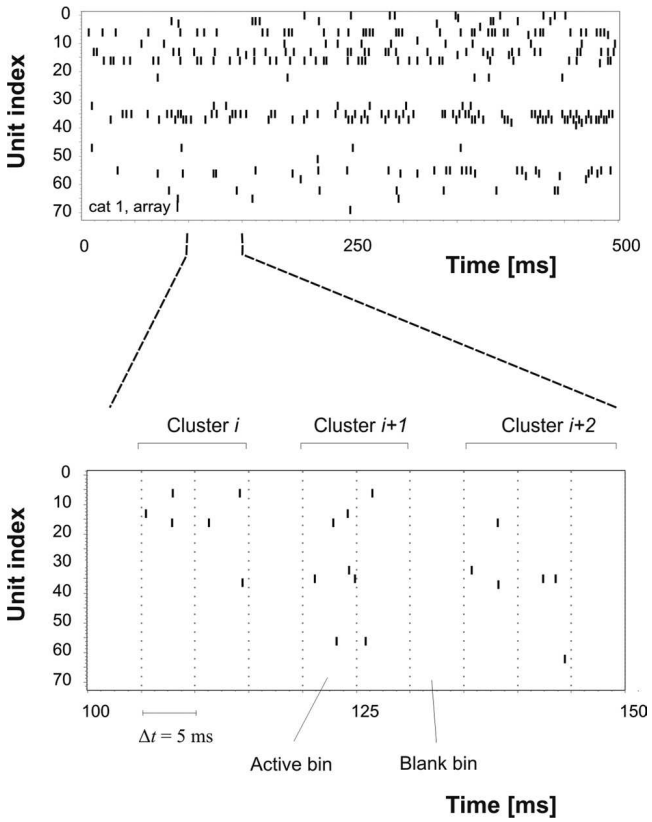

FIG. 1. Recording of extracellular unit activity and definition of spatiotemporal spike clusters in cat visual cortex. *Top*: spontaneous spiking activity for 72 neurons shown in the form of a raster plot for the duration of 500 ms (single 4 × 4 Michigan probe inserted in area 17). *Bottom*: 3 spatiotemporal spike clusters at higher temporal resolution (zoom). In this example, continuous time is discretized into time bins of width $\Delta t = 5$ ms. A spike cluster is bracketed by at least 1 bin with no activity (blank bin) and consists of a continuous sequence of bins with at least 1 spike in each (active bins). In this example, all 3 spike clusters have the same lifetime of 10 ms.

however, we did not identify these layers. All neurons recorded by the same array had overlapping receptive fields. In three cats (*cats 1, 3*, and *4*), the analyzed spontaneous activity was taken from the 1 s period before visual stimulation. For each trial, 1 s recordings of spontaneous activity preceded 4–5 s of visual stimulus presentation (sinusoidal gratings) and were followed by 1 s of recording. Intertrial periods ranged between 1 and 2 s, depending on the experiment. In one cat (*cat 2*), no visual stimulus was presented, and spontaneous activity was analyzed for the whole trial duration (10 s). The total duration of spontaneous activity obtained in each of the recordings ranged between 100 and 720 s. For each cat, we investigated activity in two different datasets (recordings). In three cats (*cats 2, 3,* and *4*), the two datasets were recorded by the same array but at different time points, the interval between recordings varying between 3 min and 67 h. In one cat (*cat 1*), the two datasets were recorded simultaneously using two different arrays. Overall, we inserted five different arrays and recorded in total eight datasets, two from each cat. During the recordings, the eyes of the cats were open, and in front of the eyes, a blank (black) computer screen was located. The ambient illumination was low as the lights in the room were strongly dimmed.

Extraction of extracellular spikes and nLFP events

Signals were amplified 1,000× and filtered between 500 Hz and 3.5 kHz for extracting multiunit activity (MUA) and between 1 and 100 Hz for extracting LFPs. MUA signals were sampled with a frequency of 32 kHz, which allowed the later application of off-line spike-

sorting techniques. LFP signals were sampled with 1 kHz. The signals were transmitted to an A/D converter and recorded by a customized LabView program running on a PC. Action potentials (spikes) were detected with a two-sided threshold discriminator adjusted manually to yield a signal-to-noise ratio of ~2:1. For each detected action potential, the time of the event (timestamp) was recorded together with the spike waveform over a duration of 1.2 ms.

After applying spike-sorting techniques based on principal component analysis, we extracted between 43 and 97 units per array (67 ± 17), the majority of which were identified as multi-units. We combined both the multi- and single-unit activity in all analyses to reduce the potential subsampling of spike clusters, which can obstruct the presence of a power law (Priesemann et al. 2009). The firing rates were computed for every unit and recording, and the values ranged between 0.01 and 69.8 Hz, and, as expected, showed a skewed distribution with an overall mean of 7 Hz and median of 2.2 Hz, resulting in an SD of 11.2 Hz. The number of spikes per recording varied between 55,037 and 251,810, with a longer recording duration also leading to the detection of more spikes. In the recordings with power law statistics, the average spike count per second was on average considerably higher [590 ± 112 (SD) spikes/s] than in recordings without a consistent power law (389 ± 179 spikes/s). However, in *cat 3*, array I–a, in which we also found a power law, the spike density was low (131 spikes/s), and in *cat 4*, array I–b, in which no power law was detected, the spike count was high (586 spikes/s). LFP events were extracted by applying a threshold of 2 SD of the noise calculated for each electrode, whereas the polarity of this threshold was determined from the polarity of the spike-triggered LFP average. In two recordings, the electrodes showed a spike-triggered LFP average with a negative deflection at the time of spike occurrence and hence we used a threshold of −2 SD. For the remaining six recordings, the unit-triggered LFP average at single electrodes was positive, resulting in a threshold of +2 SD. To determine the time of an event, we detected the point at which the LFP signal reached its maximum between the two threshold crossings at which the signal first exceeded and then returned back below the threshold.

Extraction of event clusters

The spatiotemporal organization of spike and LFP events was studied in the context of neuronal avalanches. We first identified spatiotemporal event clusters in the spiking data based on the same principles as those used for the investigation of avalanches in spontaneous LFP events in earlier studies (Beggs and Plenz 2003; Stewart and Plenz 2006). Spikes were first grouped into small time bins of width Δt, which, across most of analyses and datasets, ranged between 0.5 and 32 ms. At $\Delta t = 32$ ms, most recordings either showed a flat distribution of spiking event sizes (i.e., the probability of small and large spiking events was equal) or the number of extracted events was insufficient to compute a distribution. The bins containing at least one spike we refer to as active and to those without spikes as blank. A spatio-temporal cluster begins with a blank bin, is followed by a sequence of active bins, and ends with another blank bin. In other words, sequences of active bins were delineated by periods of no activity, as shown in Fig. 1 (zoom-in). The first and last event clusters of each segment (1 and 10 s in duration) were discarded from further analysis, because they were likely to reflect an incomplete cluster. All the analyses were restricted to neuronal spiking activity obtained from single arrays, and recordings were included into analysis only if all 16 channels of the array detected neuronal spiking activity with signal-to-noise ratio ≥2.

By applying this algorithm, we identified ≤132,400 (47,679 ± 39,684) spike clusters per recording (with $\Delta t = 1$ ms). This number depended strongly on the bin size (Δt). If Δt was small, the total number of cluster increased by splitting larger cluster into several smaller ones. Similarly, with large values of Δt, small clusters were combined into larger ones, resulting in fewer clusters. Previous work by Beggs and Plenz (2003) showed that a reasonable estimate of the optimal bin width can be obtained from the gross average of interspike interval $(ISI)_{array}$ distribution, $avg\Delta t$, which estimates the average time between successive spikes occurring anywhere in the array (see also Stewart and Plenz 2006 for a detailed explanation of the methods). ISI_{array}s were calculated always with a resolution of 0.1 ms. The ISI_{array} distribution quickly decayed to negligible values within ~50 ms (see Fig. 4*B*), and there was no requirement to impose any additional cut-off as based on maximal extend of correlations (cf. for the acute slice; Stewart and Plenz 2006). Histograms of ISIs calculated for individual units (ISI_{unit}) were computed always with a resolution of 1 ms and plotted in log-log coordinates. Both ISI_{array} and ISI_{unit} distributions were fitted with both power law and exponential functions (ISI_{array} range: 2–30 ms; ISI_{unit} range: 2–500 ms) for statistical purposes.

For each cluster, the cluster size was obtained by counting either *1*) the number of spikes across all units and active electrodes or *2*) the number of electrodes at which at least one spike was detected. For each array, histograms of cluster sizes were obtained using linear binning, normalized to probability density distributions, and plotted in log-log coordinates for further analysis. Fits of exponential and power-law functions were calculated starting from a minimal cluster size of 3 spikes and ending with ≤40 spikes for Δt values between 1 and 8 ms in four recordings and between 6 and 16 ms in one recording, representing the Δt range in which we detected a power law. The resulting R^2 values were averaged across all Δts. In the case that the estimated density plot was not continuous because of an insufficient number of data entries, the maximal cluster size was <40, in which case we truncated the rightmost end of the corresponding plot. This fitting range was optimal for the analysis of power law statistics, because cluster sizes with ≤2 spikes were not always distributed on a straight line (e.g., with $\Delta t \leq 2$ or ≤3 ms), whereas the distributions of cluster sizes >40 spikes were either curved too (e.g., when $\Delta t \leq 2$ ms) or sometimes undersampled (when Δt reached values of ~8 ms), reducing the R^2 values of the linear and exponential fits. Preliminary analysis showed no difference in the appearance of a power law and its concomitant exponent across the two definitions of cluster sizes, and thus to characterize the cluster size distributions, we restricted our analysis to the number of spikes, i.e., to definition *1*. At least two spikes needed to occur within a sequence of active bins to be counted as a cluster, which excludes from the analysis single, isolated spikes. Spike clusters were considered to be neuronal avalanches if their corresponding size distribution obeyed a power law (i.e., the distribution in a log-log plot followed a straight line and power law fitted better than exponential function). The lifetime of a spike cluster was defined as the length of the uninterrupted sequence of active bins, i.e., the count of bins within the cluster multiplied by Δt. Lifetime distributions were plotted in log-log coordinates, and both power law and exponential fits were computed for lifetimes between 1 and 40 active bins and for bin sizes between 1 and 8 ms (6 and 16 ms for 1 dataset; always in 1 ms steps).

As described for spike clusters, spatiotemporal LFP clusters were also obtained by concatenating active time bins bracketed by at least one empty time bin on each side. For LFP clusters, Δt ranged from 1 to 32 ms, and the LFP cluster size was defined as the number of electrodes for which an LFP event was detected. The histograms of LFP cluster sizes were obtained with logarithmic binning, normalization, and studied in log-log coordinates using linear regression analysis.

Correlation analysis

Normalized auto-correlation histograms (ACHs) and cross-correlation histograms (CCHs) of spontaneous spiking activity were computed first for each unit and each pair of units, respectively. We averaged the histograms across all units (ACH) and all possible pairs of units (CCH). Consequently, we obtained only one ACH and one CCH per dataset. Normalization was achieved by replacing coinci-

dence counts with Pearson's *r* computed on the trains of 1s (spike) and 0 s (nonspike) binned to 1 ms precision. The width of an ACH or CCH was estimated at half-height, i.e., at the midpoint between its baseline and the maximum. In all cases, the investigated auto-correlation window was ±50 ms and cross-correlation window was ±100 ms.

Subsampling analysis

To test whether subsampling of spiking events can account for the absence of a power law in some of our recordings, we randomly removed spikes from the recordings with power law and recomputed distributions of cluster sizes (also known as spike-train thinning). Spiking events (i.e., actions potentials) were removed randomly and independently from each unit such that, as a result, only 50, 25, or 10% of the original data were sampled. This subsampling procedure was repeated 10 times for each size of the subsample. Power law and exponential functions were fitted for cluster size distributions (see above) and for Δts (2–8 ms for 4 datasets and 6–16 ms for 1 dataset), where we had previously found a power law. We subsequently averaged across all 10 subsampling repetitions, all investigated Δts, and all tested recordings. To avoid any bias toward a better power law fit because of a distribution that was bimodal, we truncated the tales of all bimodal distributions such that only the single-curved part of these distributions were fitted. Consequently, we obtained two values per subsampling size, one for the average power law fit and one for the average exponential fit, which we compared across different levels of subsampling.

RESULTS

An example of the spontaneous activity recorded from 72 units in parallel is shown in Fig. 1. In the same figure we also show the procedure for extracting the spatiotemporal spike clusters, i.e., candidate avalanches, defined as sequences of active bins delineated by blank bins (see the zoom-in). The same procedure was used to extract LFP event clusters.

LFP cluster size distributions

The cluster sizes of LFP events from spontaneous activity in slice cultures, acute slices, and in vivo from young, anesthetized rats and awake monkeys have been found to distribute according to a power law (Beggs and Plenz 2003; Gireesh and Plenz 2008; Petermann et al. 2009; Stewart and Plenz 2006). In this study, a similar power law distribution was found for LFP cluster sizes recorded during spontaneous activity in primary visual cortex of the anesthetized cat. The density of LFP cluster sizes, $P(n)$, when plotted in log-log coordinates, followed a straight line up to the cluster size of $n = 16$ (Fig. 2*A*), which was the largest size that is expected with a 4×4 array provided that, within a cluster, LFP events are unlikely to recur, i.e., rarely return back to the electrode at which they once already occurred. This distribution is characteristic of the power law function, $P(n) \sim n^{\alpha}$, with a cut-off at the maximal cluster size, and for which the exponent α indicates the slope in the log-log plot. As shown originally for LFP events in vitro (Beggs and Plenz 2003), the power law in vivo, as well as the cut-off values for LFP cluster sizes, remained also robust across different bin sizes, Δt (in 7 of 8 recordings).

The exponent of the power law allows for a distinction between different types of dynamical systems that may give rise to avalanche-like behavior (i.e., each dynamical system displays a unique exponent) and thus restricts potential mechanisms that may be responsible for the generation of the power law (see Plenz and Thiagarajan 2007). Previous estimates of the exponent α for neuronal avalanches both in vitro and in vivo showed a monotonical increase of α from about -2.2 to -1.2 with an increase in Δt (Beggs and Plenz 2003; Gireesh and Plenz 2008; Petermann et al. 2009; Plenz and Thiagarajan 2007;Stewart and Plenz 2006), and when Δt was chosen as the average time delay between successive events on the array, α was found to be close to -1.5. Similarly, in this study, the slope monotonically increased with Δt from -2 to about –1.2 (Fig. 2*B*; $n = 7$ recordings). However, the slope remained largely above –1.5 for $\Delta t > 2$ ms. Therefore the slopes found in this study in vivo were more shallow from those found previously in vitro (Beggs and Plenz 2003), even though the same interelectrode distance of 200 μm was used in both cases.

Computer simulations of cascading neuronal activity suggested that the distributions of lifetime for clusters of short duration (i.e., less than $\sim 10\Delta t$) should follow a power law too

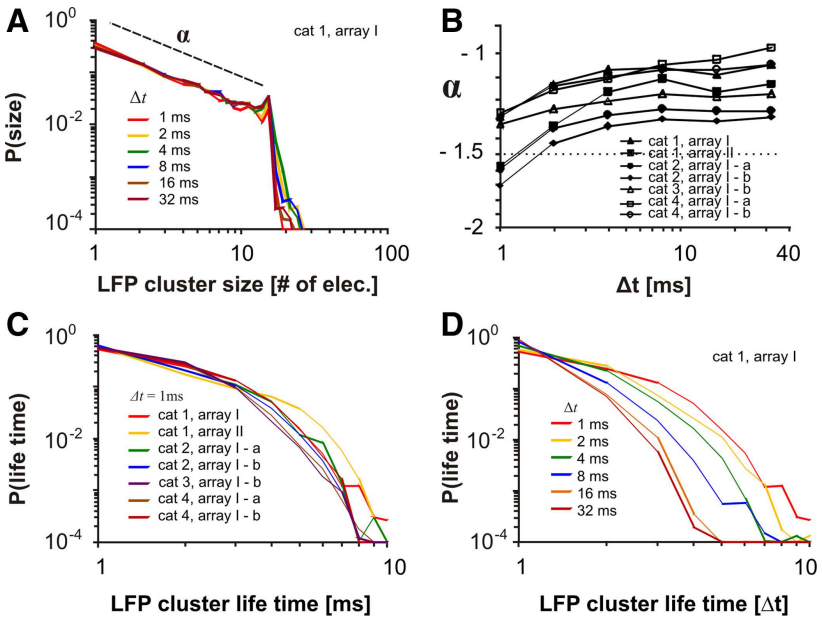

FIG. 2. The organization of spontaneous local field potential (LFP) events into spatiotemporal clusters shows the statistical features of neuronal avalanches. *A*: the probability distribution of LFP cluster sizes for 6 different bin sizes, Δt. The size is defined as the number of active electrodes in an LFP event cluster. Note the linear decay of the distribution shown in log-log coordinates and the cut-off point of size = 16 electrodes, which is the total number of electrodes of the array. *B*: dependence of the exponent α on the bin size, Δt, for 7 different arrays with a power law distribution. *C*: probability distributions of lifetimes plotted in log-log coordinates for 7 different arrays (bin size = 1 ms). *D*: lifetime distributions of 1 array computed for 6 different bin sizes in log-log coordinates.

(Eurich et al. 2002), with an exponent close to −2.0 (Teramae and Fukai 2007; Zapperi et al. 1995). Previous in vitro studies on LFPs reported results consistent with these predictions, showing a power law for the initial part of the lifetime distributions (Beggs and Plenz 2003). We obtained different results for the lifetime distributions of LFP clusters in vivo. For all recordings and with $\Delta t = 1$ ms, the entire lifetime distribution displayed curvatures, but on the other hand, deviated also from a simple exponential distribution, showing a substantial increase in long lifetimes relative to what would have been expected if LFP events clustered by chance (Fig. 2*C*). This finding is consistent with earlier reports of lifetime distributions in vitro (Beggs and Plenz 2003), which also differed from an exponential decay. Moreover, in this study, lifetime distributions of LFP events did not scale, i.e., did not collapse, with an increase in Δt (Fig. 2*D*), a result that would be expected from theory (Eurich et al. 2002) and that has been already shown experimentally in vitro (Beggs and Plenz 2003).

Spike cluster size distributions

Next, we examined whether spike clusters in vivo exhibited a power law. We varied Δt from 0.5 to 32 ms and found characteristic spike cluster distributions, which depended on Δt. An example distribution computed for different bin sizes is depicted in Fig. 3*A* (*cat 1*). For small bin sizes ($\Delta t < 1$ ms), the cluster sizes were distributed across a steep, curved line, which had a tendency to become shallower and straighter as the bin size increased. Starting with $\Delta t = 1$ ms (in some cases 2 ms; Fig. 3*A*) the distributions showed a power law that stayed ≤7 or 8 ms. At $\Delta t \geq 9$ ms, the distribution became bimodal with curvatures at the initial part and a horizontal tale, i.e., medium-size and large clusters being about equally probable. In the range 1–7 or 8 ms, with the gradual increase in Δt, the slope of the fitted line (i.e., the exponent of the power law) also gradually increased. This can be explained by the increased likelihood to concatenate spike events (see METHODS). In one dataset, the power law was detected only between $\Delta t = 6$ ms and $\Delta t = 16$ ms.

Overall, we found power law distributions of avalanche sizes in five of eight datasets independently of whether the recorded segments were short (*cats 1* and *3*) or long (*cat 2*), and the results were similar to a previous report in dissociated cultures (Pasquale et al. 2008), whereby the detection of a power law in spiking activity also depended on Δt. For each of these five experiments (recordings), we fitted the resulting size distributions for different Δts (6–16 ms in 1 recording and 1–8 ms in all other recordings) with an exponential and with a power law function, averaged across all tested Δts and compared the goodness of the two fits (i.e., averaged R^2 values). A good fit to power law suggests correlated spikes (Bak et al. 1988). A good fit to an exponential function may suggest either independence between neurons analogous to a Poisson process (Shadlen and Newsome 1998) or subsampling of event clusters, whose true size distribution exhibits a power law but is inaccessible because of a small count of recorded action potentials (Petermann et al. 2009; Priesemann et al. 2009). In these recordings, a power law function fitted the data significantly better than an exponential function (*t*-test, all $t > 2.65$; all $P < 0.001$; df ≥ 13; Fig. 3*B*), for which the distributions of spike cluster sizes are plotted in Fig. 3*C* using $\Delta t = 3$ ms for four recordings and $\Delta t = 9$ ms for one of them. One pair of recordings (*cat 1*) was obtained simultaneously from the same cat from arrays positioned in the same brain area a few millimeters apart. This suggested that the power law was present simultaneously in two spatially separated arrays. Two other recordings using the same array (i.e., the same position in the cortex) were obtained from another cat (*cat 2*) at two different instances in time (separated by ~15 min), which suggested temporal stability for at least a short period of time. The overall linear fit to distributions of event sizes in log-log plots was $R^2_{power} = 0.93 \pm 0.01$ (SD), which exceeded considerably the quality of the exponential fit ($R^2_{expon} = 0.85 \pm 0.03$; see also Fig. 3*B*). Therefore similarly to the results obtained with

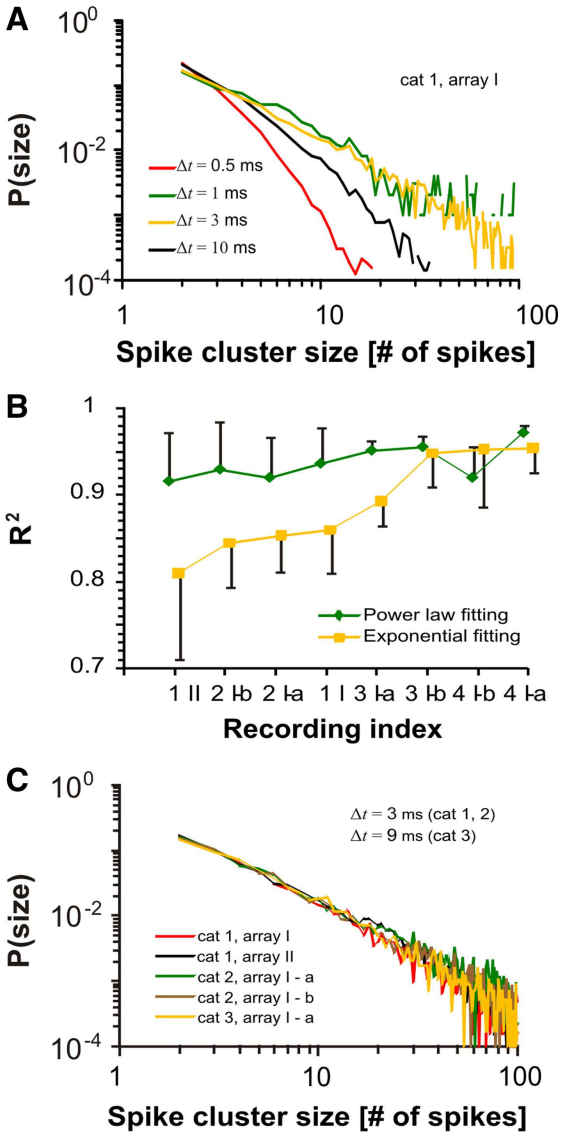

FIG. 3. Spike cluster sizes in vivo show power law statistic similar to that of neuronal avalanches. *A*: probability to observe a spike cluster of a given size *s* is plotted in log-log coordinates for 4 different bin sizes Δt. Spike cluster size is calculated as the number of spikes for the duration of the cluster and is shown for values between 2 and 100. *B*: comparison of quality with which power law and exponential functions fitted cluster size distributions in different recordings. The order of the recordings on the abscissa was organized according to the quality of the exponential fit. Error bars: SD. *C*: same as in *A* but calculated for 5 different recordings and only 1 Δt. Four of the recordings are plotted with $\Delta t = 3$ ms and 1 with $\Delta t = 9$ ms.

LFPs, the spiking events, which sample much smaller portion of neuronal activity, can show power law distributions of spatially distributed events. The cautionary note is, however, that this result is not obtained in every recording.

Exponent of the power law

A representative result for the estimated exponents of the spike cluster distributions is shown in Fig. 4*A*, where we plotted the changes in the estimated exponent as a function of the bin size, Δt, for four recordings in which we found a power law distribution for Δt = 1–8 ms (the 5th recording with a power law at Δt = 6–16 ms is not shown). In accordance with the findings based on LFPs, the slope grew with the increase in Δt. This result is expected because the concatenation of spikes at large values of Δt necessarily increases the likelihood of large spike clusters. We also estimated the value of Δt that minimizes the decomposition and concatenation of clusters. To this end, we used the methods of Beggs and Plenz (2003) and computed simply the gross average of ISI_{array}s (see METHODS; Fig. 4*B*). For the recordings that exhibited a power law, the resulting value, $avg\Delta t$, varied across different arrays but stayed within the range of Δt (close to the lower limit) where we found a power law, with the averages ranging between 1.5 and 5.9 ms (2.84 ± 1.8). Importantly, when we computed the exponents of event size distributions only for these optimal values of Δt, the values of exponents were remarkably similar across all five recordings for which we have previously established reliable power laws. These values were −1.77, −1.78, −1.81, −1.82, and −1.83, with an average of −1.8 ± 0.03 (R^2_{power} = 0.98 ± 0.01, R^2_{expon} = 0.90 ± 0.01, for the 5 fitted lines). Consequently, when these distributions of event sizes were plotted on the same graph, they largely overlapped (Fig. 4*C*). These values of the exponents were lower than those found either in this (Fig. 2*B*) or in previous studies for LFPs (Beggs and Plenz 2003; Gireesh and Plenz 2008) or those found in previous studies for spike clusters (Mazzoni et al. 2007; Pasquale et al. 2008).

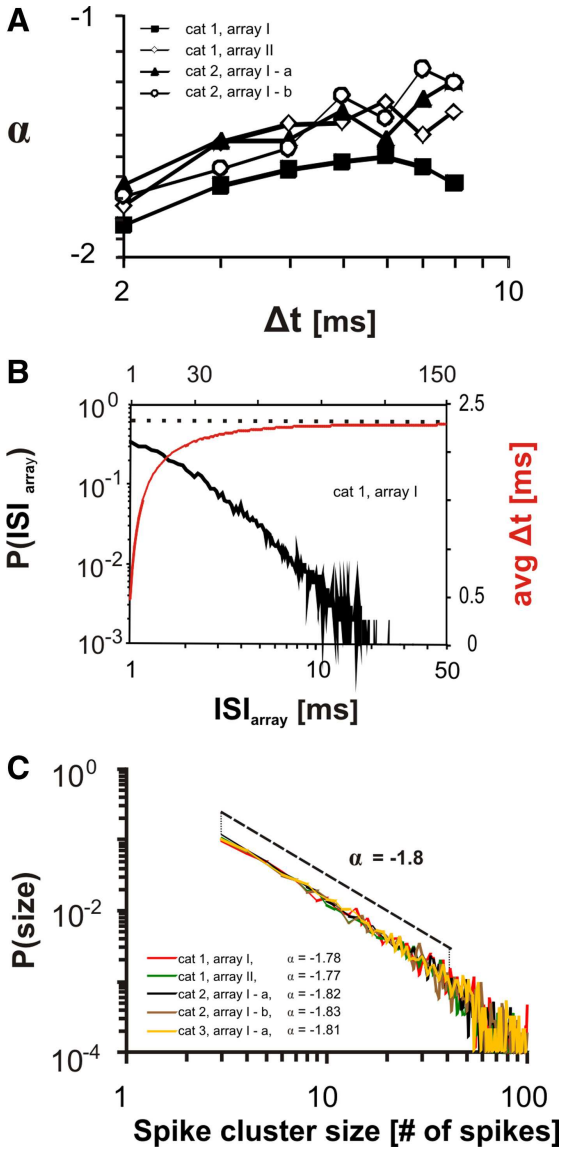

FIG. 4. The slope of the power law. *A*: change in the slope, α, shown as a function of bin size, Δt, for the 4 arrays with power law statistics in the depicted range of Δt. *B*: interspike interval $(ISI)_{array}$ distribution for the recordings shown in Fig. 3*A* plotted in log-log coordinates (black, left ordinate) and the running average of this distribution, $avg\Delta t$, computed as a function of the ISIs (red, right ordinate). The dashed line represents the value of $avg\Delta t$ (2.3 ms in this case), which was used in the analysis in *C*. *C*: distributions of spike cluster sizes calculated at corresponding $avg\Delta t$ for 5 different arrays. The slopes α for each recording are indicated in the plot.

Absence of power law statistics in event size distributions

As mentioned, in three recordings (of 8), we did not find sufficient evidence that the sizes of spike events distributed according to a power law (Fig. 3*B*). One recording without a power law (*cat 3*) was made almost 3 days (67 h) after another one that has shown a power law. The remaining two datasets were obtained from the same cat (*cat 4*) about 1 day apart (28 h). This was despite the presence of a power law in the LFP events in all cases (Fig. 2*B*). This suggests that the power law statistics might be more robustly found at the level of the LFP compared with unit activity, which is more prone to subsampling. Similarly to the datasets with a power law, for small Δt, the distribution of event sizes was steep and curved (although sometimes only to a small degree). Likewise, an increase in Δt made the distributions of both classes of recordings shallower. The main difference between the two groups was detected with the increase in Δt. Only those five recordings classified as containing a power law exhibited consistently a straight line in a log-log plot, whereas the distributions of the remaining three became gradually more and more curved as Δt increased.

These three recordings were fitted with an exponential and a power law function for bin sizes 1–8 ms. Overall, the quality of fit for exponential functions did not differ from that of a power law, when different values of Δt were taken into account (t-test, all $t < 1.71$, all $P > 0.06$, df ≥ 13). As expected, for small bin sizes, the power law fitted the distributions of cluster sizes in two recordings better than did the exponential function (R^2_{power} = 0.97; R^2_{expon} = 0.88 with Δt = 1 ms), whereas the result was reversed for higher bin sizes (R^2_{power} = 0.95; R^2_{expon} = 0.98 with Δt = 8 ms). As a result, averages of the goodness of power law and exponential fits computed across all Δts were approximately equal for these two recordings. In the third

recording, an exponential function described the distribution of event sizes better than a power law across all bin sizes (*cat 4* I-b; on average, $R^2_{power} = 0.92 \pm 0.04$ vs. $R^2_{expon} = 0.95 \pm 0.07$). Note that the qualities of the exponential and power law fits (i.e., averaged R^2 values) are higher in these three recordings than in those with consistent power law. This is because the average duration of the recording was much longer in the former case, increasing the total spike count and, by that, the quality of the fit.

Distributions of ISIs

We also studied the presence of a power law in the distributions of ISIs. These distributions were computed either for each unit separately (ISI_{unit}) or for all the units belonging to an entire array (ISI_{array}). The ISI_{unit} distributions did not exhibit a straight line in a log-log plot in either of our recordings (Fig. 5*B*). However, for the datasets that exhibited a power law in the distribution of cluster sizes, a power law function fitted also the distribution of ISI_{unit} better than did the exponential function ($R^2_{power} = 0.93 \pm 0.01$; $R^2_{expon} = 0.85 \pm 0.03$). The opposite was the case for the datasets without a power law in cluster sizes ($R^2_{power} = 0.91 \pm 0.01$; $R^2_{expon} = 0.94 \pm 0.01$). Therefore, although the distributions of ISI_{unit} were always curved, the curvature was the smallest in the recordings in which the distributions of cluster sizes obeyed a power law.

In contrast, ISI_{array} distributions were much more consistent with the analysis of event size distributions. In the recordings in which spike cluster sizes distributed according to a power law, the ISI_{array} distributions exhibited a straight line (Fig. 5*C*; $R^2_{power} = 0.96 \pm 0.01$; $R^2_{expon} = 0.88 \pm 0.03$) and vice versa; if a power law was absent in the distribution of cluster sizes, a straight line was also missing in the ISI_{array} distribution (Fig. 5*D*; $R^2_{power} = 0.92 \pm 0.01$; $R^2_{expon} = 0.97 \pm 0.02$). Thus the analysis of ISI_{array} distributions suggests conclusions similar to those reached after the analysis of the distributions of events sizes.

Lifetime distributions

The distributions of spike cluster lifetimes showed properties similar to those of the cluster size distributions. The result was dependent on the bin size and whether a power law was detected in the size distribution. In all recordings, the distribution of lifetimes was steep and curved at small bin sizes ($\leq$1 ms; see Fig. 6*A* for $\Delta t = 1$ ms) and became gradually shallower with the increase in Δt (Fig. 6*B*). In those five recordings with a power law distribution of cluster sizes, the lifetime distributions became straighter with increasing bin sizes, but nevertheless, they never exhibited fully a power law (Fig. 6*B*). The distributions were closest to a power law with bin sizes 6–7 ms (16 ms for 1 recording)—values similar to the maximum Δt for which a power law of cluster sizes could still be detected. For Δts $\geq$ 7 ms, the lifetime distributions became bimodal. In the three recordings with absence of a power law distribution in cluster sizes, the increase in Δt had the opposite effect on the lifetime distribution. Much like the cluster sizes, these distributions increased also in curvature with larger Δts (data not shown). We also quantified these results: For all recordings in which cluster sizes exhibited a power law, the lifetime distributions for Δts = 1–8 ms (6–16 ms in 1 case) were approximated more accurately by a power law function ($R^2 = 0.95 \pm 0.01$) than by an exponential function ($R^2 = 0.89 \pm 0.2$). Conversely, in the absence of a power law in cluster sizes (recordings marked with stars in Fig. 6*A*), the lifetime distributions were described better by an exponential function than by a power law ($R^2_{power} = 0.92 \pm 0.02$; $R^2_{expon} = 0.97$).

Furthermore, recordings with a power law also showed longer lifetimes, as can be seen in Fig. 6*A*. Lifetime distributions with a power law in cluster sizes were less steep and intercepted the abscissa at a later point (23 $\pm$ 4 ms) compared with the lifetime distributions of recordings lacking power law statistics (13 $\pm$ 3 ms; marked with stars). The only exception was array I-a of *cat 3*, which showed a power law in the size distribution (only for $\Delta t \geq 6$ ms) but intercepted the abscissa at a value similar to recordings without a power law (13 ms).

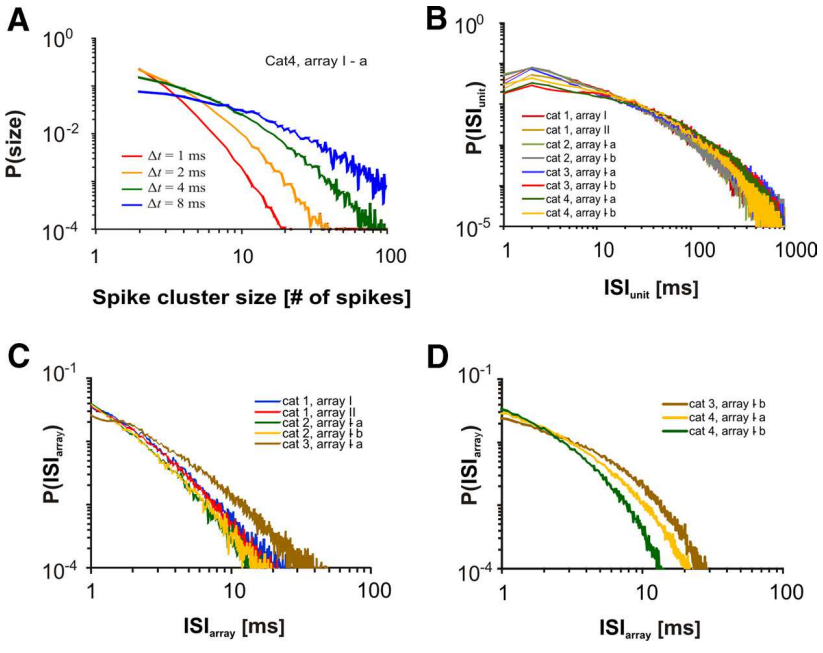

FIG. 5. Example recording in which a power law was not detected consistently across different bin sizes. *A*: spike cluster size distribution shown as a function of bin size. The notation and the analyses are the same as in Fig. 3*A*. *B*: ISI_{unit} distribution for 8 different recordings. *C*: ISI_{array} distributions calculated for recordings that exhibited a power law in the cluster size distributions. *D*: same as in *C* for datasets without a power law in the cluster size distribution.

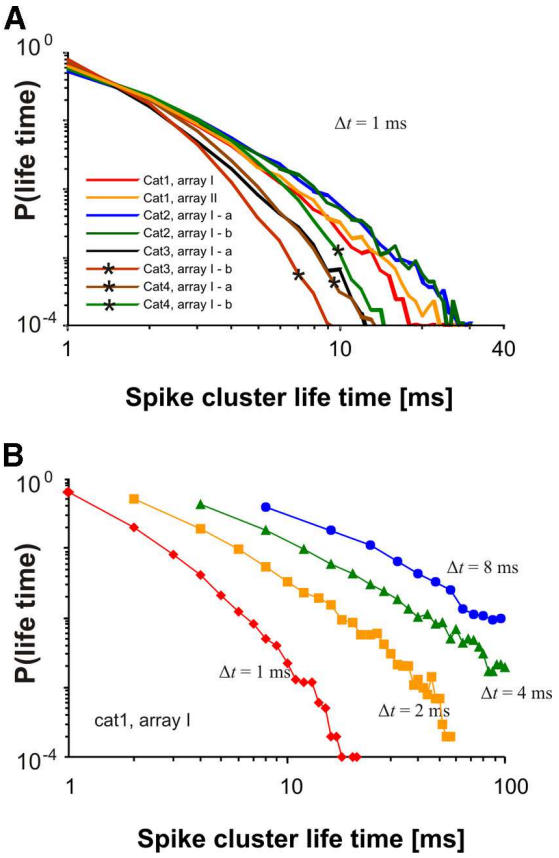

FIG. 6. Lifetime distributions of spike clusters. *A*: distribution of cluster lifetimes computed for all recordings. Star: the 3 recordings whose size distributions did not follow a power law in the size distribution. *B*: example lifetime distributions for 1 recording in area 17 calculated for different values of Δt.

Correlation analysis

In critical systems, events that occur within cascades can be correlated over long distances and often display long-range temporal correlations (Bak et al. 1988). The same was shown in in vitro experiments in which the existence of a power law in neural activity was associated with long-range correlations across neuronal events (Beggs and Plenz 2003, 2004; Mazzoni et al. 2007). To assess the role of correlations in our in vivo experiments, we computed overall ACHs and CCHs by averaging the individual ACHs and CCHs calculated for all possible units and pairs of units belonging to one array (see METHODS for more details).

In all cases, ACHs and CCHs showed center peaks that indicated correlations (auto- or cross-) higher than expected by chance. The value of the ACH at 0 time delay is by definition always 1.0 and hence was not used for the analysis. Notably, these correlations differed across arrays with and without power law statistics. Correlations were on average stronger (e.g., the center peaks were higher) in arrays with a power law in cluster sizes ($r = 0.019 \pm 0.008$ and 0.007 ± 0.001 for ACHs and CCHs, respectively) as opposed to cases where a power law was absent [$r = 0.007 \pm 0.002$ and 0.005 ± 0.001 for ACHs and CCHs, respectively; for ACH, $t(6) = 2.34$, $P = 0.027$; for CCHs, $t(6) = 1.85$, $P = 0.057$]. Example ACHs and CCHs for a power law and a non–power law case are shown in Fig. 7.

Moreover, we found a close relationship between the width of the center peak and the presence of a power law. The recordings in which the spike counts showed power law statistics had significantly wider center peaks, both in ACHs and CCHs, than the recordings in which the power law was absent. The width at the half height of the peak was 14 ± 3 ms for ACHs and 18.6 ± 7.4 ms for CCHs in arrays with power law and 8 ± 2 ms for ACHs and 3.7 ± 0.6 ms for CCHs in arrays without power law [for ACH, $t(6) = 2.63$, $P = 0.02$; for CCHs, $t(4.1) = 4.51$, $P < 0.01$]. Therefore consistent with the longer lifetimes in the recordings with power law in event sizes, the presence of a power law was associated not only with stronger correlations but also with correlations that spanned considerably longer temporal distances.

Subsampling can destroy power law statistics

As shown in previous studies (Petermann et al. 2009; Priesemann et al. 2009), subsampling, i.e., recording an insufficient number of neuronal events, can mask power law statistics of underlying neuronal dynamics. To test whether subsampling could explain the absence of a power law in our data, we randomly removed spikes from the recordings, the effect of which on the distribution of cluster sizes is shown in Fig. 8*A* for $\Delta t = 3$ ms. The straight line of the fully sampled recording gradually turned into a larger and larger curvature as further spikes were removed from the dataset. To quantify these results, we fitted power law and exponential functions for each subsampling class and for each Δt, where a power law was detected in the original data (in 4 datasets $\Delta t = 2$–8 ms, in 1 dataset $\Delta t = 6$–16 ms). The resulting fits were averaged across all Δts and all recordings with previously established power law distributions for a given level of subsampling, such that we obtained one power law fit and one exponential fit per subsampling size. Subsequently, the two types of fits were compared, and the results are shown in Fig. 8*B*. The analysis showed that fully sampled data are fitted better with a power law than with an exponential function [$t(84) = 8$, $P < 0.001$]. This difference

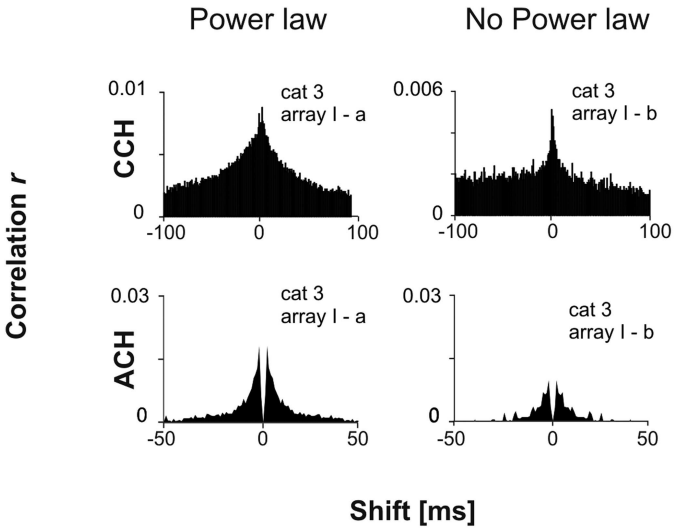

FIG. 7. Examples of cross-correlation (CCH) and auto-correlation histograms (ACH) averaged across all spikes trains or pairs of spike trains recorded from an array and obtained in recordings that either did or did not exhibit a power law in the event size distributions.

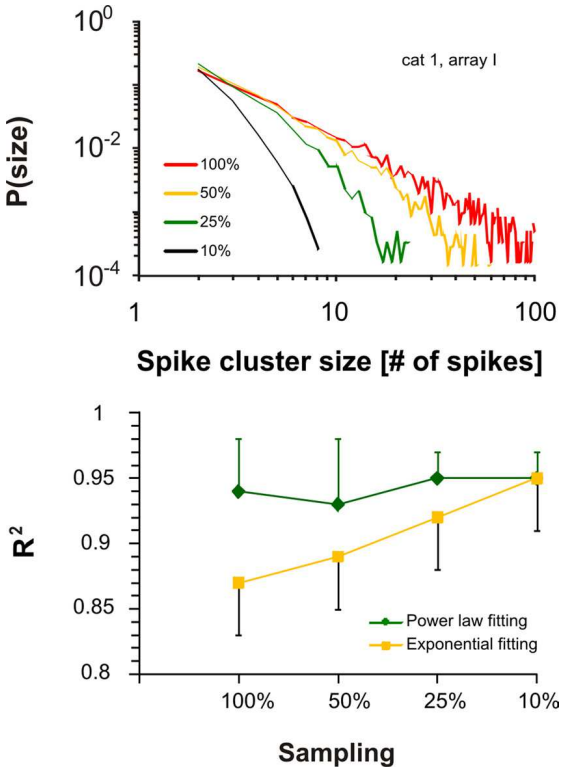

FIG. 8. Subsampling analysis. *A*: distributions of spikes clusters for a fully sampled dataset and 3 different degrees of subsampling. *B*: comparison of power law and exponential fit for 4 different sample sizes averaged across all datasets with previously established power law. Each pair of fits was obtained by subsampling 10× the original recordings at the indicated level and at different Δts (4 datasets: 2–8 ms, 1 dataset: 6–16 ms) and averaging the obtained values across all Δts and all recordings in which a power law was detected before. Error bars: SD.

reduces gradually as data are subsampled to a higher degree, the difference being only marginally significant with the sampling of 10% of the original data [$t(643) = 1.74$, $P = 0.08$]. These results show that the power law in cluster size distributions breaks down with subsampling, i.e., with random removal of spikes from the original dataset. However, we also found that the presence of a power law was not tightly linked to the average spike density (i.e., spike count per second in a given recording). Although, on average, the spike count per second was higher in the recordings with power law than in those with curved distributions of event sizes, the lowest spike density of all was found in a recording that also showed power law statistics. Thus power law can also be found with a low level of ongoing activity.

DISCUSSION

Identifying a critical state of a system, as it has been defined by Bak and others (Bak and Paczuski 1995; Bak et al. 1988; Jensen 1998), is a nontrivial task. Finding a power law in a distribution of events is apparently not sufficient proof of criticality, and other measures are necessary. Much importance has been assigned to long-range correlations between events and to scale invariance, i.e., persistence of the power law across different spatial and temporal scales. First, evidence suggesting the existence of critical dynamics in neural tissues, characterized as neuronal avalanches, was reported from the statistics of the spontaneous LFP activity in cultured neuronal networks and in acute cortical slices (Beggs and Plenz 2003, 2004). In particular, a power law distribution of the event sizes was found, irrespective of whether these sizes were defined as the number of LFP events or the sum of the amplitudes of these events. In addition, the distributions of the events' lifetimes partially obeyed a power law. These power law functions exhibited reliably exponents of −1.5 for event sizes and −2.0 for lifetime distributions, the empirically obtained values matching closely the theoretical predictions (Eurich et al. 2002; Zapperi et al. 1995). Also, the authors described long-range temporal correlations and robustness of power law statistics, when both spatial and temporal scaling operations were applied. The same results were recently obtained from ongoing activity in awake monkeys, suggesting the presence of critical dynamics in the nonanesthetized brain (Petermann et al. 2009). A power law organization of nLFP clusters was accompanied by correlations spanning several seconds in time. This organization also withstood scaling operations in nLFP amplitude threshold, which systematically removed ≤95% of nLFPs.

Our study attempted to expand these findings in two directions. First, we studied the properties of the spontaneous activity in the visual cortex in vivo, and second, we analyzed much more sparse signals based on neuronal spiking activity rather than relying on the LFP. Our results provided support for the conclusions offered by Beggs and Plenz (2003, 2004) and Petermann et al. (2009), but also provided additional information because of several differences between the in vitro and our in vivo results and also between LFP-based and spike-based analyses. We found that the spontaneous spiking activity in cat visual cortex can, under anesthesia, exhibit different types of distributions of spiking events. The distributions in some cases follow a power law, but in other cases, lack such statistics. Importantly, when the power law property was detected, it was found only across a certain range of values for the scaling parameter Δt, which is in contrast to our LFP analysis, where the power law was invariant to the chosen Δt, a scale-invariance characteristic for neuronal avalanches (Beggs and Plenz 2003). This result is similar to a previous study in vitro, in which power law statistics also depended on Δt (Pasquale et al. 2008). When in our data the value of Δt was chosen such that it was most optimal for minimizing concatenation and decomposition of events, the exponent of the power law distribution was highly consistent across different experiments. In these recordings, in which power law statistics was found for event sizes, lifetime distributions were the closest to, although did not fully exhibit, the power law statistics. A similar case was with the ISI distributions computed for an entire array (ISI_{array}), which also exhibited a power law in cases in which the event sizes did the same. Therefore we found evidence supporting the idea that the spontaneous activity in anesthetized brains is driven by processes that manifest power law statistics consistently across different measures and that are possibly based on cascades of neuronal events or so-called neuronal avalanches.

The exponent of avalanche size distribution was, however, somewhat smaller than that reported in previous studies and expected theoretically. We find consistently the value around −1.8 (as opposed to −1.5 reported previously). On the other hand, we found an exponent larger than −1.5 for LFP clusters for most of the investigated values of Δt (Fig. 2*B*). It is presently not clear how these differences in slope are related to

the type of used signals (spikes vs. LFP), why these results differed from the studies in vitro, and whether anesthesia played a role.

In three of eight recordings we did not observe a power law, but instead, a distribution of event sizes that exhibited an exponential-like distribution. The reasons for this variability in the results also need to be identified. One possible explanation of this finding is subsampling: The invariant presence of power law in LFPs suggests that avalanche-like behavior may exist also in all recordings of spiking activity but, because of the relatively small number of spikes recorded simultaneously, this property may not be detected easily or always (Priesemann et al. 2009). Our subsampling analysis points in a similar direction. Subsampling because of a too small number of electrodes (8) may be the reason that another recent study that recorded spiking activity in vivo did not find a power law distribution of event sizes (Bédard et al. 2006). However, there are also other possible explanations; as in this study, the electrode tips spanned much larger distances (1 mm), and the electrodes were aligned linearly.

At present, we cannot distinguish the subsampling explanation of the lack of power law from changes in cortical states. Spontaneous changes in the depth of anesthesia (Herculano-Houzel et al. 1999), possibly the result of a change in the concentration of acetylcholine (Rodriguez et al. 2004), may be a possible factor that underlies these changes in the properties of neuronal activity. Our findings that the shapes of auto- and cross-correlograms differed in recordings with and without power laws possibly suggest a role of state changes. This, however, does not explain why changes in power law would be observed only in spiking and not in LFP activity. A complete explanation will require accounting for this feature of our results. A similar problem is with a third class of explanation that may hypothesize changes in the statistical properties across different cortical layers. Again, if responsible for the lack of power law, one would expect this factor to affect LFP and spiking activity equally. This conclusion is supported by the finding that one of our arrays showed the differences in the presence of power law and correlations at two different time points, without moving the array to another position.

In this study, we investigated one more prediction. It is expected that cross-correlation analysis of avalanche activity shows correlations between events on a broad temporal scale (Beggs and Plenz 2003). Thus if avalanches are found in neuronal spiking activity, cross-correlation should not show a narrow center peak characteristic for neuronal synchrony associated with beta/gamma oscillations. Instead, one should observe a broad peak that reflects correlations that occur simultaneously at different time scales. This is what we found. Auto-correlation showed a similar internal structure of spike trains.

The functional implications of a putative critical state in the sensory areas remain elusive. Theoretical work (Kinouchi and Copelli 2006) reported that neuronal networks set at criticality display optimal sensitivity to stimuli, a finding that was experimentally confirmed using organotypic cultures (Shew et al. 2009). The preparation showed a maximum range of responses to stimulation by electric currents when nLFP clusters were distributed according to a power law. Possibly, the presence of power law in the visual cortex has a similar impact on processing visual stimuli.

Mechanisms other than self-organized criticality can generate a power law distribution of event sizes (Newman 2005; Plenz and Thiagarajan 2007). Touboul and Destexhe (2010) attributed the occurrence of a power law in nLFP clusters to stochastic dynamics, although with orders of magnitude steeper slopes. Our data leave open the possibility that the mechanisms that generate power laws in spiking and LFP activity are different, because we find different properties in the two types of responses. Further studies will be needed to identify the mechanisms responsible for power law distributions, or lack thereof, in different measures of neuronal activity.

In conclusion, this study provides evidence, for the first time, that not only LFP and spiking activity in vitro can exhibit power law statistics of event sizes, but the same can be the case for neuronal spiking activity recorded in vivo. These results suggest the possibility that neuronal avalanches are a common component of spontaneous brain dynamics and thus may also have implications in understanding how sensory inputs are represented and processed.

ACKNOWLEDGMENTS

We thank M. Wibral and V. Priesemann for useful discussions and for providing sand-pile simulation data on which we tested our computer code for data analysis.

GRANTS

This work was supported by the Hertie Foundation, the Max-Planck Society, a grant from Deutsche Forschungsgemeinschaft number NI 708/2–1, the Division of the Intramural Research Program of the National Institute of Mental Health, and the European Community's Seventh Framework Program (FP7) under grant agreement number PITN-GA-2009-237955.

DISCLOSURES

No conflicts of interest, financial or otherwise, are declared by the authors.

REFERENCES

Arieli A, Shoham D, Hildesheim R, Grinvald A. Coherent spatiotemporal patterns of ongoing activity revealed by real-time optical imaging coupled with single-unit recording in the cat visual cortex. *J Neurophysiol* 73: 2072–2093, 1995.

Arieli A, Sterkin A, Grinvald A, Aertsen A. Dynamics of ongoing activity: explanation of the large variability in evoked cortical responses. *Science* 273: 1868–1871, 1996.

Bak P, Paczuski M. Complexity, contingency, and criticality. *Proc Natl Acad Sci USA* 92: 6689–6696, 1995.

Bak P, Tang C, Wiesenfeld K. Self-organized criticality. *Phys Rev A* 38: 364–374, 1988.

Bédard C, Kröger H, Destexhe A. Does the 1/f frequency scaling of brain signals reflect self-organized critical states? *Phys Rev Lett* 97: 118102, 2006.

Beggs JM, Plenz D. Neuronal avalanches in neocortical circuits *J Neurosci* 23: 11167–11177, 2003.

Beggs JM, Plenz D. Neuronal avalanches are diverse and precise activity patterns that are stable for many hours in cortical slice culture. *J Neurosci* 24: 5216–5229, 2004.

Bringuier V, Chavane F, Glaeser L, Frégnac Y. Horizontal propagation of visual activity in the synaptic integration field of area 17 neurons. *Science* 283: 695–699, 1999.

Eurich CW, Herrmann JM, Ernst UA. Finite-size effects of avalanche dynamics. *Phys Rev E Stat Nonlin Soft Matter Phys* 66: 066137, 2002.

Ferezou I, Haiss F, Gentet LJ, Aronoff R, Weber B, Petersen CC. Spatiotemporal dynamics of cortical sensorimotor integration in behaving mice. *Neuron* 56: 907–923, 2007.

Gireesh ED, Plenz D. Neuronal avalanches organize as nested theta- and beta/gamma-oscillations during development of cortical layer 2/3. *Proc Natl Acad Sci USA* 105: 7576–7581, 2008.

Herculano-Houzel S, Munk MH, Neuenschwander S, Singer W. Precisely synchronized oscillatory firing patterns require electroencephalographic activation. *J Neurosci* 19: 3992–4010, 1999.

Jensen HJ. *Self-Organized Criticality*. Cambridge, UK: Cambridge University Press, 1998.

Kinouchi O, Copelli M. Optimal dynamical range of excitable networks at criticality. *Nat Phys* 2: 348–351, 2006.

Kenet T, Bibitchkov D, Tsodyks M, Grinvald A, Arieli A. Spontaneously emerging cortical representations of visual attributes. *Nature* 425: 954–6, 2003.

Mazzoni A, Broccard FD, Garcia-Perez E, Bonifazi P, Ruaro ME, Torre V. On the dynamics of the spontaneous activity in neuronal networks. *PLoS ONE* 2: e439, 2007.

Newman MEJ. Power laws, Pareto distributions and Zipf's law. *Contemp Physics* 46: 323–351, 2005.

Pasquale V, Massobrio P, Bologna LL, Chiappalone M, Martinoia S. Self-organization and neuronal avalanches in networks of dissociated cortical neurons. *Neuroscience* 153: 1354–1369, 2008.

Petermann T, Thiagarajan TC, Lebedev MA, Nicolelis MA, Chialvo DR, Plenz D. Spontaneous cortical activity in awake monkeys composed of neuronal avalanches. *Proc Natl Acad Sci USA* 106: 15921–15926, 2009.

Petersen CC, Hahn TT, Mehta M, Grinvald A, Sakmann B. Interaction of sensory responses with spontaneous depolarization in layer 2/3 barrel cortex. *Proc Natl Acad Sci USA* 100: 13638–13643, 2003.

Plenz D, Thiagarajan TC. The organizing principles of neuronal avalanches: cell assemblies in the cortex? *Trends Neurosci* 30: 101–110, 2007.

Priesemann V, Munk MHJ, Wibral M. Subsampling effects in neuronal avalanche distributions recorded in vivo. *BMC Neurosci* 10: 40, 2009.

Rodriguez R, Kallenbach U, Singer W, Munk MH. Short- and long-term effects of cholinergic modulation on gamma oscillations and response synchronization in the visual cortex. *J Neurosci* 24: 10369–10378, 2004.

Shadlen MN, Newsome WT. The variable discharge of neurons: implications for connectivity, computation, and information coding. *J Neurosci* 18: 3870–3896, 1998.

Shew WL, Yang H, Petermann T, Roy R, Plenz D. Neuronal avalanches imply maximum dynamic range in cortical networks at criticality. *J Neurosci* 29: 15595–15600, 2009.

Stewart CV, Plenz D. Inverted U-profile of dopamine-NMDA-mediated spontaneous avalanche recurrence in superficial layers of rat prefrontal cortex. *J Neurosci* 26: 8148–8159, 2006.

Stewart CV, Plenz D. Homeostasis of neuronal avalanches during postnatal cortex development in vitro. *J Neurosci Methods* 169: 405–416, 2008.

Teramae JN, Fukai T. Local cortical circuit model inferred from power-law distributed neuronal avalanches. *J Comput Neurosci* 22: 301–312, 2007.

Touboul J, Destexhe A. Can power-law scaling and neuronal avalanches arise from stochastic dynamics? *PLoS ONE* 5: e8982, 2010.

Tsodyks M, Kenet T, Grinvald A, Arieli A. Linking spontaneous activity of single cortical neurons and the underlying functional architecture. *Science* 286: 1943–1946, 1999.

Wu JY, Xiaoying H, Chuan Z. Propagating waves of activity in the neocortex: what they are, what they do. *Neuroscientist* 14: 487–502, 2008.

Xu W, Huang X, Takagaki K, Wu JY. Compression and reflection of visually evoked cortical waves. *Neuron* 55: 119–129, 2007.

Zapperi S, Bækgaard Lauritsen K, Stanley HE. Self-organized branching processes: ean-field theory for avalanches. *Phys Rev Lett* 75: 4071–4074, 1995.

7.2 Discussion

In this study, we investigated the presence of critical features in spiking and LFP data of anesthetized cat primary visual cortex. We found evidence for criticality in two thirds of the datasets in spiking activity and in the majority of datasets in the LFP. In the remaining one third of recordings power laws were absent similar to the results reported by Bédard et al. (2006). Notably, overall spiking correlations within the recorded neuronal population differed between cases with power law and those without. Datasets with power law statistics were in general more correlated with correlations that spanned longer time scales as opposed to recordings without power laws, whose correlations were weaker and less temporally extended. Further analysis revealed that the absence of power law in spiking activity can be explained by the sub-sampling hypothesis of spiking activity (Priesemann et al., 2009) which postulates that insufficient sampling of critical dynamics can destroy power laws. Since our multi-electrode only capture a fraction of the underlying neuronal activity (Buszaki, 2004), this hypothesis seems to be plausible. LFP represents the summed activity of the local neuronal population and is less likely to be affected by sub-sampling (Plenz and Thiagarayan, 2007), explaining our finding of power laws in the LFP of most datasets. However, we also put forth another hypothesis, which explains the mixed results by different cortical states and is based on our finding that the correlation structure in our data changes over time. In this framework, cortical activity would alternate between critical activity and more desynchronized dynamics without signs of criticality. This possibility will be further explored in the next chapter.

8 Neuronal Avalanches and Cortical State

Neuronal Avalanche Analysis of Different Cortical States in Vivo

Gerald Hahn[1], Cyril Monier[1], Giacomo Benvenuti[2], Arvind Kumar[3], Frédéric Chavane[2], Yves Frégnac[1]

[1] Unité de Neuroscience, Information et Complexité (UNIC), CNRS, Gif-sur-Yvette, France

[2] Institut des Neurosciences de la Timone, CNRS, Marseille, France

[3] Bernstein Center for Computational Neuroscience, Freiburg, Germany

8.1 Introduction

In 1949, Donald Hebb hypothesized that cognitive functions require an organized flow of neural activity from sensory to motor areas. He put forward the concept of cell assemblies which are formed by the spread and reverberation of excitation and are organized as phase sequences. More than half a century later, Hebbs idea of cascading neuronal activity is still appealing and found expression in the recent theory of neuronal avalanches (Beggs and Plenz, 2003; Plenz and Thiagarayan, 2007).

Neuronal avalanches are the manifestation of criticality in neural networks, a theory originating from physics which attempts to explain the emergence of complexity in a variety of natural and man-made systems (Bak, 1996). It predicts the occurrence of avalanche sizes at different spatial and temporal scales, which is captured quantitatively by power law distributions and long-range correlations. Critical dynamics are

positioned in between subcritical activity with dominant small avalanches and a supercritical dynamical state, in which activity is characterized by large avalanches that span the entire system. Criticality can be achieved by fine tuning of system parameters like during critical phase transitions in thermodynamical systems (e.g. Ising model, Brush, 1967). Critical features can also be the attractor of dynamical systems which is reached by self-organization (self-organized criticality (SOC), Bak et al., 1987). In this model, slow external input drives the system to a critical point at which small external perturbations trigger fast avalanche dynamics (Jensen, 1998). The complex spatiotemporal activity patterns observed in simulations of critical neuronal networks dynamics (Chialvo, 2010) have been suggested to endow the brain with optimal information processing (Bertschinger and Natschläger, 2004), optimal memory storage (Haldemann and Beggs, 2005) and a maximum dynamical range of stimulus responses (Kinouchi and Copelli, 2006). In particular, critical activity may provide the framework for neural communication between remote brain areas, as neuronal avalanches can easily bridge large distances through nearest neighbor interactions (Beggs and Plenz, 2003; Beggs, 2012) and small-world connectivity (Pajevic and Plenz, 2009).

Criticality predicts the presence of power laws and long-range spatiotemporal correlation in population brain activity (Chialvo, 2010) and both have been reported in local field potentials (LFP) of *in vitro* preparations (Beggs and Plenz, 2003; Shew et al., 2009; Yu et al., 2011) and *in vivo* recordings from anesthetized rats (Gireesh et al., 2008), anesthetized cats (Hahn et al., 2010) and awake monkeys (Petermann et al., 2009). Similar results were obtained in spiking activity recorded *in vitro* (Mazzoni et al., 2007; Beggs, 2008; Pasquale et al., 2008; Friedman et al., 2012) and *in vivo* during anesthesia (Hahn et al., 2010; Ribeiro et al., 2010). However, a number of studies did not find evidence for criticality, which has been either explained by insufficient sampling of neuronal avalanche activity due to the limited recording capacity fundamental to recording arrays (sub-sampling hypothesis: Priesemann et al., 2009; Ribeiro et al., 2010) or absence of critical neuronal dynamics (Bédard et al., 2006; Dehghani et al., 2012). In addition, the presence of power laws was disputed by rigorous statistical tests or explained by other mechanism than criticality (Touboul et al., 2010; Dehghani et al., 2012). Another hypothesis to account for the presence of power law and long-range correlation in some data, but absence in others, is varying cortical states (Hahn et al., 2010). A cortical state is defined by the amount of synchronized fluctuations within a population of neurons and can vary between the extremes of synchronized and desynchronized states (Harris and Thiele, 2011). Synchronized cortical activity is characterized by periods of strong neuronal firing (up-phases) followed by a phase of reduced or absent neural discharges (down-phases), while desynchronized dynamics display continuous and irregular spiking activity. Synchronized population bursts are a hallmark of *in vitro* activity (Plenz and Aertsen, 1996; Sanches-Vives and McCormick, 2000), slow wave sleep (Destexhe et al., 2007) and occur during anesthesia (Luszak et

al., 2007; Ribeiro et al., 2010). Large scale synchronization is also present in awake animals during quiet waking and drowsiness (Crochet et al., 2006; Poulet et al., 2008). Desynchronized activity is associated with active behavior (Okun et al., 2010; Poulet et al., 2012) and may also be a neuronal correlate of attention (Harris and Thiele, 2011).

According to the cortical state hypothesis, synchronized states show statistics that come closer to a power law, while desynchronized dynamics should show marked deviations from power laws. In the present study, we recorded spontaneous LFPs and spiking activity from the primary visual cortex of anesthetized cats (isoflurane) and awake monkeys in the dark, and systematically tested the differences of neuronal avalanche statistics across cortical states with different levels of population synchronization. In accordance with the hypothesis, we demonstrate that the tail of neuronal avalanche statistics in spiking activity is highly modulated by the cortical state in monkey and cat data with synchronized states coming closest to power laws. A similar modulation was found for LFP activity, but distributions close to power law were found in all states due to relatively strong population synchronization compared to spiking activity. Taken together the spiking activity results suggest a continuous switch between synchronized critical and desynchronized subcritical activity, while LFP activity indicates invariant criticality across all cortical states.

8.2 Materials and Methods

8.2.1 Preparation

Recordings were obtained from four anesthetized and paralyzed cats (isoflurane), and one awake monkey. The isolfurane concentration was kept at a constant value of ˜0.8%. Experimental protocols have been approved by the local ethical committee for animal research, and all procedures complied with the French and European regulations for animal research as well as the guidelines from the Society for Neuroscience.

8.2.2 Recording

We inserted 32 channel silicon-based micro-electrode arrays (four shanks with eight electrode contacts each, distance between electrode contacts: 400m, electrode contact impedance: 0.3-0.5 M at 1000 Hz, shank length: 3mm, Neuronexus Technologies, Ann Arbor, USA) into area 17 of four cats (one array per cat) and chronically implanted a Utah array (Blackrock Microsystems, Salt Lake City, UT, USA) into the primary visual cortex (near-foveal retinotopic region) of an adult macaque monkey (macaca mulatta - 10kg). The Utah array was composed of 96, 1 mm long, electrodes arranged in a

10 x 10 matrix with an inter-electrode distance of 400 microns. In both preparations, continuous spontaneous multiunit activity (sampling frequency: 30 kHz,) and local field potentials (LFP, sampling frequency: 1 kHz) were recorded with a Cerebus acquisition system (Blackrock Microsystems, Salt Lake City, UT, USA). For each cat we acquired one dataset lasting between 3900 and 6000 seconds, while four datasets of 600 seconds each were obtained in the monkey on four different days. The monkey was sitting in the complete dark, head fixated. For subsequent analysis the LFP was filtered between 1 and 100 Hz. Spikes were detected by manually setting a one-sided threshold that would result in a signal to noise ratio larger than ~2. Action potential waveforms were sorted and separated from remaining noise using the T-EM clustering algorithm and manual cluster cutting. (Offline Sorter, Plexon Inc, Dallas, USA). In the cat, spiking activity was extracted from an average of 21.5 +- 6.7 channels and in the monkey 8.75 +- 1.9 channels yielded spikes. Note that no attention was paid to extract single units, as during later analysis spikes from each electrode were pooled together into one population spike train. The electrode firing rate ranged between 0.61 Hz and 1.44 Hz (1.01 +- 0.38) in the cat and between 4.95 Hz to 7.32 Hz (6.31 +- 1.08) in the monkey recordings. The rates for the entire recordings were 20.64 +- 7.9 Hz for the cat data and 54.24 +- 10.57 Hz for the monkey. The cat recordings were performed with strongly reduced illumination (only the screen of the recording system was switched on), while any source of light was eliminated during the monkey recordings.

8.2.3 Separation of Cortical States

Cortical states and degrees of synchronization of neuronal activity can switch at a time scale of seconds (Harris and Thiele, 2011). In order to capture this fast dynamics a short time window of one second was chosen to analyze different synchronization levels in cortical activity. We based the separation of cortical states on differences in the frequency composition of the LFP between the one second segments. To this end we computed power spectra for each channel of a given segment with the multitaper method (see www.chronux.org) and averaged across all channels to obtain one spectrum per segment. Next, we split the power spectrum into 1 Hz frequency bins between 1 and 100 Hz and fed these 100 values as variables into a principal component analysis (PCA). As a result, we reduced the power spectrum of each segment to its first three principal components and each segment was represented by its position in a three dimensional PCA state space. In order to find segments with similar power spectra, we applied a k-means clustering algorithm with a different number of clusters (2-10 clusters) after normalization of each principal component to a value of 1. To determine the optimal number of clusters we validated the clustering results with the Dunn index (Dunn,

1973) according to the following formula:

$$DI = \min_{1 \leq i \leq n} \left\{ \min_{1 \leq j \leq n, i \neq j} \left\{ \frac{d(i,j)}{\max_{1 \leq k \leq n} d'(k)} \right\} \right\}$$

, with distance $d(i, j)$ between the centers of clusters i and j and distance $d'(k)$ between the center and elements of cluster k. This equation evaluates the compactness of clusters by calculating the ratio between the minimal distance between clusters to the maximal distance within clusters. The Dunn index was computed for the k-means results of each cluster number for a dataset and was averaged across all cat recordings and separately across all monkey datasets. The Dunn index reaches a maximum at the optimal cluster number and we hence identified five clusters for each cat dataset and four clusters for each monkey dataset (see Fig. 8.1F). The clusters of each recording were consistently color coded according to their position in the state space, such that the clusters were comparable across datasets and species. All the segments of a cluster were concatenated and used as separate datasets in subsequent analysis.

8.2.4 Correlation Analysis

To investigate the correlation characteristics of the recorded neuronal population, we pooled the spiking activity of all channels into one population spike train. Correlations were assessed by computing the auto-correlation histograms (ACH) and Fano factor curves of the population trains. An ACH was calculated for each 1 second segment and subsequently averaged across all segments of a cluster. We also subtracted a shift predictor that was calculated from the average of 100 randomly shuffled surrogates with the same firing rate to normalize the baseline for each segment. All ACHs were normalized to a center peak of one and quantified based on the peak amplitude (i.e. after removal of the peak at zero time lag) and the integral between the ACH curve and the baseline for time lags between -250 and 250ms. In order to allow a comparison between different datasets and species these measures were normalized such that the cluster with the maximum value for each dataset was set to one.

We estimated the Fano factor as $var(count)/mean(count)$of the population spike trains across time windows t within each one second segment and then averaged across all segments of a cluster. For the Fano factor curve we used t = 1, 2, 5, 10, 25, 100 and 200 ms. The Fano factor is a measure of synchrony between the spike trains constituting the population trains at a time scale given by t. A Fano factor of one indicates complete independence between the spike trains and is equal to the superposition of independent Poisson processes. Any synchronization between the neurons increases the variance of the spike count and thus the Fano factor becomes > 1.

We also estimated the correlation between spiking activity and the LFP by constructing spike triggered averages (STA) for each cluster of a given dataset. The STAs of all clusters and datasets showed negative deflection. LFP was z-scored and STAs were quantified by calculating the amplitude of the deflection peak and the integral of the negative deflection and the zero crossings. Like with the ACH, these two measures were normalized to the cluster with the maximum value which was set to one. In addition, correlations between the LFP signals of different channels were estimated by computing the average pairwise correlation coefficient between iLFPs (see below) of all channel pairs in a dataset.

8.2.5 Neuronal Avalanche Analysis

The spiking data were binned with bin size t and event clusters were defined as groups of consecutive bins containing at least one spike that were separated by empty bins. The cluster size is equal to the number of events within a cluster. In accordance with previous studies (Beggs and Plenz, 2003; Ribeiro et al., 2010), t was chosen as the average inter-spike interval of the population spike trains (also denoted as ISI_{pop}) which reflects a compromise between spurious concatenation of small clusters (large t) and separation of larger clusters (small t). Distributions of cluster sizes were plotted in log-log coordinates and further analyzed. We refer to this procedure as neuronal avalanche analysis.

In order to statistically characterize the distribution of cluster sizes s, we used maximum-likelihood estimation (MLE) to fit a lognormal distribution with the probability density function:

$$P(s, \mu, \sigma) = \frac{c}{\sigma s \sqrt{2\pi}} ^{-\frac{(\ln s - \mu)^2}{2\sigma^2}} ;\ \sigma > 0, \mu \geq 0$$

with scale parameter σ (sigma) and location parameter μ. Sigma gives an indication of the tailness of the estimated distribution with higher values signaling heavier tails and smaller values indicating lighter tails. Thus, this variable estimated how closely the cluster size distributions in different states approached a power law distribution:

$$P(s, \alpha) = cs^{\alpha}$$

with exponent α. The models were fitted over the entire range of cluster sizes s. In some cases we encountered a horizontal tale which we truncated before fitting to avoid a bias towards too high values of sigma.

Previous studies investigated neuronal avalanche properties of LFP by converting the continuous signal into a point process through thresholding and applying a neuronal avalanche analysis to the extracted event trains as described above (Beggs and Plenz,

2003; Petermann et al., 2009; Dehghani et al., 2012). In this study we chose a different approach and used integrals of negative LFP deflections as building blocks for the analysis. First, we z-scored the LFP and binned the data with varying bin-sizes t. Then, we computed the integral between the signal and the baseline (z-score=0) of each bin for a given channel that contained a negative LFP deflection, since these were associated with spiking activity. These integrals are referred to as iLFP in the rest of this study. Finally, we computed the sum of iLFPs for all channels in a given bin and studied the distribution of these summed iLFPs ($iLFP_{sum}$). In order to investigate the heavy tail properties of the $iLFP_{sum}$ distributions, we fitted gamma distribution, whose PDF is given by:

$$P(s, \alpha, \beta) = c\frac{s^{\alpha-1}}{\beta^{\alpha}\Gamma(\alpha)}e^{-\frac{s}{\beta}};\ \alpha > 0, \beta > 0$$

with shape parameter α(alpha), scale parameter β and the gamma function $\Gamma(\alpha) = \int_0^{\infty} t^{k-1}e^{-t}dt$. Alpha is <1 for heavy-tailed distributions and approaches a Gaussian function with $\alpha>1$, as expected from independence between LFP signals across recording channels (Dayan and Abbott, 2001).

We also calculated the inter-spike interval distributions of the population spike trains (ISI_{pop}) for all clusters of each dataset. The tailness of these distributions was measured by computing the coefficient of variation, defined as $std(ISI_{pop})/mean(ISI_{pop})$, for ranges between 0 and 100ms as well as 0 and 1000ms. Coincident spikes within the population spike trains were assigned an interval of zero.

8.2.6 Shuffling Analysis

We created surrogate data to test how correlations at different time scales contribute to the presence of heavy tails in spike cluster size distributions. The population spike trains of each cluster in a dataset were first jittered at three different bin-sizes (50ms, 100ms and 250ms). Then we created an inhomogenous Poisson process by randomizing spike times within each segment. The resulting spike train represented a non-stationary random process with fluctuations at a one second time scale. In addition, we constructed a homogenous Poisson process with the same firing rate as the given cluster dataset. For the iLFP analysis, we permuted the one second segments within each channel and thereby destroyed existing correlations between the electrodes.

8.3 Results

For this study, we recorded spontaneous spiking activity and local field potentials (LFP) from the primary visual cortex of four anesthetized cats (area17) and one awake monkey

(V1) using 32-channel silicon probes (cats) and a chronically implanted 96-channel Utah array (monkey) (Fig. 8.1A). To avoid interference of ongoing dynamics with visually evoked activity all recordings were performed in the dark. The LFP spectrogram of cat and monkey datasets showed non-stationary dynamics with fast and large power fluctuations in a frequency band between 1 and 15 Hz and prominent alpha oscillations (9-13 Hz) in the monkey recordings (Fig. 8.1B).

8.3.1 State Separation

In order to capture this variable dynamics, we attempted to pool short segments of the data into groups which are characterized by a similar frequency composition of the power spectrum. Each group is referred to as a different cortical state in accordance with previous studies (Okun et al., 2010; Renart et al., 2010; Harris and Thiele, 2011).

We first divided all the datasets into non-overlapping segments of one second and computed the power spectrum between 1 and 100 Hz for each segment separately with a frequency resolution of 1 Hz. The resulting 100 frequency variables per dataset were fed into a principal component analysis (PCA) and reduced to it first three principal components (PC). As illustrated in Fig. 8.1C, each component represented a different part of the frequency spectrum and differed mainly in a frequency range between 1 and 15 Hz. This result was consistent across all cat and monkey datasets. The first three principal components explained on average between 97% of the variance of the cat data and 99% of the monkey recordings (Fig. 8.1D). Next, we represented each data segment in a three dimensional principal component space and observed a characteristic pattern of segment clusters, which was similar across cat and monkey data. Most segments were concentrated at the origin of the PC space around which the remaining segments were scattered along the axis of the three components. Representative examples of this pattern are shown in Figure 8.1E. Then, we applied a clustering algorithm (k-means) to extract different clusters in each dataset. Since k-means requires to set the number of desired cluster manually, we fitted a varying number of clusters and validated the number of clusters with the Dunn index (DI) which measures the separation and compactness of a given number of clusters (see Materials and Methods section). The DI has a maximum at the cluster number with the best clustering and was found to peak on average at five clusters in the cat datasets and four in the monkey recordings (Fig. 8.1F). In order to compare states across different datasets and species, we coded clusters at the same location in the PC space with the same color (see the color code in Figs. 8.1E). Analysis of cluster duration revealed that the time the cortex spends in a specific state is asymmetrically distributed. Cortical activity is dominated by data segments in the central black cluster (on average 58% and 75% of the data in the cat and monkey, respectively), while the cortical dynamics represented in the other clusters is much less frequent (Fig. 8.1G).

Next, we computed the average power spectrum across all data segments in one cluster and the result confirmed that the separation algorithm extracted power spectra with a similar frequency composition across time (Fig. 8.2A). The black clusters consistently represented dynamics with little power in lower frequencies (1-5 Hz, delta band) as opposed to the red and green clusters in which the power in slower (red) or faster frequencies (5-15 Hz, green) was high. The blue and magenta clusters had intermediate power at slower frequencies approaching either the black or red cluster, respectively. In the subsequent analysis we will refer to the states with low power in slower frequencies as desynchronized states, high power in slower frequencies as slow synchronized states and high power in faster frequencies as fast synchronized state. The finding of power spectra with different power particularly in lower frequencies is in line with previous reports of a continuum of cortical states that lie in between the extremes of synchronized and desynchronized states (Curto et al., 2009; Okun et al., 2010; Harris and Thiele, 2011).

An example of spiking activity that was associated with each state is depicted in Figure 8.2B. This figure shows examples of LFP traces of one second duration for each state recorded in a cat along with the recorded spike raster and the evolution of the spike count in time. The firing properties of neurons change consistently with cortical state. During epochs of desynchronized LFP with small amplitude fluctuations the spiking activity is characterized by continuous and irregular firing of neurons without apparent synchronization across the different channels (black and blue cluster). When the LFP shifts to dynamics with larger amplitude fluctuations, the underlying firing pattern of neurons is characterized by burst of spiking activity that occur synchronously across all channels and are followed by periods of silence. The duration of these population bursts depends on the frequency of the LFP and is longer for slow frequency fluctuations (red and magenta clusters) and shorter for higher frequency modulations of the LFP (green cluster). Similar transitions from desynchronized to synchronized spiking activity were observed in the monkey (not shown).

To further quantify the relationship between spikes and LFP we computed spike-triggered averages (STA) for each dataset and cortical state. Two examples for a cat and a monkey for all states are shown in Figure 8.2C. In all cases spikes were associated with negative LFP deflections and their amplitude varied between states. In the desynchronized states the LFP peaks were small and thin, while they increased in amplitude and width in more synchronized cortical states. The synchronized cluster with faster deflections displayed peaks with the highest amplitude, but its width was smaller than synchronized states with lower frequency fluctuations. These results were confirmed across all datasets and both species, when the size of these peaks was measured based on their amplitude as well as the area between the negative deflection and the zero baseline (Fig. 8.2D). Thus, the dynamics of the LFPs is tightly linked with the underlying population spiking activity.

8.3.2 Spike Rate and Correlation Analysis

Next, we investigated the properties of the spiking activity in each state by comparing firing rates and correlation statistics between clusters. The mean channel firing rates across all cat and monkey recordings for a given state are illustrated in Figure 8.3A. It demonstrates that the firing rates consistently vary across different states, but show opposite behavior for the cat and the monkey data. In the anesthetized cat, more desynchronized states were associated with a low firing rate which increases as the state switches to more synchronized dynamics. In contrast, neurons in the awake monkey fired more vigorously during more desynchronized states and decreased their firing rate during synchronized activity. These results suggest that desynchronized activity in the cat may be due to a suppressive effect caused by the anesthetic agent (Isoflurane), while other mechanisms are at work in the awake monkey that both increase and decorrelate neuronal firing.

Then, we attempted to quantify the level of correlation in the population spiking activity. The spikes of all channels were thus pooled into one population spike train and different correlation measures were applied to study interdependence between spikes. First, we estimated the Fano factor (FF) for each state and across different bin-sizes which gives insight into the degree of synchronization between the neurons within the population. We found that the FF is close to one with very small bin-sizes (1ms) and increases with larger bin-sizes for cat and monkey datasets (Fig. 8.3B). However, this increase was larger for cats resulting in higher FF values than in the monkey. Importantly, the Fano factor differed across the various states in both species indicating different dynamics with fluctuating levels of correlations. The FF of the black cluster was on average small compared to the other clusters across all datasets and bin-sizes (Fig. 8.3C), while the FF was highest for the most synchronized clusters (red and green). The other clusters had FFs in between these two extremes. Similar results were obtained computing the auto-correlation histograms (ACH) of the population spike trains for each state. As shown in Figure 8.3D, the red and green clusters were accompanied by center peaks with much larger amplitude and area compared to the black cluster. Similar to the FF the other clusters showed center peaks with height and area in between the largest and smallest peaks. This result was consistent across all datasets and species, as illustrated in Fig 8.3E which shows the average ACH peak amplitude and area across datasets. In conclusion, these findings are congruent with the STA results and indicate the presence of highly correlated spiking activity between different recording channels during large LFP deflections and decreased correlation during episodes of desynchronized LFP.

8.3.3 Neuronal Avalanche Analysis of Spiking Activity

Systems in a critical state generate highly correlated population events (avalanches, Bak et al., 1987) that are characterized by power law distributions in various measures (Lowen and Teich, 2005). Beggs and Plenz (2003) introduced a new measure to detect power law scaling which was used in many subsequent experimental (Petermann et al., 2009; Hahn et al., 2010; Ribeiro et al., 2010) and theoretical studies (Priesemann et al., 2009; Benayoun et al., 2010; Rubinov et al., 2011). This algorithm is based on binning point processes like spike trains and extracting clusters defined as consecutive bins with a least one event separated by empty bins (Fig. 8.4A). The cluster size is then given by the sum of event counts in all bins of a cluster. Size distributions are plotted in log-log coordinates (shown here with logarithmic binning for better illustration) and their shape analyzed for power law (detected as straight line in log-log plot). In this study, we used the same algorithm to investigate neuronal avalanche properties of different cortical states. Figure 8.4B illustrates examples of cluster size distributions for all separated dynamical clusters in cat and monkey recordings. The distributions of the most desynchronized clusters (black solid lines) were visibly curved and did not follow a power law. However, moving from desynchronized to more synchronized clusters, the tail of the cluster size distribution increased and came closest to a power law in the most synchronized clusters (red lines). This pattern was evident in both cat and monkey data, and indicated a state dependent modulation of the tail of the cluster distribution.

Previous studies attempted to compare the goodness of fit for power laws and various other distributions to measure the presence of criticality in neuronal network dynamics such as the exponential distribution (Hahn et al., 2010; Ribeiro et al., 2010; Klaus et al., 2011). Here, we use a different approach and quantify the size of the cluster distribution tail to measure how close a given distribution comes to a power law. To this end we fitted a lognormal function to the cluster size distributions and estimated its scale parameter sigma, whose value is an indication of the distributions' tailness. A high value of sigma indicates a heavier tail than lower sigmas. Note that we avoid testing the presence of a mathematical power law, as proposed by previous studies (Clauset et al., 2009) and rather compare the tailness of the distributions across different states based on sigma values of fitted lognormal distribution. Therefore, we calculated cluster size distributions for each state and estimated sigma which was subsequently averaged across all datasets of a species. The results are shown in Figure 8.4C. Similar to the STA and correlation results, sigma was the lowest in the desynchronized black clusters and increased with the degree of correlation present in the recorded neurons. The clusters with the highest degree of synchronization (red) also had the heaviest tail and hence came closest to a power law. We fitted a power law to the red clusters using liner regression in logarithmically binned distributions and estimated the exponent alpha.

Interestingly, the average exponent for each species varied around the experimentally found and theoretically predicted value of -1.5 (cats: 1.62+-0.15, monkey: 1.42+-0.23; note that in one monkey dataset alpha was 1.12, which explains the larger SD) (Zapperi et al., 1995; Eurich et al., 2002).

We also investigated how close the dynamics in the desynchronized black clusters was to a random Poisson process as expected from an asynchronous irregular state (Renart et al., 2010; Tetzlaff et al., 2012). To this end we first jittered the original data at different time scales and created an inhomogenous Poisson process by randomizing the spike times within each one second segment of a state cluster. This allowed us to study the contribution of rate non-stationarity across different segments to the tail of the black clusters. Finally, we replaced the original spike train by a homogenous Poisson process, in which rate modulations at longer time scales were destroyed. Lognormal functions were fitted to all surrogate data and sigma estimated for comparison across these different types of shuffling. The results for each cluster were averaged across all datasets of a species and are shown in Figure 8.4D. In the cat, jittering at increasing time scales revealed the presence of remaining correlations within each data segments indicating that the black clusters do not represent fully desynchronized states. In contrast, jittering in the monkey recordings had little effect on the tail of the cluster size distributions suggesting the absence of correlations at this time scale. However, a clear difference in tailness between the homogenous and inhomogenous Poisson process was found for both the cat and monkey data. This is a clear indication that a significant part of the tail in the black clusters originated from rate inhomogeneities across different one second samples. This non-stationarity dominates in the black clusters of the monkey data and contributes to the tail in the cat recordings along with correlations at shorter time scales. In conclusion, these findings reveal that even though statistical analysis suggests the absence of heavy tails and correlations at short time scales (<1s), tails may still arise from correlations at longer time scales due to rate fluctuations.

So far we have found that the level of LFP fluctuations influences the amount of correlations within the population spiking activity. In addition, the degree of spike synchronization determines the tail of cluster size distributions. We quantified the correlation between the LFP fluctuations represented by the STA area and the population synchrony in spiking activity measured by the area of the population ACH. Figure 8.5A shows that as the LFP peaks become larger, the ACH area and thus the mean spike synchronization increases as well. Likewise, the tail of the cluster size distributions and sigma grow with increasing population correlation in spiking activity. Hence, the size of the LFP fluctuations is directly translated into the degree of synchronization in spiking activity and consequently the tail of the spike cluster size distributions. As the LFP varies with cortical state, the results of the neuronal avalanche analysis change from more power law like to more curved distributions indicating the absence of correlated population activity.

8.3.4 State Dependence of ISI_{pop} Distributions

Previous studies reported power laws in the inter-spike interval distributions of individual neurons (Teich et al., 1997; Safonov et al., 2010) and spike trains of neuronal populations (Segev et al., 2002; Hahn et al., 2010). In this study, we also compared inter-spike interval distributions of population spike trains (ISI_{pop}) for each dynamical cluster (Fig. 8.5B). The tail of the distributions was measured by the coefficient of variation (CV) for a shorter interval range of 0-100ms and a longer range of 0-1000ms. Visual inspection showed a straight line in synchronized states of the cat data between ISI_{pop}= 5ms and ISI_{pop} = 100ms, while desynchronized clusters were more curved. In this interval range the average CV across all cats for the black, most desynchronized activity was ˜ 1, indicating a Poisson process, while the CV in the other clusters was slightly above this value (Fig. 8.5C). As visible in Figure 8.5B, marked tails occurred and differed the most between clusters at intervals $>$ 100ms. The CV not only increased in all clusters, but showed a pattern similar to the previously computed average Fano factors and ACH statistics. In the monkey recordings, ISI_{pop} distributions were curved in all clusters up to intervals of ˜50ms (Fig. 8.5B) and the CV was close to 1 in an interval range until 100ms even in synchronized states (Fig. 8.5C). However, heavy tails were found for intervals $>$ 100ms in more synchronized states, while a tail was absent in the black cluster. Likewise, the CV for the most desynchronized cluster remained close to one, while it increased in synchronized clusters, showing a CV distribution similar to the cat recordings. In conclusion, ISI_{pop} distributions also exhibit state dependent tails, which resemble those in other statistics of spiking activity.

8.3.5 Neuronal Avalanche Analysis of LFP

First evidence for neuronal avalanches accumulated in LFP data from *in vitro* (Beggs and Plenz, 2003) and later also *in vivo* recordings (Petermann et al., 2009). These studies established a new method that transforms the continuous LFP signal into a point process by thresholding the LFP and extracting events (so called nLFPs), whenever the signal crosses the threshold. The resulting discrete data were subsequently analyzed with correlation and neuronal avalanche statistics. However, the thresholding approach extracts only a fraction of the original signal and discards all LFP fluctuations that lie below the threshold. Especially desynchronized cortical dynamics with only small LFP deflections may be neglected by this method. Moreover, introducing a threshold may generate spurious power laws as demonstrated by a recent study (Touboul and Destexhe, 2010). In order to avoid these shortcomings, we employed a different approach that takes the entire LFP signal which is associated with spiking activity into account. The new method is illustrated in Fig. 8.6A (top) based on two channels. We first binned the z-scored LFP data with varying bin-size t and then calculated the integral

between the signal and the zero baseline within each bin (black and grey areas). These integrals are denoted as iLFP. As spiking activity is in general associated with negative LFP deflections (see Fig. 8.2C), we restricted our analysis to negative fluctuations of the signal. Then we summed up the integral of all channels in a given bin (Fig. 8.6A, bottom) and plotted the distribution of the summed iLFPs ($iLFP_{sum}$) for further analysis.

First, we investigated the correlation structure between iLFPs and calculated the mean correlations coefficient (CC) across all channel pairs. The results for the cat and monkey data are shown Figure 8.6B (t = 25ms). The mean correlation between electrodes was generally high and ranged between 0.87 and 0.94 in the cat and between 0.73 and 0.85 in the monkey data. Notably, the correlation was graded between the different states and showed a pattern similar to the spiking activity. This means that the average CC was lowest in the black desynchronized cluster and increased with the size of the LFP fluctuations in cat and monkey recordings. This indicates a state dependence of correlated dynamics also in LFP signals despite the overall high levels of correlation.

Next, we investigated the statistical properties of the $iLFP_{sum}$distributions. Examples for cat and monkey distributions calculated with different values of t are displayed in Figure 8.6C. As a reference, we also plotted the segment shuffled surrogate of the black cluster, where all spatial correlations between the electrodes were destroyed and the $iLFP_{sum}$ distribution approached a Poisson distribution in accordance with theory (Dayan and Abbott, 2001). In the cat recordings, the distributions of all clusters followed a straight line for all tested t and significantly deviated from the shuffled data. Importantly, this straight line showed a cut off at smaller bin-sizes, which was smaller for the more desynchronized states and higher in synchronized clusters. This cut-off moved to larger $iLFP_{sum}$ sizes, as t increased, resulting in a straight line that stretched about three orders of magnitude. With very large t (>100ms), the distributions started to become markedly bell-shaped and approached a Poisson distribution (not shown). The monkey data displayed similar results except that the $iLFP_{sum}$distributions started to converge to the Poisson distribution at smaller values of t (˜50ms). In addition, the initial part of the distribution (iLFP size < 10ms) became more curved with increasing t, while the tails were preserved and also extended up to three orders of magnitude.

Then, we fitted a gamma distribution to the $iLFP_{sum}$ distributions in order to quantify potential differences in their tail across different states. The shape parameter alpha of the gamma distribution was used to estimate these tails. Alpha <1 indicates heavy tails, while distributions with alpha >1 approach a Gaussian distribution, which comes closer to the segment shuffled distributions. In Figure 8.6D, alpha is plotted as a function of state and t. For both monkey and cat data, alpha remained well below one for smaller t indicating the presence of heavy tails. As t increased, alpha also rose and became larger than one for very large t (200ms). Interestingly, differences for alpha

across different states were similar to those already observed for the various statistics of the spiking activity above. In general, the black clusters had the largest values of alpha, while alpha decreased in clusters with higher levels of synchronization. Thus, despite the presence of heavy tails for a large range of t, the degree of the tailness varied as a function of the cortical state.

8.4 Discussion

Even though the presence of power laws and long-range correlations is widely accepted at the macroscopic scale (see Werner, 2010 for review) and the single cell level (Teich et al., 1997; El Boustani et al., 2009), the existence of criticality and avalanche dynamics at the mesoscopic scale is still under debate. A number of previous studies have reported power laws in local field potentials from various *in vitro* (Beggs and Plenz, 2003; 2004; Shew et al., 2010; Stewart and Plenz, 2006; 2008; Shew et al., 2009; 2011) and *in vivo* preparations (Gireesh et al., 2006; Petermann et al., 2009; Hahn et al., 2010), while a recent study questioned the presence of power laws in LFPs of awake monkeys, cats and humans (Dehghani et al., 2012). In spiking activity, researchers have found evidence for criticality in slices and cultures (Mazzoni et al., 2007; Pasquale et al., 2008; Beggs, 2008; Friedman et al., 2012), but recordings from intact animals drew a more complicated picture. A first report from awake and sleeping cats discovered more exponential distribution rather than power laws (Bédard et al., 2006), a finding which was further substantiated by Dehghani et al. (2012). However, two other studies reported both the presence and absence of power laws in multi-electrode recordings coming from the same animal (Hahn et al., 2010; Ribeiro et al., 2010). In the first study, power law statistics changed over time during halothane anesthesia in cats (Hahn et al., 2010), while in the second study (Ribeiro et al., 2010) power laws emerged only during ketamin-xylazin anesthesia and were replaced by lognormal distributions in behaving and sleeping rats. Petermann et al. (2009) also analyzed spiking activity in awake monkeys, but initially did not find a power law. Only when units that were synchronized within an electrode, as indicated by significant correlations in the CCH, were used for analysis, the spike cluster distribution became heavy-tailed, albeit not showing a full power law. The results of these studies raised the question about the causes for the presence of curved distributions rather than power laws and absence of correlations in spiking activity under certain conditions.

One line of argument to explain the lack of power law statistics revolves around sub-sampling cascading events of a critical system. Multi-electrode recordings inevitably sample only a very small and random fraction of the spiking activity in the neuronal network, while the remaining spiking events of a potential power law process remain hidden (i.e. they are deleted from the fully-sampled spike train). As pointed out by

Lowen and Teich (2005), power laws are gradually replaced by curved distributions, when events are randomly removed from a point process like spiking activity. Indeed, random deletion of spikes from spike trains in awake monkeys (Petermann et al. 2009) and anesthetized cats (Hahn et al. 2010) yielded similar results. A similar case has been made by Priesemann et al. (2009) for datasets in awake monkeys and Ribeiro et al. (2010) in awake and sleeping rats. They put forward sub-sampling of neuronal events to account for absence of power law in their data. According to the sub-sampling hypothesis, avalanches do not spread or spread only partially through the area sampled by the electrodes. An avalanche may also be cut and sampled as several smaller avalanches. As reviewed by Cohen and Kohn (2011) correlations need to be interpreted carefully and are not only a result of neuronal network dynamics, but also subject to measurement problems imposed by the experimental setup. In particular, using spike trains with only few spikes is prone to yield only small correlations. This effect is exacerbated by spike-sorting errors that erroneously eliminate spikes from individual neurons (Pazienti and Grün, 2006). Within this framework, the sub-sampling argument may be viewed as insufficient capturing of existing correlations that are generated by critical avalanche dynamics. This insufficiency is caused by using arrays with too few electrodes and with large inter-electrode spacing. As a consequence, an inadequate number of spikes is recorded to reach a level of spatiotemporal correlations that shows power law distributions.

An alternative explanation for curved distributions is that the recorded dynamics is indeed subcritical and does not create correlations and power law statistics as expected from a critical state. To date, a number of neuronal network models have described such dynamics, in which neurons are continuously active with irregular firing and mean correlation close to zero. (van Vreeswijk and Sompolinsky, 1996; Destexhe, 2009; Renart et al., 2010; Benayoun et al., 2010; Tetzlaff et al., 2012). This dynamics was coined asynchronous irregular (AI state; Brunel, 2000). The hallmark of these networks is that the AI regime results from a correlation between excitation and sufficiently strong and fast inhibition, such that excitation is prevented from spreading as it is rapidly tracked by inhibition (Renart et al, 2010; Tetzlaff et al., 2012). In this case, the network activity, even if all spikes are sampled, is characterized by statistics that resemble more a Poisson process than highly correlated critical dynamics. Accordingly, the lack of avalanche dynamics leads to subcritical distributions in this type of network (El Boustani et al., 2007). Recent experimental evidence suggests that cortical networks *in vivo* can indeed display asynchronous irregular firing with mean correlations near zero (Ecker et al., 2010; Renart et al., 2010). Importantly, the dynamics of these networks can change to synchronous population burst activity (Brunel, 2000), whose size distribution can follow a power law within a certain parameter range (Benayoun et al., 2010). A similar switch between asynchronous and synchronous cortical dynamics can be seen in anesthetized preparations (Clement et al., 2008; Renart et al. 2010)

and underlies the transition between awake/REM state to SWS state (Destexhe et al., 2007). Notably, even in the awake state, epochs of desynchronized and synchronized activity can be distinguished depending on the behavioral state of the animal (Crochet et al., 2006; Poulet and Petersen, 2008). However, it has been argued that the cortex can produce various states showing different levels of synchronization with the asynchronous and synchronized state representing only two extremes of a continuum (Curto et al., 2009; Okun et al., 2010; Harris and Thiele, 2011).

As discussed by Harris and Thiele (2011) synchronized states are characterized by population bursts of spiking activity (up-phases) which are followed by periods of absent or reduced neuronal firing (down phases). Both phases last ˜100ms and are accompanied by high power in slow frequencies (<5 Hz). In contrast, these frequencies are suppressed in desynchronized states and spiking activity is tonic and irregular without any apparent structure in the population activity. Importantly, the average correlation between neurons is positive in more synchronized states, while mean correlation in the desynchronized state is close to zero. Similar differences in the correlation structure of spiking activity and cortical state have been found over the course of Halothane anesthesia in the primary visual cortex of the cat (Hahn et al., 2010) and hypothesized to be the reason for the presence of power law in some and absence in other recordings. In this study, we further tested this hypothesis and systematically separated different dynamical states in dark room recordings from the primary visual cortex of anesthetized cats (isoflurane) and awake monkeys. We found that LFP power highly fluctuated in both cat and monkey recordings and we delineated four to five classes of cortical states which differed in their mean power in the LFP at slower (1-5 Hz) and higher frequencies (5-15 Hz). Dynamics with high power at slower and faster frequencies were associated with population bursts in spiking activity followed by periods of silence (synchronized state), while lower power entailed continuous, irregular and unstructured neuronal firing. As cortical activity moved from more desynchronized to synchronized dynamics, average correlation and fluctuation depth (measured by the ACH of the population spike train and the Fano factor) increased to reach a maximum in the most synchronized states. Importantly, the cortex in cats and monkey data spent more than 60% in more desynchronized states, which were interrupted by occasional periods of highly synchronized activity. We then conducted a neuronal avalanche analysis and instead of quantifying the goodness of fit for power laws we estimated the tail of the obtained cluster size distributions by the scale parameter sigma of fitted lognormal distributions. As hypothesized, sigma was indeed a function of the cortical state. It was high in synchronized states coming closer to a power law and smaller in desynchronized dynamics with more curved distributions. Likewise, the tail and coefficient of variation of population inter-spike intervals increased with more synchronization and was lower in more desynchronized states. Moreover, we found that despite the absence of correlation and large fluctuations in short time periods within the most desynchronized state, non-

stationarity of firing rate can significantly increase the tail of cluster size distributions. These findings not only hold for the anesthetized cat recordings, but were similar in the monkey indicating that heavy-tailed distributions can be found in the awake monkey, if synchronized activity is selectively extracted from the data. Note that these tails are expected to be averaged out if the whole recording is used for analysis, since most activity is rather desynchronized. This may partially account for previous reports of curved distributions in awake animals, in which epochs of synchronized and desynchronized activity were not separated (Ribeiro et al., 2010; Deghani et al., 2012). In summary, these results indicate that the dynamical state and its correlation profile has a strong impact on various distributions previously used to test for criticality and state differences may indeed explain the presence of both, power law and subcritical distributions in spiking data of *in vivo* recordings.

We also looked for state dependent modulation of correlations and tails in the LFP of the cat and monkey data. Similar to the spiking data, average correlations between negative LFP deflections across all channels were higher in synchronized than in desynchronized states. However, the overall correlation in the LFP signal was very high (>0.7). This may explain why we found heavy tails that came close to power laws in all separated states, even the most desynchronized one. However, even these tails were modulated by the state, when quantified by the shaping parameter of a fitted gamma distribution, with synchronized states being slightly more heavy-tailed than desynchronized dynamics. A similar dichotomy between the results in spiking activity and LFP has been described previously by a number of studies (Petermann et al., 2009; Hahn et al., 2010; Dehghani et al., 2012). An important question is whether the strong correlations in the LFP are partially confounded by spurious signals originating in volume conduction, as proposed by Dehghani et al. (2012). Alternatively, the LFP might sample much larger portions of the underlying neuronal signal than the spiking activity and absence of power law in desynchronized states in neuronal firing is indeed a consequence of sub-sampling as outlined above. In this case, one would expect a decrease of population firing rate as the synchronization level goes down, which is true for the cat recordings in this study. However, in the monkey data the firing rate is on average the highest for the most desynchronized state and thus more spikes are available to capture potential correlations. All the same, correlations decrease making sub-sampling a less likely candidate mechanism to account for curved distributions in the monkey.

Our findings suggest that the cortex can switch between different cortical states that either resemble synchronized dynamics in critical systems or approach a more asynchronous dynamical regime without long range correlations typical for critical cascading dynamics. Several mechanisms have been suggested that enable the cortex to make transitions between varying states (for review see Harris and Thiele, 2011). Synchronized states have been interpreted within the framework of excitable media (Curto et al., 2009), in which recurrent excitation builds up and spreads as a traveling wave

through the network, analogous to avalanches in critical systems. The spread of excitation stops, when it is counterbalanced by various mechanisms that decrease the efficacy of excitatory transmission between neurons. These adaptation mechanisms include synaptic depression (Tsodyks and Markram, 1998; Rigas and Castro-Alamancos, 2009), depletion of ATP (Cunningham et al., 2006) and increase in K+ conductances (Sanchez-Vives and McCormick, 2000). Interestingly, several modeling studies have highlighted the role of resource depletion and synaptic depression in the emergence of self-organized critical states linking critical dynamics directly with synchronized cortical states (Levina et al., 2007; Millman et al., 2010). The synchronized up-down dynamics is also the most prevalent type of activity in cortical slices and cultures (Plenz and Aertsen, 1996; Sanches-Vives and McCormick, 2000; Timofeev et al., 2000). It is thus not surprising that the first evidence for criticality came from these preparations (Beggs and Plenz, 2003; 2004; Stewart and Plenz, 2006), as they generate activity with large spatio-temporal correlations in line with predictions from criticality theory (Jensen et al., 1998; Chialvo, 2010).

Desynchronization is mediated by various neuromodulators like acetylcholine (Buszaki et al., 1988; Manns et al., 2000; Goard and Dan, 2009; Lucas-Meunier et al., 2009), serotonine (Vanderwolf et al., 1986) and noradrenaline (Constantinople et al., 2011). Studies on criticality in slices so far have not tested the impact of these neuromodulators, but rather inhibited excitation directly to produce hypoexcitable, subcritical states (Beggs and Plenz, 2003; Mazzoni et al. 2007; Gireesh et al., 2008; Shew et al., 2009; 2011; Yang et al., 2012). Only in one study, acetylcholine was applied to cultured networks of leech ganglion neurons and a transition was found from synchronized bursting activity with power law distributions to continuous irregular firing with decreased population synchrony and subcritical distributions (Pasquale et al., 2007). Another mechanism to reduce synchronous population fluctuations in neural activity was recently found in a study by Poulet et al. (2012) which reported an increase in thalamic firing rate as an important driver of desynchronized activity in the barrel cortex of awake rats during whisking. According to the theory of self-organized criticality, a sufficiently slow drive is necessary to trigger avalanches with power law distributions (Bak, 1996). If the external drive is too strong, avalanche dynamics are destroyed and criticality abolished (Jensen, 1998). Accordingly, a recent theoretical paper observed a transition from critical to asynchronous dynamics in a neuronal network model, when external drive to the network was increased (Benajoun et al., 2010). Thus, from the standpoint of criticality theory, it is not surprising that increased external input from the thalamus induces a switch from critical to subcritical and desynchronized activity.

A variety of functions have been attributed to criticality in neuronal networks (Beggs, 2008; 2012; Shew and Plenz, 2012), among which enhanced neuronal communication plays an important role. In this framework, neuronal avalanches create dynamic correlations between remote brain areas and allow for effective exchange of information.

In contrast, subcritical avalanches would remain too small to link more distant neural networks, while supercritical dynamics would rather spread across the entire brain and thus prevent selective communication. According to this hypothesis, one would expect that cortical processing and communication is optimized during more synchronized cortical states. However, evidence form the experimental and theoretical literature suggests a different scenario. First, synchronized states in the awake state are prevalent in drowsy and immobile animals that are not engaged in a task (Petersen et al., 2003; Luszak et al., 2007; 2009; Okun et al., 2010). In contrast, desynchronization of cortical activity has been associated with active behavior (Crochet and Petersen, 2006; Poulet and Petersen, 2008; Niell et al., 2010) and reduction of slow frequency fluctuations in local cortical networks has also been observed during attention (Fries et al., 2001; Khayat et al., 2010). Moreover, gamma oscillations, a prominent candidate of cortical communication (Fries, 2005), have been reported to predominately occur during the desynchronized cortical state (Munk et al., 1996; Herculano-Houzel, 1999). In general, global synchrony has been regarded as detrimental for coding and information processing (Zohary et al., 1994; Shadlen and Newsome, 1998; Kumar et al., 2008), while fine grained synchronization between groups of neurons established within coherent gamma oscillations might be used to faithfully process and transmit information (Siegel et al., 2011). Likewise, studies on feedforward networks, another framework for neuronal communication, found that propagated patterns of synchrony can only be read out in other brain areas during desynchronized states, while these synchronous spiking patterns disappear in more synchronized background activity (Kumar et al., 2008). These results indicate that large population fluctuations and global synchrony need to be suppressed in order to allow specific activity patterns to be propagated and read out by distant cortical networks. However, it is conceivable that slower fluctuations in cortical activity modulate the emergence of fine grained activity patterns, a phenomenon which has been recently studied within the context of frequency coupling. According to this framework (Buszaki and Wang, 2012), slower oscillations (e.g. in the alpha band) determine the phase and amplitude of higher frequency oscillations (e.g. in the gamma band). Thus, larger scale synchronization may determine which brain areas can be coupled through more precise communication. Further studies are required to disentangle the role of global synchronization and asynchronous activity in cortical networks.

The present study revealed that only epochs of cortical activity with population synchronization are consistent with criticality and a large part of cortical activity reflects more desynchronized dynamics. Interestingly, a similar conclusion has been reached by a recent fMRI study that described both critical and non-critical dynamics in resting state activity of humans (Tagliazucchi et al., 2012). Taken together, these results indicate that the cortex evolved mechanisms to synchronize and desynchronize its activity according to computational needs, thereby switching continuously between critical and more asynchronous dynamics.

8.5 Figures

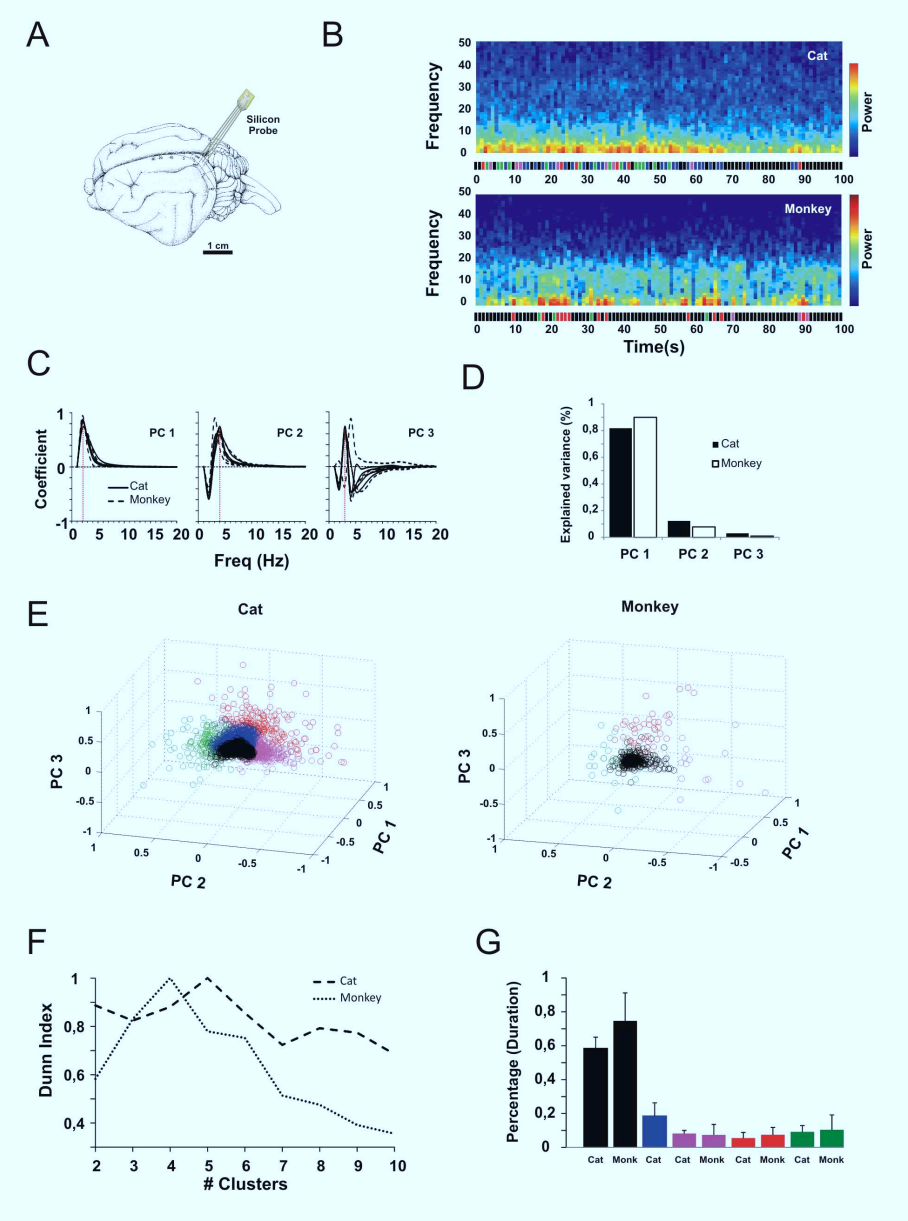

Figure 8.1: Separation of cortical states in spontaneous activity of anesthetized cat and awake monkey. A: Recording position in primary visual cortex (anesthetized cat: 32 channel silicon probes). (B) Spectrograms of two 100s segments computed with non-overlapping windows of 1s. Bottom: colored bars indicate cortical state as defined below. C: Coefficient for first three principal components as a function of power spectrum frequency. D: Variance explained by the first three principal components. E: Principal component space for two entire datasets (cat: 6000s, monkey: 600s). Each circle represents a data segment of 1s duration. Colors indicate different cortical states. F: Dunn index as a function of cluster number extracted by k-means. G: Average (+SD) duration of different states across all datasets of a species.

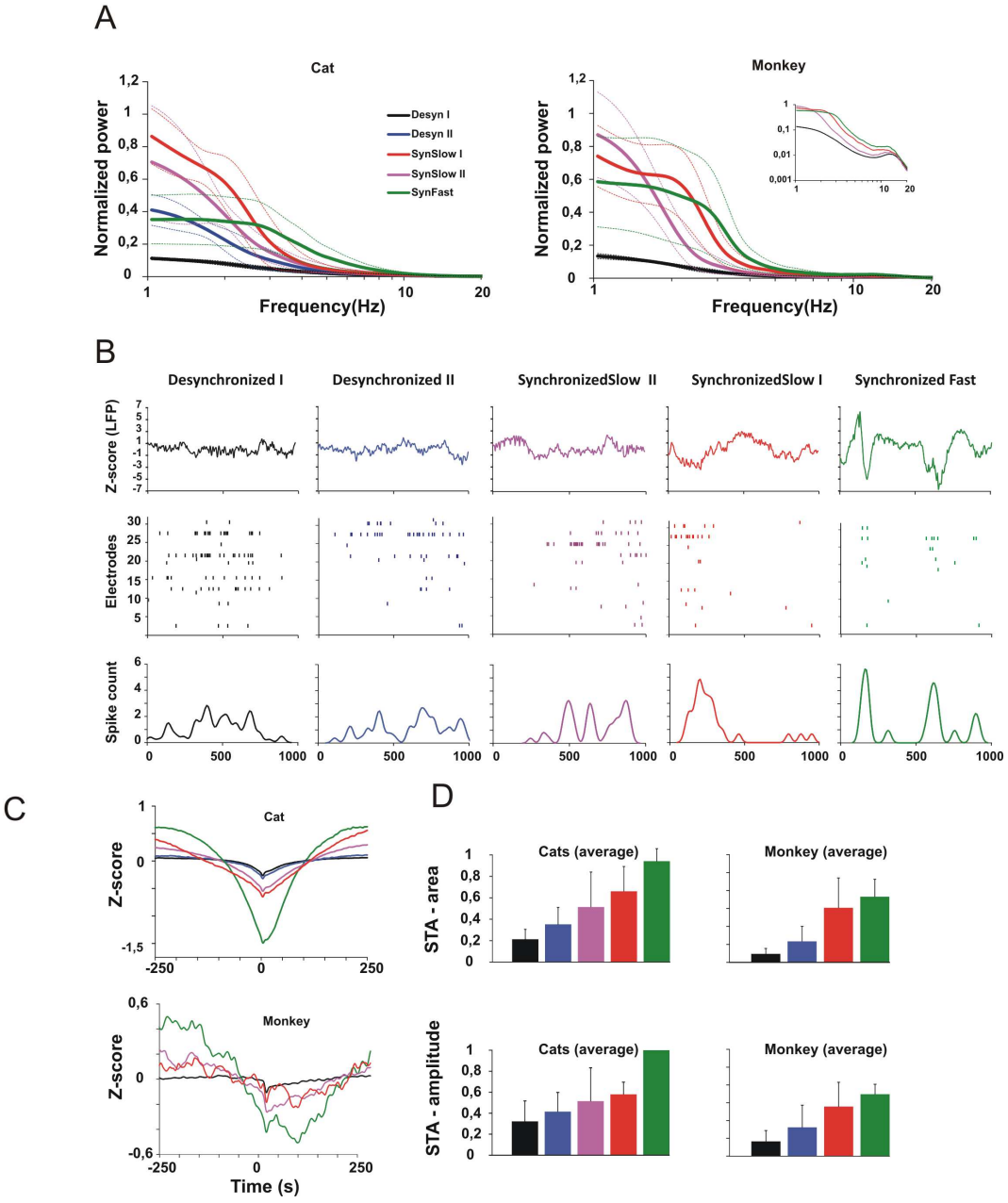

Figure 8.2: Characteristics of LFPs and LFP-spike relationship for different cortical states. A: Power spectrum of different cortical states for a cat and monkey dataset. Dashed lines indicate standard deviation (+-SD). Inset: same as in main figure, but in log-log coordinates to show peak in alpha band. B: LFP, spike raster plots and spike count for 1s segments of cortical states from one cat dataset. Spike counts were computed with a Gaussian kernel (20ms window). C: Examples of spike-triggered averages (STA) for different cortical states. D: Average (+SD) STA area and amplitude across all cat and monkey datasets. Area and amplitude are normalized to the dataset with largest value.

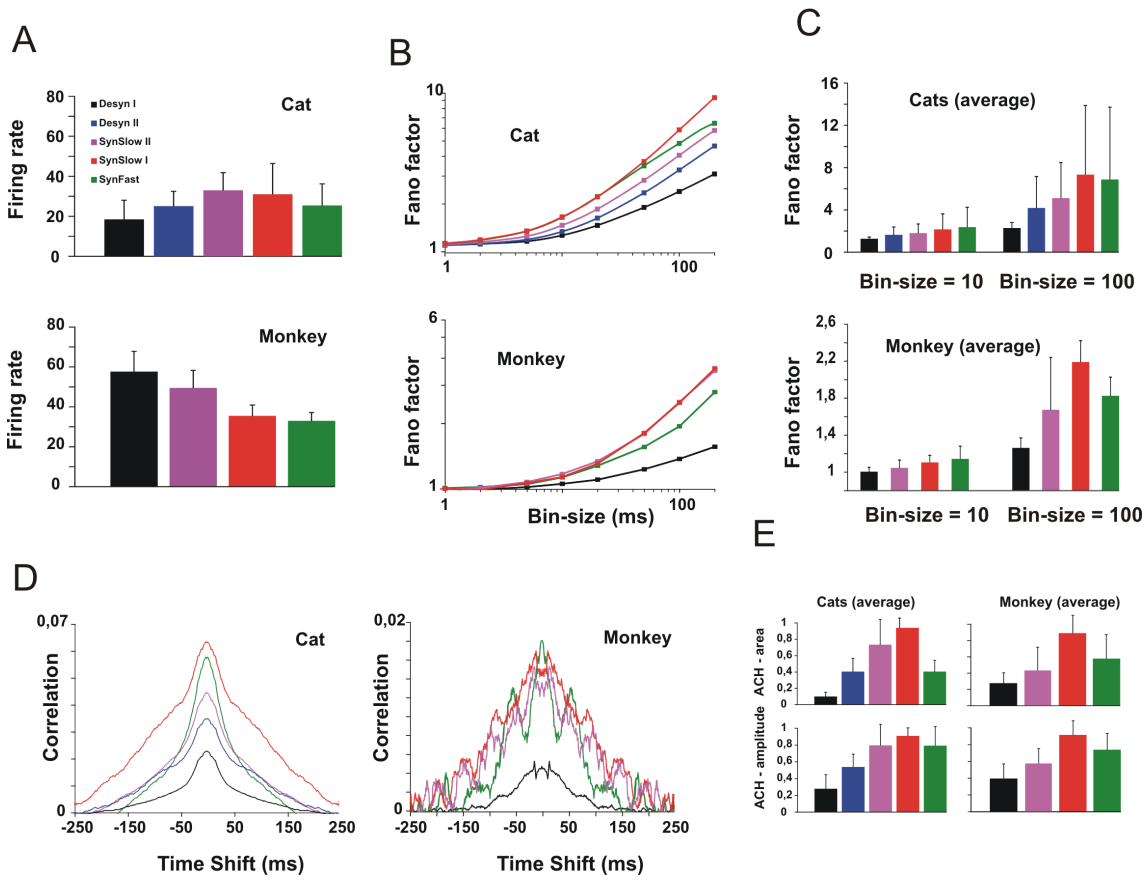

Figure 8.3: Firing rate and correlation analysis of different cortical states. A: Average (+SD) population firing rate for all recordings of a species. B: Two examples for Fano factor curves plotted as a function of bin-size. C: Average (+SD) Fano factor across all cat and monkey datasets. D: Autocorrelation histograms (ACH) of the population spike train for one cat and one monkey recording. E: Average (+SD) area and peak amplitude of ACHs computed for all cat and monkey datasets. The values were normalized to the dataset with maximum area and amplitude within a species.

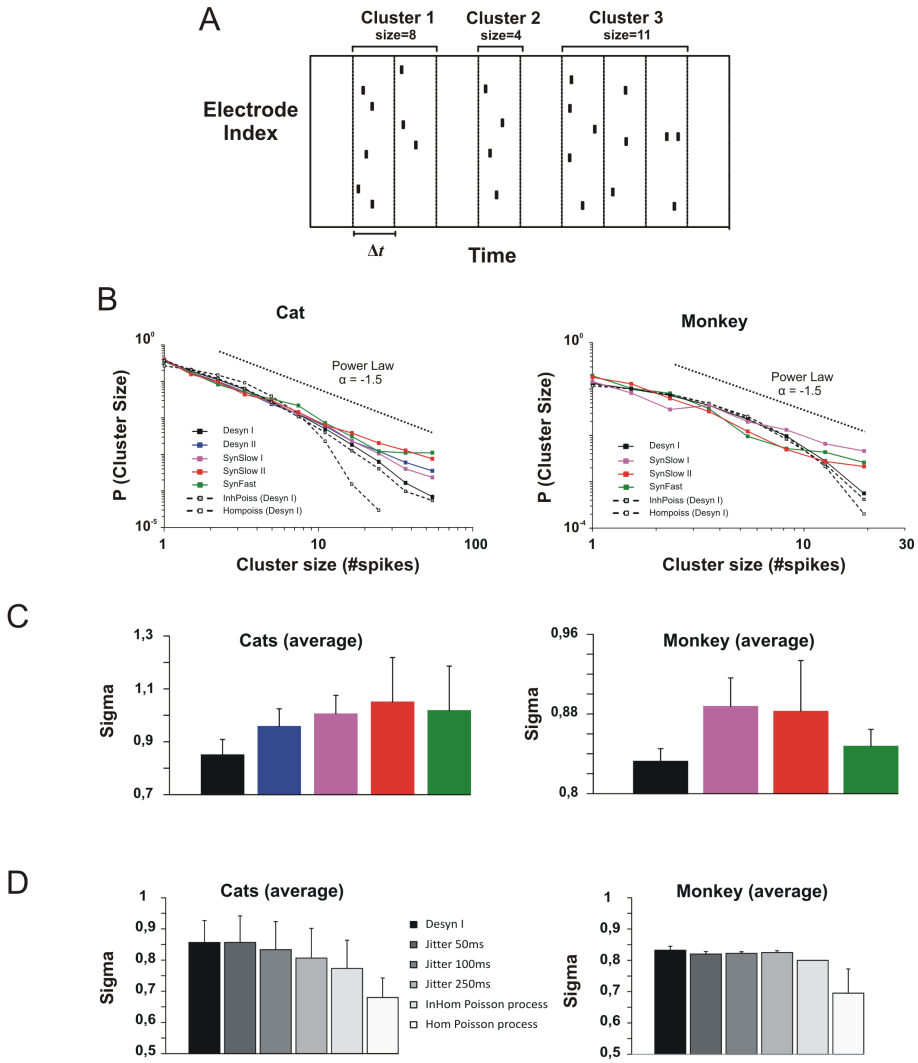

Figure 8.4: Neuronal avalanche analysis of spiking activity. A: Spike clusters were defined as a sequence of bins containing at least one spike delineated by bins without spiking activity. The size of a spike cluster is given by the total number of spikes within a cluster. t was chosen as the average ISI_{pop} interval of the population spike train for each state. B: Cluster size distributions of different states. Dotted black lines indicate power law with exponent = -1.5. Dashed lines with gray squares represent an inhomogenous Poisson process created from the desynchronized I state by spike time randomization within all 1s segments. Dashed lines with empty squares indicate an homogenous Poisson process with the same rate and duration as the original desynchronized I state. C: Average (+SD) sigma values of a lognormal function fitted to the cluster size distributions across all cat and monkey data. D: Same as in C, but with different types of surrogate data constructed from the desynchronized I state.

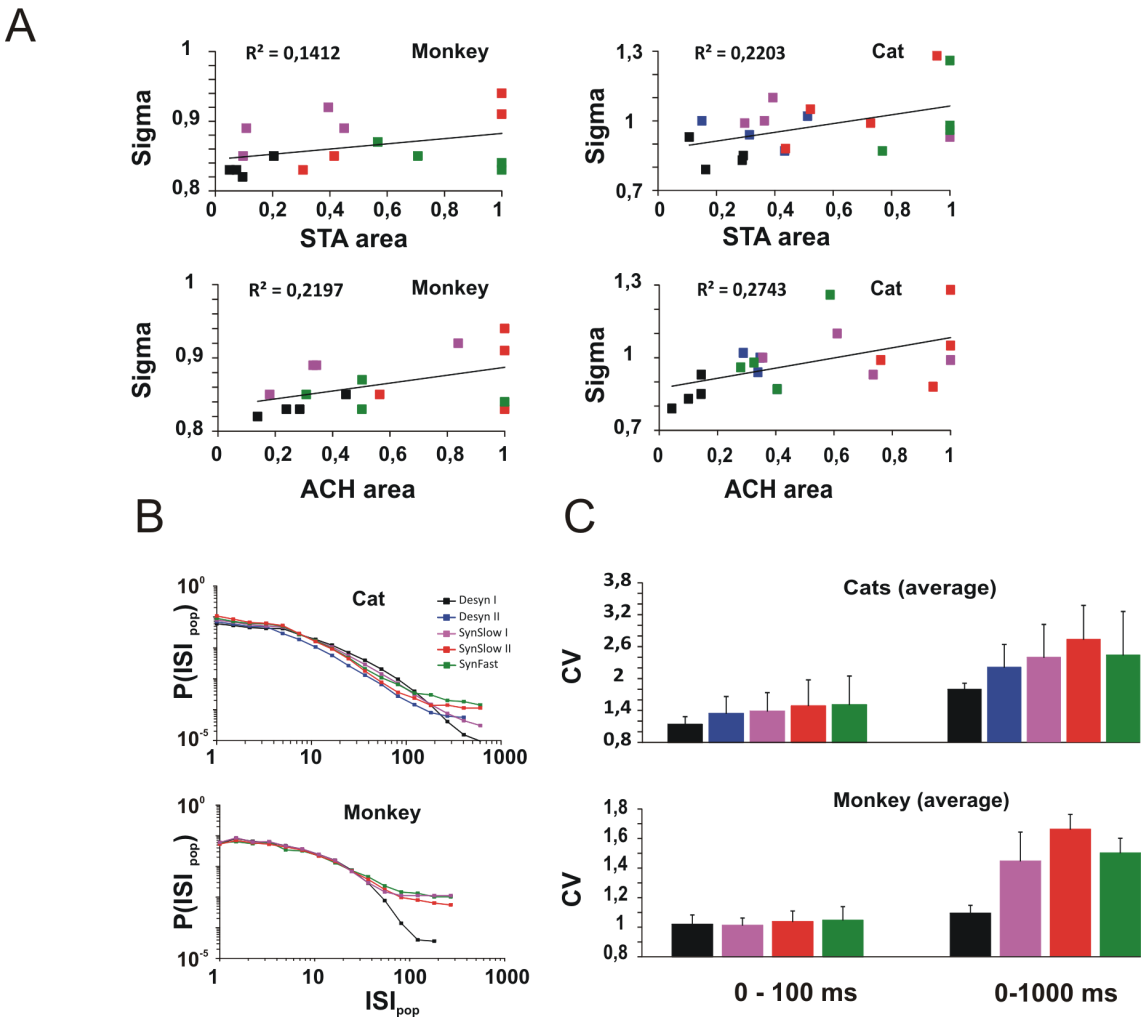

Figure 8.5: ISI_{pop} analysis and relationship between tailness of cluster size distribution and correlation variables. A: Lognormal sigma as a function of area and amplitude of the STA and ACH of population spike trains for different states. Each rectangle represents one dataset. B: Inter-spike interval distributions of population spike trains for one cat and one monkey recording. C: Average (+SD) coefficient of variation for ISI_{pop} distributions across all cat and monkey datasets and two interval ranges.

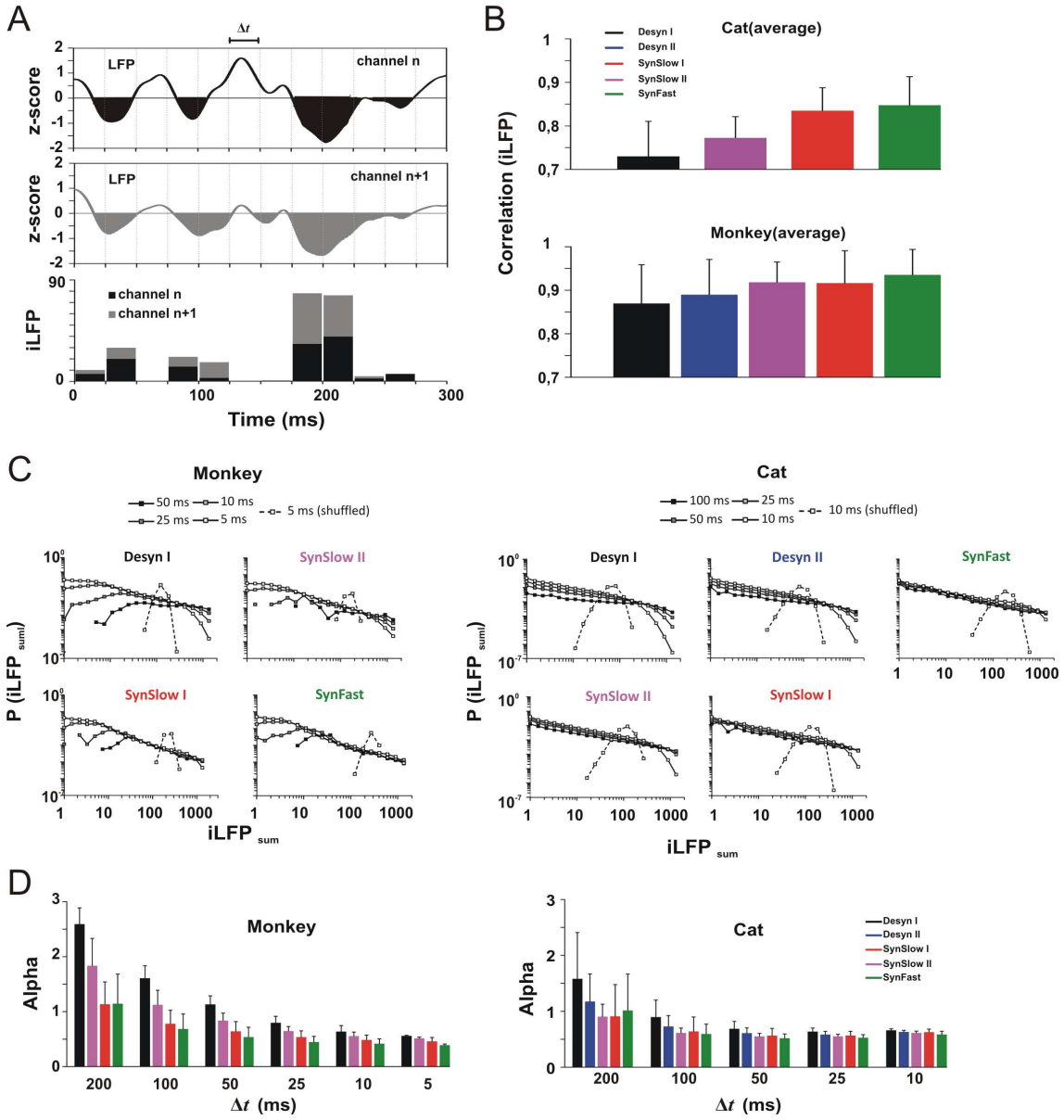

Figure 8.6: Neuronal avalanche and correlation analysis of LFPs. A: Z-scored data were binned with bin-size t and the negative z-score integral (iLFP) for every bin of each channel was calculated (top).$iLFPs$ for each bin were summed up across all channels ($iLFP_{sum}$, bottom). B: Average (+SD) of pairwise $iLFP$ correlation coefficient for different cortical states computed with t=25ms. C: Two examples of $iLFP_{sum}$ distributions computed for all states. D: Gamma distributions were fitted to $iLFP_{sum}$ distributions and the average (+SD) of their shaping parameter alpha is plotted as a function of t and cortical state.

9 Precise Neuronal Communication: Synfire Chains and Gamma Oscillation

Synfire Chains and Gamma Oscillations: Two Sides of the Same Coin?

Gerald Hahn[1], Alejandro Bujan[2], Ad Aertsen[2], Yves Frégnac[1], Arvind Kumar[2]

[1] Unité de Neuroscience, Information et Complexité (UNIC), CNRS, Gif-sur-Yvette, France

[2] Bernstein Center for Computational Neuroscience, Freiburg, Germany

9.1 Introduction

During waking the brain receives a continuous stream of input from its environment through a variety of sensory organs. At the same time, the brain generates meaningful output which influences the environment through coordinated muscle movement and actions. Ever since Donald Hebb (1949), systems neuroscience has tried to understand the principles of the neural processes that lie in between input and output which humans experience as percepts, emotions and thoughts or remain unconscious. These processes must extract objects from the sensory inputs, link these objects to behaviorally relevant decisions based on internal goals and map these decisions onto motor output. A simplified example of such a perceptual decision making process (Heekeren et al., 2008; Hernandez et al., 2010; Siegel et al., 2011) is shown in Figure 9.1A, in which a monkey was trained to indicate the color of a stimulus by a button press (Bak, 1996). To accomplish such a simple task, Hebb proposed the existence of cell assemblies which reflect groups of neurons defined by a specific connectivity structure. Different cell assemblies may be activated sequentially and form processing cascades, so called phase sequences, which intercede between the stimulus and the finger movement.

His framework imposes several requirements on neural activity implementing a cell assembly. First, cell assemblies are selective for a particular stimulus or action, such that each input or task only activates one specific ensemble of neurons at a time. This allows

downstream neurons to distinguish between different stimuli or actions. Second, each time a stimulus is present or an action needs to be accomplished, a cell assembly needs to be reliably activated. This enables neural activity to repeatedly signal the presence of a stimulus or perform a given task. Third, neural activity needs to remain flexible to permit the formation of novel assemblies for new stimuli, actions or their combinations into different tasks. In addition, once new assemblies or phase sequences have emerged they are stabilized by strengthening their connections through synaptic plasticity (Hebbian learning rule). Importantly, this flexibility necessitates mechanisms by which novel stimuli and actions can be processed before they are enhanced by synaptic plasticity. Figure 9.1B illustrates the requirement for neuronal assemblies to be formed by strong connections (familiar stimuli and actions) and weaker connections (novel stimuli and actions). According to Hebb, incorporating cell assemblies and phase sequences in the brain essentially becomes a problem of transmission of excitation from sensory to motor cortex. This transmission needs to be selective, reliable and yet flexible enough to allow new representations of stimuli and novel actions to be formed.

9.1.1 Synfire Chains

An elaborate model that implements Hebbian assemblies is the synfire chain (Abeles, 1982; 1991; 2009; Diesmann et al., 1999; Gewaltig et al., 2001; see Kumar et al., 2010 for review) and its generalized versions (synfire braids: Bienenstock, 1995; polychronization: Izhikievich, 2006). A synfire chain is a feedforward network with numerous layers which are connected through divergent and convergent connections. Transmission of excitation is achieved by propagating synchronous volleys of spikes from one layer to the next. The necessity of synchrony is warranted by the established physiological fact that single spikes create too small EPSPs to trigger another spike. Only a sufficient number of spikes arriving at the postsynaptic neuron within a sufficiently small time window is able to generate a new spike (Abeles, 1982; Azouz and Gray, 2000; Salinas and Sejnowski, 2000; Léger et al., 2005; Rodriguez-Molina, 2007; Rossant et al., 2011). Thus, synchronous presynaptic spike volleys are particularly likely to have a strong effect on the spiking activity of downstream neurons (Salinas and Sejnowski, 2001; Tiesinga and Sejnowski, 2008). A sufficiently strong synchronous input to the first layer of a synfire chain will be preserved and faithfully propagated across subsequent layers through well timed and sufficiently strong divergent and convergent connections between the layers (Fig. 9.2A). In a Hebbian sense, one layer might represent a cell assembly and the propagation of a synchronous volley may be considered as a phase sequence.

Initial models of synfire chains were studied in isolation and showed that these networks can implement reliability as they transmit activity to the end of a chain with high fidelity (Diesmann et al., 1999). However, first attempts to embed synfire chains in a neuronal

background with balanced excitation and inhibition violated the selectivity principle. Synchrony did not only spread along enhanced connections within the synfire chain, but activated the entire network (Mehring et al., 2003). Later it was shown that synchronous volleys remain restricted to the chain, when either lateral inhibition is introduced (Aviel et al., 2003; Vogels and Abbott, 2005) or the chain is embedded in asynchronous-irregular (AI) background activity with realistic synapses (Kumar et al., 2008). This AI activity (Brunel, 2000) prevents synchrony to spread outside the chain by quickly tracking down growing excitation through inhibition (Renart et al., 2010; Tetzlaff et al., 2012), while synchronous excitation within the chain remains strong enough to overcome the asynchronous inhibition and spread along the chain. Subsequent studies have also demonstrated that a set of interacting synfire chains can be used to bind together simple features to a more complex object (Bienenstock, 1996; Abeles et al., 2004; Hayon et al., 2005) or perform a variety of cognitive tasks (Izhikievich, 2006). Synfire chains have also been used to explain the generation of bird songs out of single syllables (Hahnloser et al., 2002; Jin, 2007; 2009) and to construct sequences of motor actions (Schrader et al., 2011; Hanuschkin et al., 2011). Despite new analysis techniques (Schrader et al., 2008; Gerstein et al., 2012), experimental evidence for synfire chains remains scarce. Evidence comes primarily from findings of repeating patterns of precise spike timing (Abeles et al., 1993; Prut et al., 1998; Ikegaya et al., 2004; Shmiel et al., 2005; 2006; Long et al., 2010).

Even though the current synfire chain models display stable and selective dynamics, their lack of flexibility remains a problem that has not been resolved yet. Synfire chains require specific connectivity and strong synapses that need to be explicitly designed by the modeler and thus rather represent Hebbian cell assemblies that have been already strengthened by synaptic plasticity after repeated activation. Several studies have investigated how synfire chains can emerge in neuronal network with different learning algorithms (Prugel-Bennet and Hertz, 1996; Levy et al., 2001; Izhikievich, 2006; Kunkel et al., 2011; Trengove et al., 2012). However, in these models stimuli can only be processed after some time until synfire chains have been learned. In contrast, novel stimuli presented for the first time are not processed.

Despite the absence of a synfire chain for a given stimulus/task configuration, there may exist diluted synfire chains with well-timed divergent/convergent connections, but insufficient synaptic weights (Abeles, 1991; Abeles, 2009). The anatomical connections within these diluted chains do not produce enough excitation that can overcome background inhibition and fail to reliably propagate activity across the synfire network. The question arises, if there are mechanisms that can increase excitation and synchrony in each layer such that activity can spread along weaker connections. At the same time, this mechanism would also need to induce synaptic plasticity (Markram et al., 1997) to enhance these connections and transform a diluted into a fully functional synfire chain.

9.1.2 Gamma Oscillations

A suitable mechanism to increase excitation may be represented by synchronous inhibition (Tiesinga et al., 2004; 2008; Börgers et al., 2005; Womelsdorf et al., 2007; Börgers and Kopell, 2008; Fries, 2009). When excitatory input is fed to a network which has just been released from synchronous inhibition the response of the excitatory neurons in the network is larger than an input arriving at times of asynchronous inhibition (Tiesinga and Sejnowski, 2009). This increased excitation will have a stronger impact on downstream neurons and might also be amplified, if it arrives precisely at the time of release of synchronous inhibition. Thus, coordinating excitation with synchronous inhibition within and between layers of a diluted synfire chain may improve the propagation characteristics of the chain.

Synchronous inhibition in the brain has been found to be linked with oscillation in particular in the gamma frequency range (Eckhorn et al., 1988; Gray and Singer, 1989). The mechanism of synchronous gamma oscillations have been explored in detail theoretically (Wang, 2010) and experimentally (Bartos, 2007; Cardin et al., 2009; Sohal et al., 2009; Buszaki and Wang, 2012). At the core of this concept are paralvabumin (PV) positive basket cells, a subtype of GABAergic interneurons. This type of cell has special characteristics that allow them to effectively provide synchronous inhibition to a local population of excitatory cells. Their connections to principal cells are highly divergent and they mediate their inhibition through perisomatic inhibition (Mann et al., 2005) which is particularly suited to modulate the firing of postsynaptic targets. In addition, PV positive basket cells are mutually connected (Buhl et al., 1994; Cobb et al., 1995; Kisvarday, 1993; Tamas et al., 1998) and interact with strong IPSCs (Bartos et al., 2002) and shunting inhibition (Fries, 2005; Vida et al., 2007). Moreover, communication between basket cells is enhanced by gap junctions (Galarreta et al., 1999; Tamas et al., 2000). This strong mutual interaction allows basket cells to effectively synchronize their firing and locally transfer synchronous inhibition to pyramidal cells.

Theoretical studies have investigated how synchronous oscillations in the gamma frequency range emerge in networks of excitatory and inhibitory neurons (E-I networks). Two different mechanisms have been identified. It has been found that tonic drive to mutually connected interneurons (e.g. through activation of metabotropic glutamate receptors, Whittington et al., 1995), lead to rhythmic synchronous discharges of inhibitory neurons which in turn also entrain tonically driven pyramidal neurons. Importantly, this mechanism does not require direct input from the pyramidal cells to the inhibitory neurons and is purely generated by the interneuron network (ING mechanism, Brunel and Hakim, 1999; Brunel, 2000). In contrast, the PING mechanism (Wilson and Cowan, 1972; Brunel and Wang, 2003) is based on phasic excitatory input of the pyramidal cells to the inhibitory neurons. This input drives the inhibitory

neurons which in turn feed synchronous inhibition back to the pyramidal neurons. The latter stop firing until inhibition fades and the process starts again, thereby creating an oscillation, whose frequency is dependent on the membrane time constant of the inhibitory neurons. Both mechanisms work independently, but may also cooperate to create gamma oscillations (Wang and Buszaki, 2012). Another potential mechanism was described recently (Moca et al., 2012) and highlights the role of resonance properties of inhibitory neurons in the generation of gamma oscillations (resonance induced gamma, RING).

9.1.3 Oscillation Chains

Rhythmic synchronous inhibition created within gamma oscillations might be a suitable mechanism to enhance the propagation of excitation in diluted synfire chains. The key idea is that weak external input to a pool of excitatory neurons drives a gamma oscillation, which in turn increases the gain of the excitatory response cycle by cycle (Fig. 9.2B). The amplified excitation of this pool drives a gamma oscillation in a subsequent pool, which again increases excitation that is sent to downstream neurons. Since the oscillation in a given pool is driven by the previous one through the PING mechanism, the excitation always arrives at the time, when neurons are most susceptible to input, i.e. when synchronous inhibition has decayed. This also guarantees that the oscillations in these two pools have the same frequency and oscillate coherently with a phase that is given by the transmission delay between the pools (Fries, 2005). Note that coherent oscillations are not necessarily restricted to the gamma range, but may also occur in the beta frequency band (Buehlmann et al., 2010).

One can hence construct a chain of oscillations, in which the oscillation in each pool of neurons is driven by the previous pool and a coherent oscillatory activity propagates along the chain. We denote this oscillating feedforward dynamics as oscillation chain. Depending on the frequency, we call this activity gamma or beta chain. The characteristic of this dynamics is the progressive increase of excitation in each layer, until it is strong enough to spread to the next pool. Thus, with more oscillation cycles, the activity spreads further within the chain. An example of the dynamics within an oscillation chain is shown in Figure 9.2C. The first pool receives a rhythmic spike volley as input which is transmitted to subsequent layers. Due to the weak connections the volley is not transmitted beyond layer two. However, because of the oscillatory nature of the input, excitation builds up in layer two, until it is sufficient to trigger the same amplification mechanism in layer three. With each oscillation cycle, the initial spike volley in layer one spreads a little further down the chain. After a sufficient number of cycles, excitation reaches the final layer of the oscillation chain and transmission is completed. Importantly, to establish a coherent oscillation, the input needs to be

presented for a prolonged period of time either as an oscillation or as a sufficiently long increase of firing rate, which is converted into a oscillation (Brunel, 2000). This is in contrast to synfire dynamics, in which the presentation of a single spike volley is enough for a successful propagation of excitation across the chain.

The dynamics in an oscillation chain is fully compatible with the concept of communication through coherence (CTC, Fries, 2005; 2009). This concept is based on the notion that two oscillating groups of neurons can communicate effectively, if they oscillate in phase such that the output of one group drives neurons in a second group just at the time, when inhibition fades. In an oscillation chain, each pool communicates with other pools further downstream through coherent oscillations and can thus effectively transmit synchronous spike volleys along the chain. Coherent oscillations in the gamma range across different brain areas have been studied in both multi-site unit recordings (Roelfsema et al., 1997; Brecht et al., 1998; Womelsdorf et al., 2007) and large scale recordings (EEG and MEG, Varela et al., 2001). They have been associated with visual (Singer, 1999; Tallon Baudry, 2009) and somatosensory perception (Gross et al., 2007), consciousness (Engel and Singer, 2001; Melloni et al., 2007) and execution of movements (Crone et al., 1998; Pfurtscheller et al., 2003; Siegel et al., 2011; van Wijk et al., 2012)

9.1.4 Transformation Oscillation Chains - Synfire Chains

In the Hebbian framework, a novel stimulus activates a new cell assembly which is stabilized after repeated presentation through learning. Learning is triggered by consistent coincidences of neural discharges within the assembly and increases the excitatory weights such that even the presentation of an incomplete stimulus activates the same assembly (Hebb's learning rule). If an oscillation chain represents the processing of novel stimuli and a synfire chain reflects more familiar stimuli, how can oscillatory dynamics be transformed into a more synfire mode of activity? In accordance with Hebb's hypothetical learning rule, theoretical (Gerstner et al., 1996) and experimental studies (Markram et al., 1997; Bi and Poo, 1997; Zhang et al., 1998) have confirmed the importance of precise spike timing between pre- and postsynaptic neurons to enhance (long-term potentiation, LTP) or suppress (long-term suppression, LTD) synaptic strength and the results are formalized within the framework of spike-timing dependent synaptic plasticity (STDP; Song et al., 2000).

Importantly, coherent gamma oscillations provide an ideal environment to induce LTP, as the precise phase relationship between two oscillating pools provides a consistent timing relationship between pre- and postsynaptic neurons. Thus it was proposed that this correlated firing of neurons within gamma oscillations (Axmacher et al., 2006; Jutras and Buffalo, 2010) activates STDP and thus promotes the formation of memories

and better communication between different brain regions (Fell and Axmacher, 2011). Since the different pools within an oscillation chain oscillate in phase, one might thus expect that LTP is switched on and strengthens the excitatory connections between the different layers. The more often a stimulus is presented the larger the enhancement of these connections. As these weights increase, less and less amplification is needed and hence fewer oscillation cycles to propagate a synchronous volley across the chain. After a sufficient number of stimulus repetitions, the weights may become strong enough for the chain to support synfire dynamics such that a spike volley is transmitted to the final layer in one sweep (i.e. in one oscillation cycle). Thus, STDP might strengthen synapses between the layers of an oscillation chain and reduce the number of cycles needed for spike volley transmission until weights are sufficiently strong to allow synfire dynamics.

To test the framework outlined above we constructed a layered feedforward network with an architecture similar to Diesmann et al. (1999), but added inhibitory neurons recurrently connected with excitatory neurons in each layer to induce oscillations based on the PING mechanism. We found coherent oscillations that spread across the network and a decrease in oscillation cycles needed to transmit spike volleys to the final layer with increasing weights. Synfire chain activity was established with sufficiently strong weights. These results confirm the hypotheses developed above and demonstrate that oscillatory chains and synfire chains are two complementary ways to transmit synchronous spiking activity in neural networks.

9.2 Materials and Methods

9.2.1 Neuron Model

The network was modeled with current-based leaky integrate-and-fire neurons, whose membrane potential is given by $\frac{dV}{dt} = -\frac{1}{\tau_m}V + \frac{1}{C_m}I_{syn}(t)$. τ_m represents the membrane time constant, C_m the membrane capacitance and I_{syn} synaptic current. In the simulations τ_m was 20ms. A spike was elicited, when the membrane potential crossed a fixed threshold which was set at 20mV above the resting potential. After a refractory period of 1ms the membrane potential was reset to its resting value of 0 mV (Tuckwell, 1988). Postsynaptic currents (PSC) followed an α-function $I_\alpha(t) = \frac{e}{\tau_\alpha}te^{\frac{-t}{\tau_\alpha}}$ with rise time τ_α which was 0.5ms for excitatory and 2.5ms for inhibitory neurons in this study. Synaptic weights J were given by the peak amplitude of the PSC. All simulations were performed with NEST (see www.nest-initiative.org) using an integration step of 0.1ms.

9.2.2 Network

Details of the network architecture are shown in Figure 9.3A. The simulated network consists of 20 layers of excitatory neurons (400 per layer, blue circles) which are connected in a feedforward fashion with weights J_{syn}, connection probability of 0.1 and a delay of 0.5ms. In the simulations, J_{syn} was varied between 0.7 and 1.9mV.. Each excitatory neuron connects to other randomly chosen excitatory and inhibitory neurons within the same pool (100 per layer, red circles) with weights J_{exc} (0.08mV). Each inhibitory neuron is reciprocally connected with other inhibitory neurons and feeds back to the excitatory pool. Inhibitory connections between the layers were omitted. All inhibitory weights were set to $J_{inh} = g * J_{exc}$ with g=10. Delays of 2.5ms were given to recurrent excitatory and inhibitory connections, while transmission between the excitatory and inhibitory pools was delayed by 0.5ms. Recurrent and in between pool connections were established with a probability of 0.2 and 0.1, respectively. Moreover, each neuron received an external Poissonian drive with rate ν_{ext} = 9.8kHz and weight J_{exc} . Input to layer one consisted of a spike volley with 100 spikes and a Gaussian temporal profile (sigma = 1ms). After allowing spontaneous network dynamics to settle for 1200ms, we either presented single or oscillating spike volleys with frequencies ranging between 10 and 30Hz.

9.3 Results

We simulated a layered network (Fig. 9.3A) with 20 layers and 500 neurons per layer (400 excitatory and 100 inhibitory neurons). The excitatory and inhibitory populations in each pool were recurrently connected and mutual synaptic links between the neurons within a pool were added. The different layers communicated with the nearest layers through feedforward connections, which were purely excitatory and projected to excitatory neurons only. Each layer may be viewed as a local cortical E-I network, which interacts with more remote networks through long-range excitatory connections. As illustrated in Figure 9.3B, the population activity within each layer displayed asynchronous irregular (AI) activity (Brunel, 2000), when the network was driven by an external Poisson input.

9.3.1 Amplification of Excitation during Oscillatory Spike Volley Input

We presented single or oscillating synchronous spike volleys to the first layer of the network and studied differences in propagation between these two types of input as a function of the connection strength (J_{syn}) between the layers. First, we investigated the effect of oscillatory input on the inhibition characteristics of excitatory neurons in

the first layer of the chain. An example of membrane potentials (V_m) and their average (in color) recorded from excitatory neurons in layer one during an oscillating stimulus at 20Hz is shown in Figure 9.3C. It demonstrates that an initially weak inhibitory response to an input pulse is amplified cycle by cycle until a steady state response is reached after the presentation of four spike volleys. Thus, oscillatory input at this frequency leads to progressive recruitment of inhibitory neurons which in turn inhibit an increasing number of excitatory neurons. Next, we analyzed the impact of the growing inhibition on the number of excitatory neurons that fired in response to the presented spike volleys. To this end we counted the number of spikes (alpha) within a short time window (10 ms) following a pulse in each layer. The onset and offset of the window was corrected for the conduction delays between the layers. In addition, we quantified the synchronization degree between the excitatory neurons by calculating the temporal dispersion (sigma) of the spikes within the window which we measured as the time between the first and last spike. The temporal evolution of and for excitatory neurons in the first four layers is illustrated in Figure 9.3D, where each dot represents one input pulse. In general, alpha increased with the number of input oscillation cycles and ended in an attractor, in which the number of excitatory spikes remained stable at around 300 spikes. Notably, the number of cycles needed to reach this attractor was a function of the layer index and was smaller for the first layers and larger for further downstream layers. The temporal dispersion sigma decreased, as more spike volleys were presented to layer one and similar to alpha approached an attractor with values between 1 and 5ms. Interestingly, this attractor was layer specific with average sigma being higher in first layers and smaller in later layers. These results indicate that repeated spike volley input not only amplifies excitation in each layer, but also increases the temporal precision of excitatory spikes, as the oscillation advances in time. In addition, this precision increases, as the spike volley spreads across the layers in line with previous studies (Reyes et al., 2003; Rosenbaum et al., 2011).

9.3.2 Emergence of Oscillation-and Synfire Chains

Having established the presence of amplification during oscillatory input, we examined the spread of spike volleys across the network as a function of J_{syn} in more detail. The raster plots in Figure 9.4 illustrate the characteristics of pulse packet propagation for three different weights J_{syn} after stimulation with either a single spike volley (left) or a sequence of spike volleys presented with a frequency of 20Hz (right). For small and medium weights a single pulse packet did not propagate beyond layer two. Only with strong weights a synfire chain emerges (Abeles, 1991; Diesmann et al., 1999) and a synchronous spike volley is transmitted faithfully to the last layer. When a rhythmic train of spike volleys is presented to the network with small J_{syn}, synchronous activity builds up during subsequent cycles and spreads further than in the case of single pulse

packet input. However, the propagation of synchrony does not reach the final layer and is characterized by a waxing and waning pattern of activity spread and collapse. This pattern changes, when J_{syn} is increased to medium values. Now, synchronous volleys spread further and further along the chain, as the input oscillation progresses. Even though the weights are not strong enough to allow synfire propagation, they are sufficient to trigger the amplification mechanism as described above in all layers. As a consequence, excitation can build up in each layer during the oscillation and spread to subsequent layer, where amplification is repeated. In each oscillation cycle, synchrony spreads further down the network and after a sufficient number of cycles the synchronous volley reaches the final layer. The result is a coherent oscillation that spreads across the network and allows faithful communication between remote layers through synchronous spike volleys. This type of activity is equivalent to the oscillation chain hypothesis described above. When $J_{syn}$is further increased, the initial pulse packet is propagated to the final layer in the first cycle without the necessity of further amplification. Oscillation chains are thus transformed into synfire chains with sufficiently strong excitatory weights between the layers.

In order to further quantify this result, we systematically varied J_{syn} and determined values for which synchrony did not propagate, spread within an oscillation chain or supported synfire transmission. In addition, we counted the number of cycles needed to transmit a spike volley in an oscillation chain from layer one to the last layer. The results are shown in Figure 9.5. For small weights, synchronization did not spread to the final layer of the chain. However, with increasing J_{syn} oscillation chains emerged and the number of cycles necessary to propagate a volley to the final layer decreased non-linearly with larger values of J_{syn}. Note that if J_{syn}becomes too large, spontaneous oscillation and synfire chains are triggered in random layers of the network that are independent of the stimulus (not shown).

9.3.3 Oscillation Chains and Resonance

The above analysis was performed with input pulses that oscillated at a frequency of 20 Hz. We next investigated the emergence of oscillation chains as a function of the input frequency. To this end we presented oscillatory input between 10 and 30Hz to the network with a value of J_{syn}that supported oscillation chain propagation above. For each frequency we checked the presence of oscillation chains that transmit synchronous volleys to the final layer. An example for a frequency, at which a propagating oscillation was absent, is shown in Figure 9.6A. At this frequency, the input volley arrived at a time, when activity in the layer was either too inhibited or has already returned to baseline activity. Thus, inhibition and consequently excitation were not consistently amplified, as shown in Figure 9.6B. Varying the frequency systematically

revealed that oscillation chains only evolved within a narrow frequency band (17-20 Hz, see Fig. 9.6C), while other frequencies did not support transmission of synchrony through coherent oscillations. These results indicate that the amplification process is due to a resonance phenomenon, which appears at frequencies that are network specific.

9.4 Conclusion

In the present study, we propose a new framework to overcome shortcomings of the synfire chain hypothesis by introducing the concept of oscillation chains. An oscillation chain compensates for too weak synaptic links within diluted synfire chains by progressive amplification of excitation through oscillating synchronous inhibition. As a consequence, during the prolonged presentation of a stimulus, a coherent oscillation propagates across the chain and takes several cycles to transmit a spike volley. Coherent oscillatory activity induces synaptic plasticity which strengthens the synaptic weights between layers of a diluted synfire chain. This promotes faster transmission and reduces the time a stimulus needs to be presented in order to be processed. In the limit, only one cycle is necessary for reliable transmission, in which case the oscillation chain is converted into a synfire chain.

We tested this framework in a layered network, in which each layer contained a recurrently connected E-I network. We found that this type of architecture supports oscillation chains, when input is presented at the resonance frequency of the local E-I network. Importantly, the number of cycles necessary to transmit synchronous volleys to the final layer was dependent on the excitatory weights between the layers. Our results also show that the network can propagate pulse packets in one cycle only, when inter-layer weights are sufficiently strong. Thus, the model supports the idea that synfire chains are a special case of oscillatory chains.

Depending on the parameters, local E-I networks may resonate at different frequencies. In our model, parameters were tuned such that the network resonated at beta frequency (~20Hz). Several studies have indeed reported long-distance coherence not only in the gamma band, but also at beta frequencies (see Engel and Fries, 2010 for review). Moreover, a recent theoretical study demonstrated that a local oscillating network can communicate with more distant networks through coherence in both the beta and gamma band (Buehlmann et al., 2010; Deco et al., 2011). These findings indicate that oscillation chains may occur at different frequencies and the exact frequency is a function of the resonance properties of the local networks.

An important prediction of our model is the appearance of coherent oscillations only during stimuli that are presented during a sufficiently amount of time. This time is necessary to trigger the amplification mechanism and transmit synchrony during a number

of cycles through the network. In a recent EEG study by Melloni et al. (2007), a stimulus was presented for a brief period time to human subjects, after which it was either rendered invisible by a mask or remained visible for a larger amount of time. In line with our prediction, coherent gamma oscillation only emerged during the visible condition with phase synchrony across widespread cortical networks. However, even during the invisible condition, subjects performed significantly better during a matching task indicating that even the briefly presented stimulus was processed. This is in accordance with other studies that found a priming effect for short and unperceived stimuli in subsequent tasks (Thorpe et al., 1996; Thorpe and Fabre-Thorpe, 2001; see Fabre-Thorpe, 2011 for review) suggesting that visual information can be already analyzed during the first wave of cortical activity. We hypothesize that brief stimuli activate networks with already established and strong connections in which synchrony may spread very fast and without the need of further amplification. Only when a stimulus is presented for a longer time, also previously unfamiliar aspect of a stimulus can be processed by enhancing the spread of synchrony along weaker connections through amplification in oscillation chains.

Another prediction is the presence of precise temporal firing patterns not only during synfire chain dynamics, but also within oscillation cycles, since the underlying connectivity remains the same in both dynamics. Notably, a recent studies found consistent firing delays between neurons (Schneider et al., 2006) and precise firing sequences of different neurons (Havenith et al., 2011) within cycles of beta/gamma oscillation evoked by drifting gratings in anesthetized cat primary visual cortex . Importantly, these delays and firing patterns were stimulus specific and changed with the directions of the grating. Within our framework, these patterns may arise during the generation of gamma/beta chains and are due to the spread of synchrony along precise, but presumably weak anatomical connections organized as diluted synfire chains. Since each stimulus activates networks with a different connectivity, patterns within synchronized oscillations should change as a function of the stimulus properties.

Oscillation chains may not only arise in neural networks after stimulation by the environment, but may also be created internally. In this case, neuronal networks need to maintain spatiotemporal patterns of neuronal activity for a limited amount of time, which provide input to the rest of cortex and may allow the formation of oscillation chains. Interestingly, there is an increase of coherence in beta/gamma frequencies between areas in the frontal and parietal areas during maintenance of information in working memory (Lutzenberger et al., 2002; Babiloni et al., 2004; see Fell and Axmacher, 2011 for review). Moreover, recent experimental and theoretical evidence suggest that spatiotemporal activity patterns in the gamma range can be embedded and maintained in beta oscillations in the absence of external stimulation (Roopun et al., 2008; Kopell et al., 2011). This opens up the possibility that persistent patterns of beta oscillations may provide the prolonged input to subsequent processing stages, which allows the

formation of oscillation chains in the beta range.

In conclusion, we propose a novel theoretical framework for transmission of synchronous spike volleys and neuronal communication that combines synfire chains, coherent oscillations and synaptic plasticity. In this framework, coherent oscillations arise in diluted synfire chains through resonance and amplification of weak synaptic input. Synfire chains are regarded as a special case of oscillation chains and emerge after sufficient strengthening of synaptic weights through plasticity induced by the coherent oscillation.

9.5 Figures

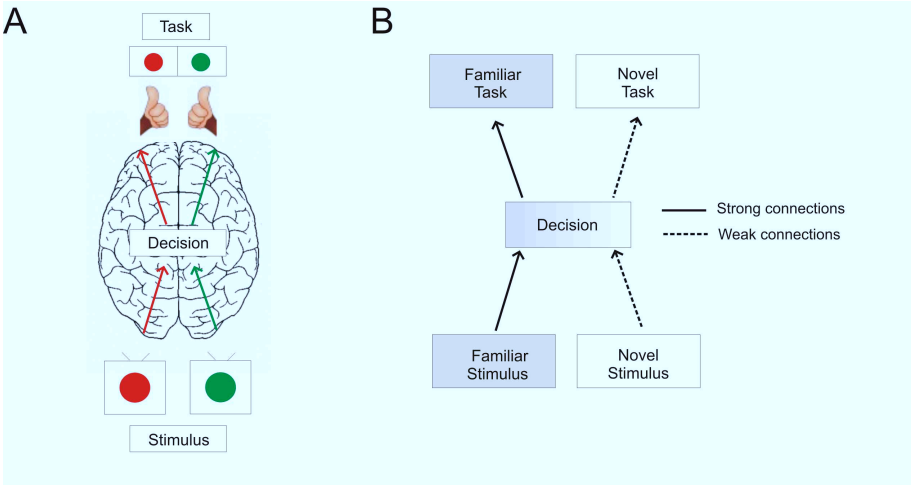

Figure 9.1: Simplified version of a decision making process in the brain. A: Two different stimuli (red and green dot) are shown to the animal, whose presence has to be confirmed by a button push of the respective color. Red and green lines indicate the neuronal processing cascades for each stimulus/task pair in the brain. B: Scheme of neural processing for novel and familiar stimulus/task pairs and putative connectivity strength.

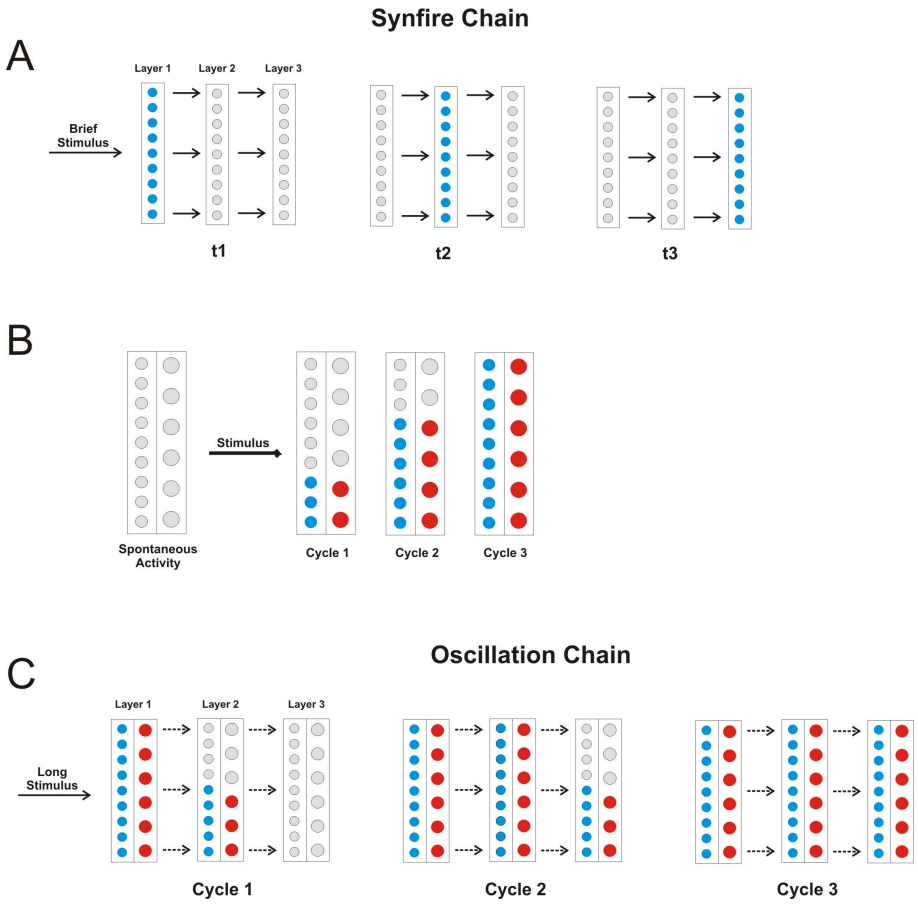

Figure 9.2: Models for propagation of synchronous spike volleys. A: Spread of pulse packets across three layers of a synfire chain with strong connections (arrows) illustrated at three different points in time t. Blue filled circles indicate spikes from excitatory neurons. B: Amplification of a weak, but prolonged excitatory input in layer one of a diluted synfire chain during several cycles of an oscillation as a consequence of synchronous inhibition (red). C: Amplification is exploited to transmit input across three layers of a diluted synfire chain with weak synapses (dashed arrows).

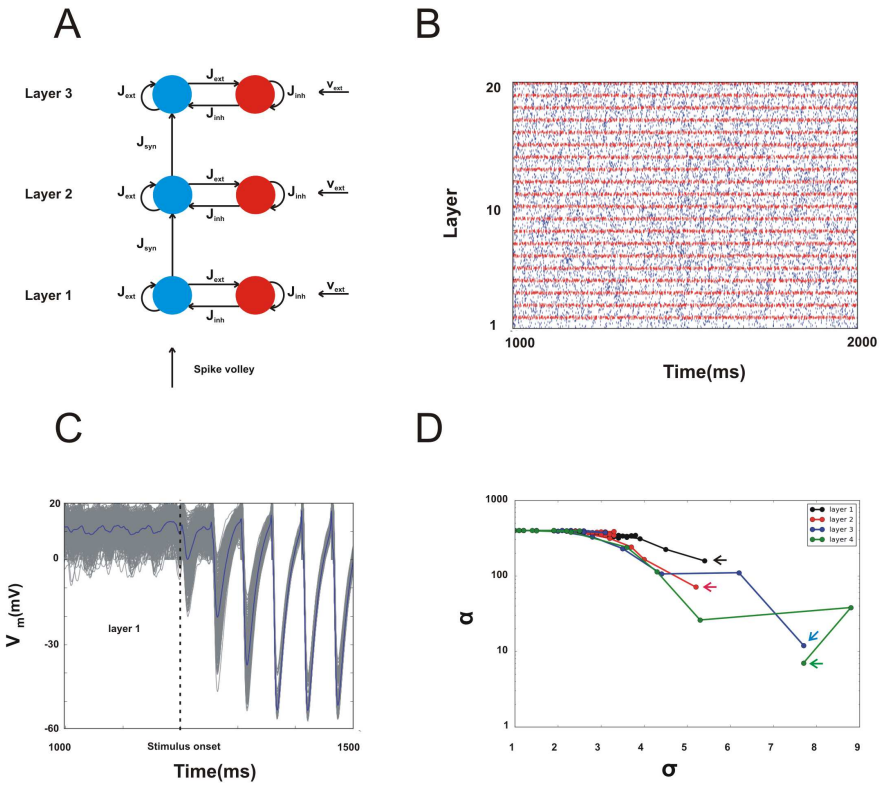

Figure 9.3: Architecture and spontaneous activity of the investigated neural network. A: The network consists of 20 layers each containing a recurrently connected network of excitatory and inhibitory. These layers are connected through feedforward connections. In addition, neurons within the excitatory and inhibitory pools of each layer are mutually connected. All neurons receive an external Poisson drive with rate v. B: Example of 1s spontaneous activity without spike volley input. Blue dots indicate excitatory neurons and red dots represent inhibitory neurons. C: Membrane potential of all excitatory neurons (gray) and their average (blue) during spontaneous activity and rhythmic stimulation with spike volleys at a frequency of 20Hz. D: Spike count of excitatory neurons (alpha) and temporal dispersion of spikes (sigma) measured within a window of 10ms for the first four layers of the network. Each dot indicates alpha and sigma of the excitatory response to 1 out of 20 oscillatory spike volleys (20Hz) presented to layer 1. The first cycle of the stimulus is represented by the arrows and time is indicated by the colored lines.

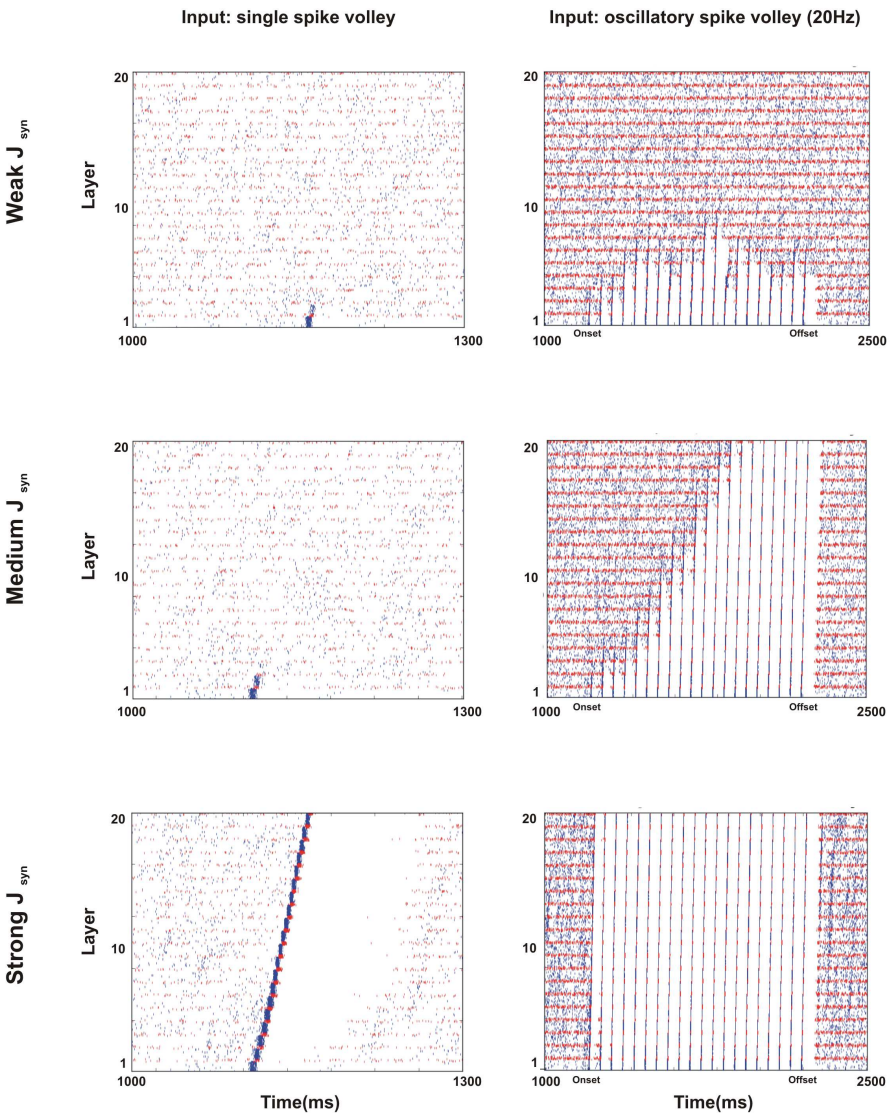

Figure 9.4: Comparison between synfire chain and oscillation chain propagation for different excitatory coupling strengths between layers. On the left, layer one receives a single synchronous spike volley. The pulse packet propagation across a network of 20 layers and for three different levels of layer coupling is shown. Note that only with strong coupling the pulse packet travels to layer 20. On the right, the first layer receives a sustained oscillatory spike volley with a frequency of 20Hz. An oscillation chain starts to form with sufficiently strong weights and reliably propagates the initial pulse packet to layer 20 after a number of cycles.

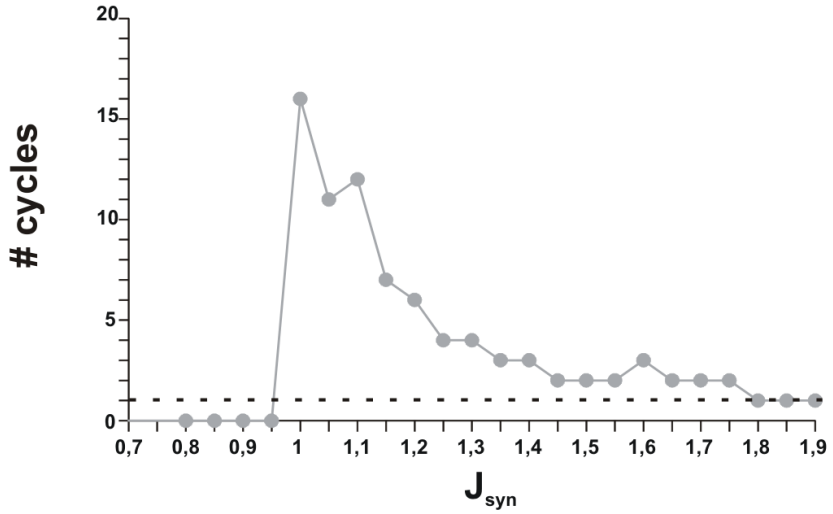

Figure 9.5: The number of cycles needed to propagate a spike volley within an oscillation chain is plotted as a function of the coupling strength. A value of zero cycles indicates failure of propagation. The dashed line represents synfire chain propagation, i.e. only one cycle is necessary to transmit a pulse packet.

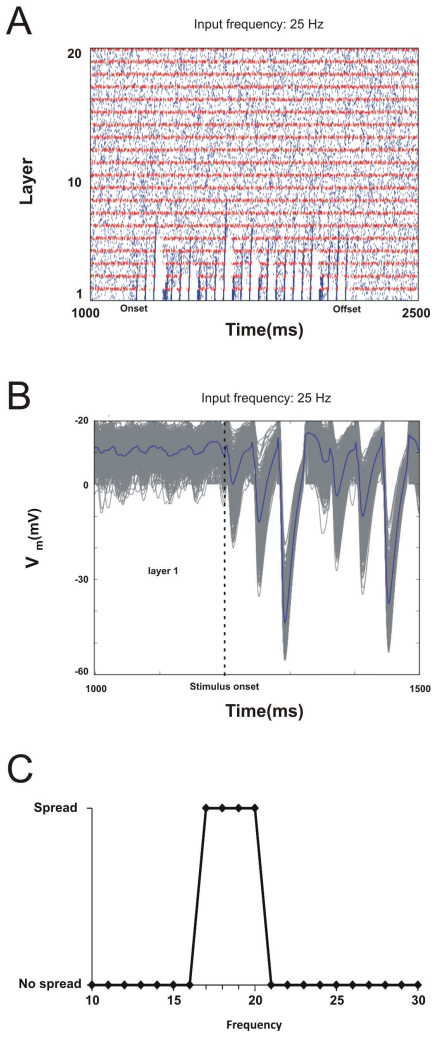

Figure 9.6: Emergence of an oscillation chain only occurs with oscillatory input at resonance frequencies. A: The purely feedforward network was given an oscillatory input with frequency of 25Hz. Note that the same network responded with an oscillation chain to an input frequency of 20Hz. B: Voltage traces of individual layer one excitatory neurons and their average during a 25Hz input. C: Oscillation chains only spread for a small range of input frequencies, but fail to emerge at other frequencies.

Part III

Discussion

10 The Problem of Neuronal Communication

How do different brain areas communicate with each other? How is neuronal activity reliably and at the same time flexibly routed across different brain structures during neuronal processing? The problem of how different neuronal networks communicate has recently received increased attention and a variety of theories have been proposed and investigated in neurobiological experiments. The aim of this thesis was to experimentally test certain aspects of neuronal communication and gain new theoretical insights on how the brain may use complementary strategies to get information from the environment across different stages of neuronal processing.

Several recent reviews have highlighted the importance of understanding the processes underlying communication between different brain areas (Vogels et al., 2005; Kumar et al., 2010; Beggs and Timme, 2012), but the formulation of the problem already dates back to Hebb (1949) and Bak (1996). Hebb realized that *"The central problem with which we must find a way to deal can be put in two different ways. Psychologically, it is the problem of thought: some sort of process that is not fully controlled by environmental stimulation and yet cooperates closely with that stimulation...Physiologically, the problem is that of transmission of excitation from sensory to motor cortex"*. He was interested in the neuronal activity that implements communication between sensory input and the motor output, and introduced the concept of cell assemblies to explain how excitation is reliably transmitted across the brain (Fig. 10.1A). Another description of the problem was introduced by Bak (1996) and referred to as the monkey problem. He imagined a monkey sitting in front of a computer screen and being presented either with a red or green dot stimulus. The monkey was trained to link the presentation of one color with a button press of one thumb and the other color with the thumb of the other hand (Fig. 10.1B). Bak wondered how neuronal networks can learn and achieve such a precise input-ouput matching and reliably communicate messages through a vast number of neurons interceding between sensory and motor regions of the cortex.

Evidently, any mechanism implementing neuronal communication must fulfill a number of criteria to solve the monkey problem. First, communication must be reliable, such that a message that is generated in sensory areas by environmental stimuli is faithfully processed and transmitted to the motor cortex. This means that the neuronal signal representing and processing the stimulus must not fade away before reaching the motor cortex. Second, neuronal communication needs to be selective so that a given input signal only targets its associated output without activating other output areas. Finally, the routing of neuronal signals must be flexible to allow learning and the formation of new input-output links. A number of theories have been developed, which account for these three prerequisites of neuronal communication in different ways. These include the criticality hypothesis (Plenz and Thiagarayan, 2007; Beggs, 2008), the synfire chain

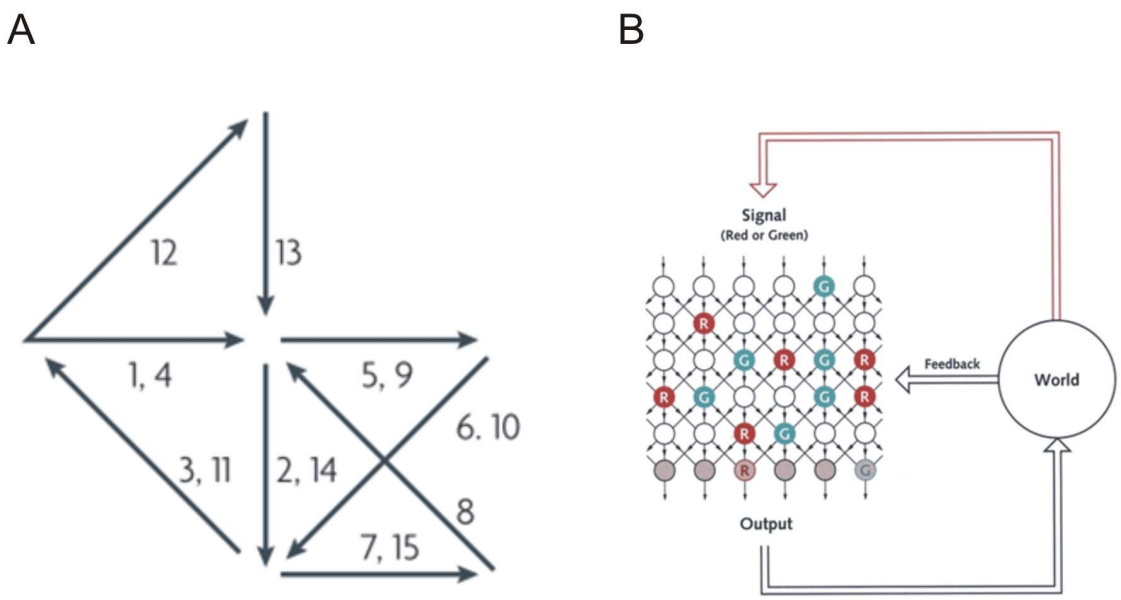

Figure 10.1: A: Sequence of cell assemblies spreading through the cortex. Adapted from Hebb (1949). B: Block diagaram of brain interacting with the outer world. The world shows a red or green signal or green signal to the brain. The signal is fed into the brain at arbritary neurons. The bottom row represents the action resulting from the processes going on in the brain. This is transmitted to the environment, which provides a feedback. If the response is correct, the environment provides food; if the response is not correct, the environment does not provide food. Taken from Bak (1996).

hypothesis (Abeles, 1982; 1991) and the communication through coherence hypothesis (Fries, 2005; 2009). In this thesis, we have experimentally explored the criticality hypothesis and tested for the presence of critical features in spontaneous activity of anesthetized cats and awake monkeys. Moreover, we proposed a new theoretical framework that potentially bridges the gap between the seemingly different concepts of synfire chains and communication through coherence, and evaluated its validity in numerical simulations.

11 Neuronal Avalanches and Criticality In Vivo

As reviewed in the introduction, the concept of criticality originated in the field of statistical physics during the last century and was used to characterize peculiar features of second order phase transitions in thermodynamical systems. These features included the emergence of complex spatiotemporal patterns with long-range correlations and power laws in various measures. While the original notion of criticality was restricted to closed thermodynamical system and required fine tuning of critical parameters (e.g.

temperature or pressure), it was later extended by Per Bak and colleagues (Bak et al., 1987; Bak, 1996) and included self-organization as the driving force to achieve critical states. Self-organized criticality (SOC) attempted to explain the ubiquitous presence of complexity and power laws in natural and man-made systems. Bak also speculated that brain activity might be self-organized critical (Bak, 1996) and inspired neuroscientists to test the applicability of his ideas to brain dynamics. Since SOC explains complexity through cascading events in a critical system, criticality in brain activity was henceforth referred to as neuronal avalanches A number of studies searched for signs of neuronal avalanches in LFP and spiking activity of both *in vitro* and *in vivo* preparations. The results were mixed and depended on the type of preparation and signal used. Power laws were most often found in local field potentials in *in vitro* and *in vivo* studies (Beggs and Plenz, 2003; Gireesh et al., 2008; Petermann et al., 2009), even though some studies refuted the presence of power laws with rigorous statistical methods (Touboul and Destexhe, 2010; Dheghani et al., 2012). The most ambiguous results were obtained in spiking activity, where *in vitro* studies generally displayed robust critical features (Mazzoni et al., 2007; Pasquale et al., 2008; Friedman et al., 2012), while power laws were in general absent *in vivo* (Bédard et al., 2006; Petermann et al., 2009; Ribeiro et al., 2010; Dheghani et al., 2012), except during ketamin-xylazin anesthesia (Ribeiro et al., 2010). The seemingly general existence of criticality in local field potentials prompted some authors to postulate that neuronal avalanches serve as a substrate for Hebbian cell assemblies (Plenz and Thiagarayan, 2007) and establish communication between different brain areas through spreading neuronal activity and long-range correlations (Chialvo, 2010; Beggs and Timme, 2012). The widespread absence of critical features in spiking activity was accounted for by the small number of neurons recorded by multi-electrode arrays, which leads to significant sub-sampling of the local neuronal population (Priesemann et al., 2009; Ribeiro et al., 2010). This problem is less prominent in LFP recordings, as much larger populations of neurons are sampled and thus reflect critical features more faithfully.

11.1 Neuronal Avalanches in Spontaneous Activity In Vivo

In order to further clarify the dichotomous results in spiking activity and local field potentials, we recorded LFP and action potentials in the primary visual cortex of anesthetized (halothane) cats with 16 channel multi-electrode arrays. We performed standard neuronal avalanche analysis as described in Beggs and Plenz (2003) for LFP and spiking activity, and in addition analyzed inter-spike intervals and computed average auto- and crosscorrelation histograms of the recorded spike trains. The results showed clear power laws in cluster size distributions for the majority of datasets in the LFP, while the analysis of spiking activity had an ambiguous outcome. In about two thirds of the datasets visual inspection showed power laws with a significantly better power

law fit compared to an exponential function which indicates statistical independence. Similar results were found for lifetime distributions. Notably, the power law exponent was similar across these datasets with a value of ~-1.8. A power law also fitted the inter-spike interval of the population spike trains or averaged across individual units better than an exponential distribution. However, cluster size and lifetime distributions of the remaining datasets were visibly curved and power law fits did not exceed fits of exponential distributions. Similar results were obtained for the inter-spike interval distributions. Another notable difference between these two types of datasets was visible in their correlation structure. Peaks in auto - and crosscorrelation histograms of recordings with power laws were higher and broader compared to datasets, in which a power law was absent. This result indicates that correlations were on average stronger and spanned a longer timescale, when a power law was present. In order to explain these different results, we proposed two hypotheses. First we considered the sub-sampling hypothesis (see above), which attributes the lack of power law to insufficient sampling of the spiking activity generated by the local neuronal network. To test this hypothesis, we randomly removed a varying number of spikes from datasets with power laws and indeed the power law was gradually replaced by curved distributions, as the number of deleted spikes increased. These findings make sub-sampling a viable hypothesis for the absence of power laws. However, we also suggested an alternative explanation, which postulates the existence of cortical states with different dynamics. The foundation of this hypothesis was our observation that the correlation structure between the two types of datasets was significantly different, which may be a consequence of fundamentally different dynamics rather than insufficient sampling of spiking activity. The cortex may display critical activity at one point in time, but can also exhibit activity that deviates from criticality at other times.

11.2 Neuronal Avalanches and Cortical States

Cortical state has been traditionally defined as the amount of slow fluctuations (1-5 Hz) in population signals like the EEG and LFP, and varied between synchronized states with large amplitude in slower frequencies during slow-wave sleep and desynchronized activity during waking. Recent studies (see Harris and Thiele, 2011 for review) related the synchronized state to population bursts (up-phases) in spiking activity that are coherent across all recorded neurons and followed by periods of no activity (down phases) (e.g. Luszak et al., 2007; Renart et al., 2010). In contrast, desynchronized states and suppression of slow activity in the LFP are accompanied by continuous and irregular population spiking activity without the burst structure found during synchronization (Curto et al., 2009; Renart et al., 2010). This type of activity resembles the asynchronous irregular (AI) state found in neuronal network models of cortical activity (Brunel, 2000). Importantly, synchronous activity is not only found during deep sleep,

but is also seen in awake animals during immobility and quiet wakefulness (Petersen et al., 2003; Crochet et al., 2006; Poulet and Petersen, 2008). Moreover, the degree of synchronization fluctuates along a continuum and is not restricted to the extreme ends of synchronized and desynchronized states (Curto et al., 2009). Thus, we hypothesized that synchronized cortical dynamics with its large population fluctuations and long-range correlations comes closer to the definition of criticality, while more desynchronized states significantly deviate from critical activity.

In order to test the hypothesis that different cortical states can account for the presence in some, but absence in other datasets of our previous study, we conducted more experiments in the primary visual cortex of anesthetized cats (isoflurane) and one awake monkey. We used 32 channel silicon probes in the cat and 96 channel Utah arrays in the monkey to record spontaneous activity. Cortical states were separated based on differences in the frequency composition of the LFP power spectrum averaged across all electrodes in short time segments of one second. These differences were evaluated using principal component analysis and k-means clustering, and resulted in the separation of four to five different states, which mostly differed in the frequency bands between 1-5 Hz and 5-15 Hz. These states reflected a continuum of synchronization levels with strongly synchronized and desynchronized activity on both ends. Synchronization in spiking activity was assessed by calculating auto-correlation histograms (ACH) and Fano factors (FF) of the population spike train. More synchronized states displayed higher and broader ACH center peaks as well as larger Fano factors compared to more desynchronized activity, where peaks were less prominent and Fano factors smaller. Interestingly, while the population firing rate decreased with desynchronization in the cat, it increased in the monkey recordings. Moreover, spike-triggered average analysis yielded an association of spiking activity with large amplitude LFP deflections during synchronized states and smaller deflections during desynchronization. Thus, our analysis confirmed the presence of different cortical states with varying degrees of synchronization at the spiking level in both anesthetized cats and awake monkeys.

Next, we performed neuronal avalanche analysis and quantified the tail of the cluster size distributions with the scale parameter (sigma) of a lognormal distribution. Larger values of sigma indicate heavy tails close to power laws, while smaller values reflect stronger deviation from power laws. Indeed, upon visual inspection cluster size distributions of synchronized states showed a power law and yielded larger values of sigma, while desynchronized activity was characterized by markedly curved distributions with smaller values of sigma. However, shuffling analysis revealed that even in the most desynchronized states some synchronization remained, which we attributed to firing rate fluctuations at longer time scales due to non-stationarity of the spiking activity. Heavier tails were also found in the inter-spike interval distributions of the population spike trains during synchronized states as indicated by larger values of the coefficient of variation as opposed to desynchronized states, in which distributions rather indicated

statistical independence between spikes.

Finally, we tested the LFP for signs of criticality and devised a new method that takes the entire signal into account without the need of thresholding as in previous studies (Beggs and Plenz, 2003; Touboul and Destexhe, 2010; Dehghani et al., 2012). Surprisingly, in contrast to the spiking activity and similar to our previous results, distributions close to power laws were present in all states, even though the power law cutoff was shifted to higher values in more synchronous states due to the larger amplitude of LFP deflections. Shape parameter values of fitted gamma distributions indicated strongly heavy-tailed distributions across all states. Importantly, despite slight differences in the LFP correlation structure between states, the overall average correlation between electrodes remained very high (>0.7).

Taken together, these results show a clear dependence of power law distributions on cortical state in spiking activity, while the dynamical state of the cortex has little impact on power law distributions in the LFP due to an overall high level of correlation. These findings raise the question about the origin of the dichotomous character of spiking activity and LFP with respect to signs of criticality. As mentioned above, a possible answer is the fact that current multi-electrode technology highly sub-samples the activity of individual neurons, while the LFP records the summed activity of a much larger neuronal population. The detrimental effect of sub-sampling on power laws statistics has been shown by theoretical studies (Priesemann et al., 2009; Ribeiro et al., 2010) and used to explain the absence of power law in spiking activity during waking and sleep in rats (Ribeiro et al., 2010). Within this framework, all neuronal activity is critical even during seemingly desynchronized states, but signs of criticality remains hidden due to insufficient sampling of spikes. Even though Ribeiro et al. (2010) did not find power laws in their spiking data, they found evidence for criticality even in desynchronized states using a scaling approach and supported the sub-sampling hypothesis. Our findings seem to be consistent with sub-sampling as power laws in the LFP are indeed invariant to the cortical state, while spiking activity has critical features only in synchronized states.

However, an alternative scenario is that the cortex can switch between critical states with large-scale synchronization and non-critical dynamics with rather desynchronized activity. In case of cortical desynchronization, even the sampling of all spikes from all neurons of a local population would still result in a deviation from power law statistics as demonstrated in computer simulations (El Boustani et al., 2007). Some studies suggested that cortical activity is in general non-critical (Bédard et al., 2006; Dehghani et al., 2012), but they did not separate states at a fine temporal scale like in our study which reveals short epochs of population synchronization even in the awake monkey. Importantly, previous reports of power law in spiking activity came from experiments in reduced *in vitro* preparations with alternations of up-and down phases (Mazzoni et

al., 2007; Pasquale et al., 2008) that are associated with widespread synchronization or rats anesthetized with Ketamin-Xylazin (Ribeiro et al., 2010), which produces a regular oscillation of up- and down activity. A study by Friedman et al. (2012) tested other predictions by criticality theory in spiking activity of *in vitro* experiments and found robust evidence for a critical state during large-scale synchronization of spiking activity. Two recent studies have reported asynchronous activity in awake monkeys (Ecker et al., 2010) and anesthetized rats (Renart et al., 2010), and it was argued based on theoretical grounds that the cortex has mechanisms that enforce desynchronization of neuronal activity (Renart et al., 2010; Tetzlaff et al., 2012). According to these studies, inhibition plays an important role in preventing neuronal excitation to build up and hence the generation of spreading neuronal avalanches. Importantly, inhibition seems to dominate during desynchronized activity (Rudolph et al., 2007; Haider et al., 2013) and thus destroy the balance of excitation and inhibition found during critical neuronal dynamics (Shew et al., 2009; Yang et al., 2012). Changes in cortical state are triggered by neuromodulators like acetylcholine, noradrenaline or serotonine (Harris and Thiele, 2011), whose effects at the cellular and synaptic level induce state transitions. In addition, glutamatergic input from subcortical structures like the thalamus plays an important role in desynchronizing cortical activity as demonstrated by a recent study (Poulet et al., 2012). Even though it seems possible that the cortex generates genuine desynchronized activity away from a critical dynamical regime, the presence of power laws and strong correlation in LFP despite neuronal desynchronization at the spiking level argues against an asynchronous state in cortical activity. However, it is conceivable that a considerable amount of correlation between channels in the LFP is spurious and due to passive spread of electric signals through volume conduction, as already pointed out by other neuronal avalanche studies (Touboul and Destexhe, 2010; Dehghani et al., 2012). This claim received support by a recent study based on current source density analysis which found passive spread of neuronal activity up to 6mm of cortex (Kajigawa and Schroeder, 2011). This in contrast to previous reports which suggested a purely local origin of the LFP (Katzner et al., 2009; Xing et al., 2009), not exceeding a spread of 200-400m. Volume conduction across the entire electrode array may thus explain the high average correlation in the LFP despite clear signs of desynchronization. However, pharmacological manipulations during *in vitro* studies on neuronal avalanches changed the synchronization profile of the LFP between different recordings channels indicating that volume conduction alone cannot fully account for large scale synchrony in the LFP (Beggs and Plenz, 2003; Shew et al., 2009; Yang et al., 2012) In summary, our results on neuronal avalanches in anesthetized cats and awake monkeys are consistent with both the sub-sampling hypothesis and the idea that the cortex can generate genuinely desynchronized activity, if volume conduction is considered as a potential source of spurious correlations in the LFP.

From a functional point of view, criticality has been viewed as a dynamical state which

creates complex spatiotemporal activity patterns and hence optimizes neuronal network functions like information processing, storage and transmission as well as the dynamical range of stimulus responses (see Beggs, 2008 for review) . It was argued that large fluctuations of neuronal activity inherent to critical neuronal dynamics and visible in the long tail of the power law facilitate neuronal communication across long distances in the brain (Beggs and Thimme, 2012). In this view, a stimulus would trigger a neuronal avalanche in sensory cortices, which would spread across the cortex carrying the stimulus information to other brain areas, where it is further processed. However, as pointed out by Vogels et al. (2005), this scenario may be too simple to solve the problem of neuronal communication. Even though criticality makes communication between neuronal networks highly flexible, as it can easily create new complex activity patterns and open up new communication pathways, it is not obvious how neuronal avalanches can solve the problem of stability. Power law distributions of fluctuation sizes indicate that despite the presence of large fluctuations, most neuronal avalanches remain small and may not be able to successfully spread across the processing chain of an environmental stimulus. Thus, trial to trial variability is high leading to successful transmission of activity, but in many cases also to propagation failure. This behavior poses serious limitations on the reliability of neuronal communication implemented by neuronal avalanches. Moreover, as demonstrated by our results, critical features are mainly seen, when the cortex exhibits large-scale synchronization, which affects large parts of the local network and presumably the rest of the cortex (Harris and Thiele, 2011). It is likely that freely spreading neuronal avalanches will not only activate areas representing a particular stimulus, but also spread to neighboring areas which process other stimuli. Thus, selectivity is not guaranteed by collective avalanche dynamics as seen during critical states. Rather, neuronal networks must create activity that spreads along specific and well defined pathways without affecting the rest of the network. Fine grained synchronization that affects only a subset of neurons in large neuronal networks is the foundation of two other theoretical frameworks of neuronal communication: the synfire chain (Abeles, 1982; 1991) and communication through coherence hypotheses (CTC; Fries, 2005; 2009). Notably, synfire chains have been shown to effectively transmit neuronal synchrony either with strong external background noise (Diesmann et al., 1999) or internal desynchronization generated by the neuronal network itself (Kumar et al., 2008). The CTC hypothesis is associated with synchronous oscillations in the beta/gamma band which predominately occur during cortical desynchronization (Munk et al., 1996; Herculano-Houzel et al., 1999). Thus, it is possible that the cortex actively suppresses large-scale synchronization and enforces desynchronization to allow the formation of precise patterns of synchronization that will process incoming stimuli selectively and with high fidelity. It remains to be seen, whether desynchronized cortical activity still has critical features (Ribeiro et al., 2010) or represents a truly asynchronous dynamical regime as suggested by various theoretical models (El Boustani et al., 2007; Renart et al., 2010; Tetzlaff et al., 2012).

12 Synfire Chains and Coherent Oscillations

The classical model for neuronal communication and information transmission is the synfire chain first introduced by Abeles more than 30 years ago (Abeles, 1982). Given the small effect of individual action potentials on postsynaptic targets he postulated that volleys of presynaptic spikes will drive downstream neurons most effectively, if they arrive nearly synchronously. He constructed a layered network, in which excitatory neurons of each layer are connected to neurons of the next layer through divergent-convergent connections with similar delays. This connectivity structure enables the network to faithfully propagate synchronous activity along its layers. A stimulus would trigger enough synchrony in layer one of a synfire chain, which is stably relayed to other cortical areas, represented by the various layers of the chain. Synfire chains were successfully implemented in a variety of theoretical studies (e.g. Diesmann et al., 1999; Gewaltig et al., 2001) and precise spatiotemporal spiking patterns, a consequence of the successive activation of neurons with stable delays in the chain, were reported in experimental studies (e.g. Shmiel et al., 2006). The synfire chain model reflects a highly stable way of neuronal communication and in addition can also provide selectivity, as synchronous volleys only spread within the organized synfire chain structure without affecting the asynchronous background activity, first shown by Kumar et al. (2008). However, a synfire chain is a rather inflexible structure, as the connections and their weights need to be set by the modeler and no convincing learning mechanism is yet known that would flexibly create a synfire chain architecture with sufficiently strong synapses as a function of ever changing computational needs imposed by the environment.

While synchrony in synfire chains is generated by common drive from previous layers, synchronization in the communication through coherent oscillation model (CTC; Fries, 2005; 2009), another framework for neuronal communication, is thought to arise from very different mechanisms. The basis for the CTC hypothesis are local oscillations generated by the interaction of excitatory and specialized inhibitory neurons (basket cells) which provide synchronous spiking activity that can effectively drive neurons in other local networks. In order to establish communication between two brain areas, oscillations in both areas need to create a consistent phase relationship, such that excitatory spike volleys of one oscillation arrive at the receptive phase (i.e. when inhibition is weak) of the other oscillation. The resulting coherent oscillation allows the exchange of information between different neuronal networks (Womelsdorf et al., 2007; Buehlmann et al., 2010). The role of such coherent oscillations in the beta/gamma band in cognition and mental diseases like schizophrenia has been shown by a variety of studies (Varela et al., 2001; Uhlhaas and Singer, 2006; Siegel et al., 2011).

In this thesis, we asked the question, whether there is a link between the synfire chain

and CTC hypotheses, since both operate with synchronization of excitatory activity. We hypothesized that synchronization in these frameworks may have a common origin and both types of communication are a manifestation of different computational demands. More specifically, we put forward the idea that a spreading coherent oscillation may arise in diluted synfire chains, with a connectivity that is insufficient to faithfully transmit synchrony. Recurrent interaction between excitatory and inhibitory neurons in each layer of the synfire chain amplifies excitation generated by small common drive from previous layers through a resonant oscillation. This mechanism compensates for the weak connections in the diluted chain and leads to the stable propagation of a coherent oscillation across the network, a process, which we call "oscillation chain". Notably, these oscillation chains can spread along weak connections and thus have access to a large number of diluted synfire chains (Abeles, 2009), thereby allowing for more flexible routing of synchronous activity. Moreover, we conjectured that the precise spike timing relationship between neurons within the coherent oscillation may induce synaptic plasticity and potentiation, which would reduce the number of oscillation cycles required to propagate synchrony. Once the excitatory connections between the layers of the network are sufficiently strong, oscillation chains are transformed into synfire chains, i.e. synchrony can be transmitted through a single synfire wave without the need of amplification in several oscillation cycles. Thus, oscillation chains can exploit weak connections in neuronal network, which are initially inaccessible to synfire chains, and process novel stimuli hitherto unknown to the neuronal network. However, they require a temporally prolonged presentation of the stimulus, so that excitation can be amplified and transmitted within several oscillation cycles. In contrast, synfire chains transmit synchrony even with a brief presentation of the stimulus and process already familiar stimuli learned previously within the coherent activity of an oscillation chain.

We tested this framework by simulating synfire chain networks of integrate and fire neurons which in addition contained a population of inhibitory neurons in each layer. These neurons were driven by the local excitatory population and provided feedback inhibition to the excitatory neurons. The first layer of the network was stimulated with either rhythmic or single synchronous spike volleys, and the propagation characteristics of the chain were investigated as a function of the input and the synaptic strength of the connections between the layers. We indeed found spreading coherent oscillations, when rhythmic input was provided at the resonance frequency of the network and connections were sufficiently strong. As predicted, the number of cycles needed to propagate synchrony to the end of the chain decreased with increasing synaptic weights and resulted in complete transmission of the spike volley within on cycle with strong synapses. Hence, synaptic potentiation resulted in the transformation of oscillation chains into synfire chains. In summary, the simulation results bridge the gap between the seemingly different concepts of synfire chains and the communication through coherence hypothesis, and link both of them through synaptic plasticity.

13 An Integrated View of Neuronal Communication

Neuronal communication is thought to be based on fine-grained spatiotemporal patterns of activity (Siegel et al., 2011). This may allow the brain to effectively code and process different stimuli without interference between them. As shown and discussed in this thesis, the brain is able to generate both large-scale synchronization of activity, which affects large parts of the brain, and potentially also precise patterns of synchronization through synfire chains and coherent beta/gamma oscillations. Importantly, precise neuronal activity is associated with globally desynchronized cortical states, as shown theoretically for synfire chains (Kumar et al., 2008) and experimentally for oscillations in the gamma range (Munk et al., 1996; Herculano-Houzel et al., 1999, Rodriguez et al., 2009). In addition, studies have provided evidence that natural scenes are best represented during desynchronization in rat visual cortex (Goard and Dan, 2009), and stimuli evoke cortical desynchronization (Poulet et al., 2008; 2012) and widespread inhibition that only allows very local spread of excitation (Haider et al., 2013). In contrast, neuronal activity associated with absent or reduced cognitive abilities during, e.g. during slow wave sleep and drowsiness, shows patterns of global synchronization linked with slow oscillations of up- and down phases (Petersen et al., 2003; Nir et al., 2011). Thus, effective cortical processing and cognitive functioning seems to require cortical desynchronization and suppression of large fluctuations of activity. Note that this desynchronization could be realized as an asynchronous-irregular state (Brunel, 2000) or as synchronous chaos with local broadband synchronization and global decorrelation (Battaglia and Hansel, 2011) Desynchronized activity might enable the brain to route activity along specific pathways that can escape the strong inhibition found during desynchronization (Rudolph et al., 2007; Renart et al., 2010; Haider et al., 2013). According to the synfire chain model, these pathways are endowed with specialized connections that create strong and synchronized excitatory activity and allow the faithful and selective spread of excitation along a processing hierarchy despite the influence of inhibition. Alternatively, in case these connections are insufficient, excitation may be amplified within a resonant oscillation and propagate as a coherent oscillation chain across the network, as suggested in this thesis.

However, the question remains how criticality can be reconciled with the notion of cortical desynchronization and precise communication with synfire-and oscillation chains. Most studies of criticality in neuronal networks are based on the notion of a critical sandpile, in which individual avalanches slide down the pile separated by periods of silence, during which new sand needs to be supplied. Not surprisingly, these studies are mostly based on synchronized states found *in vitro* (Beggs and Plenz, 2003; Pasquale et al., 2008; Shew et al., 2009; Friedman et al., 2012), *in vivo* during anesthesia (Ribeiro et al., 2010) or *in silico* (Benayoun et al., 2010; Millman et al., 2010), in which each up-state can be conceptualized as a single neuronal avalanche that is

separated by another avalanche by down-phases. Thus, avalanches are triggered at the beginning of an up-phase spread across cortical areas, which are in an excitable, but silent down-phase. This enables avalanches to access widespread parts of the brain, which is seen as global synchronization. In contrast, during continuous and desynchronized activity, avalanches soon encounter inhibition and are prevented from spreading unselectively across the entire cortex, unless relayed across organized and strong connections or propagated along resonant and coherent oscillations, as argued above. Hence, these precise avalanches (synfire- and oscillation chains) are embedded in desynchronized background activity, unlike those found during cortical synchronization, which spread across inactive cortical areas. It is conceivable that these fine-grained patterns of cortical synchronization still reflect critical activity, in a sense that their patterns are complex and enable the brain to flexibly process and represent ever changing input from the environment. In this context, global desynchronization would be necessary to make these patterns stimulus specific and prevent cross-over of activity to neuronal networks that represent other stimuli, as presumably seen during large-scale synchronization. However, since these patterns are formed within desynchronized activity, power laws and large-scale synchronization, as predicted from criticality theory, are lost due to the mixing of fine-grained correlations with decorrelated background dynamics (Hahn et al., 2011). In line with the criticality hypothesis, evidence for critical dynamics in spiking activity beyond power laws was found in desynchronized activity of awake rats, when scaling approaches were used (Ribeiro et al., 2010). In this thesis, we also found power laws and strong synchronization during epochs of desynchronized activity in the LFP, while spiking activity showed clear signs of decorrelation. This seems to be consistent with the idea that the LFP preferentially picks up local synchronized activity, which might reflect fine-grained spatiotemporal patterns of synchrony, which cannot be easily detected by spiking activity. It is also in accordance with a variety of reports based on other macroscopic signals like the EEG or MEG which found evidence for criticality in the brain (see Werner, 2010, for review). However, it remains to be seen how much the LFP is contaminated by spurious correlation due to volume conduction which was recently shown to be significant across large patches of the cortex (Kajigawa and Schroeder, 2011).

14 Outlook

In this thesis we have investigated critical features of cortical activity as a function of cortical state and attempted to find a common theoretical framework for precise neuronal communication through synchrony. Our results clearly indicate that classical critical features such as power laws and long-range correlations are state dependent in spiking activity, whereas they are still present in the LFP during all observed states.

Further studies need to explore, whether seemingly desynchronized cortical activity is still compatible with the notion of a critical state as pioneered by Ribeiro et al. (2010). These studies will also have to establish, whether absence of power law is due to subsampling or may be interpreted as a result of mixing fine-grained correlation potentially created by synfire-or oscillation chains and decorrelated background activity. Moreover, the exact role of volume conduction for large-scale synchronization and the presence of power laws need to be determined in population signals like the LFP, as already pointed out by Dehghani et al. (2012). Significant long-range volume conduction as described by Kajigawa and Schroeder (2011) may necessitate a reevaluation of power laws reported in the LFP of multi-electrode recordings *in vivo* (e.g. Petermann et al., 2009).

Furthermore, our novel theoretical framework and modeling results suggest an intimate link between synchronization provided by synfire chains, coherent oscillations in the gamma/beta range and synaptic plasticity. However, our simplified simulation needs to be extended in several ways. First, we used biologically unrealistic current-based synapses, which need to be replaced by more biologically plausible conductance-based synapses. Second, in our study we mimicked synaptic potentiation by increasing the synaptic weights between different layers of the network externally. Thus, synaptic plasticity should be implemented directly in the network and it remains to be seen, whether realistic plasticity rules can transform coherent oscillations into synfire chains. Third, gamma oscillations in the brain are subject to cycle skipping, i.e. that excitatory neurons only fire during a fraction of the entire oscillation. However, in our study excitatory neurons discharged at almost every cycle, a finding, which requires further investigation. Moreover, we used purely feedforward connectivity in our network, which seems unrealistic given the dense network of feedback connections in the brain. However, there is growing evidence that feedforward and feedback connections do not originate in the same cortical layers (Wang, 2010) and more importantly do not use the same spectral signature to transmit neuronal signals. While gamma activity is mainly found during feedforward processing (e.g. Roelfsema et al., 2012), feedback signals are carried through beta (Engel and Fries, 2010; Siegel et al., 2011) or alpha band activation (Roelfsema et al., 2012). Thus, unidirectional oscillation chains may not seem unrealistic and further research needs to be undertaken to study the interaction of bidirectional chain activity with different frequencies. Finally, the oscillation chain hypothesis needs to be tested in experiments using large-scale recordings and manipulation techniques (e.g. optogenetics) by studying the role of precise excitatory synchronization patterns in the generation of coherent oscillations.

15 Bibliography

References

[1] M. Abeles. Local cortical circuits: An electrophysiological study. 1982.

[2] M Abeles. Role of the cortical neuron: integrator or coincidence detector? *Israel journal of medical sciences*, 18(1):83–92, January 1982.

[3] M. Abeles. *Corticonics: Neural Circuits of the Cerebral Cortex*. Cambridge University Press, 1991.

[4] M. Abeles. Synfire Chains. *Scholarpedia*, 2009.

[5] M Abeles, H Bergman, E Margalit, and E Vaadia. Spatiotemporal firing patterns in the frontal cortex of behaving monkeys. *Journal of neurophysiology*, 70(4):1629–38, October 1993.

[6] M Abeles, G Hayon, and D Lehmann. Modeling compositionality by dynamic binding of synfire chains. *Journal of computational neuroscience*, 17(2):179–201, 2004.

[7] C Adami and NJ Cerf. Physical complexity of symbolic sequences. *Physica D*, 137:62–69, 2000.

[8] ED Adrian. *The basis of sensation: the action of the sense organs*. Christophers, London, 1928.

[9] A. Aertsen, M. Diesmann, and MO Gewaltig. Propagation of synchronous spiking activity in feedforward neural networks. *Journal of physiology-Paris*, 90(3-4):243–247, 1996.

[10] DJ Amit. *Modeling brain function: The world of attractor neural networks*. Cambridge University Press, 1989.

[11] T Andrews. The Bakerian lecture: On the continuity of gaseous and liquid states of matter. *Philosophical transactions of the royal society*, 159:575–590, 1869.

[12] HM Arnoldi and W Brauer. Synchronization without oscillatory neurons. *Biological cybernetics*, 74(3):209–23, March 1996.

[13] HM Arnoldi, KH Englmeier, and W Brauer. Translation-invariant pattern recognition based on Synfire chains. *Biological cybernetics*, 80(6):433–47, June 1999.

[14] W Ashby. Principles of the self-organizing dynamic system. *J. Gen. Psych.*, 37:125–128, 1947.

[15] Y Aviel, C Mehring, M Abeles, and D Horn. On embedding synfire chains in a balanced network. *Neural computation*, 15(6):1321–40, June 2003.

[16] N Axmacher, F Mormann, G Fernández, CE Elger, and J Fell. Memory formation by neuronal synchronization. *Brain research reviews*, 52(1):170–82, August 2006.

[17] R Azouz and CM Gray. Dynamic spike threshold reveals a mechanism for synaptic coincidence detection in cortical neurons in vivo. *Proceedings of the National Academy of Sciences of the United States of America*, 97(14):8110–85, July 2000.

[18] C Babiloni, F Babiloni, F Carducci, F Cincotti, F Vecchio, B Cola, S Rossi, C Miniussi, and PM Rossini. Functional frontoparietal connectivity during short-term memory as revealed by high-resolution EEG coherence analysis. *Behavioral neuroscience*, 118(4):687–97, August 2004.

[19] R Baddeley, LF Abbott, MC Booth, F Sengpiel, T Freeman, EA Wakeman, and ET Rolls. Responses of neurons in primary and inferior temporal visual cortices to natural scenes. *Proceedings of the royal society London B*, 264(1389):1775–83, December 1997.

[20] P Bak. *How Nature Works: The Science of Self-Organized Criticality*. Springer, 1996.

[21] P Bak and D R Chialvo. Adaptive learning by extremal dynamics and negative feedback. *Physical review. E, Statistical, nonlinear, and soft matter physics*, 63(3 Pt 1):031912, March 2001.

[22] P Bak and K Sneppen. Punctuated equilibrium and criticality in a simple model of evolution. *Physical review letters*, 71(24):4083–4086, 1993.

[23] P Bak, C Tang, and K Wiesenfeld. Self-Organized Criticality: An Explanation of 1/f Noise. *Physical review letters*, 59(4):381–384, 1987.

[24] SN Baker and RN Lemon. Precise spatiotemporal repeating patterns in monkey primary and supplementary motor areas occur at chance levels. *Journal of neurophysiology*, 84(4):1770–80, October 2000.

[25] GJ Ball, P Gloor, and N Schaul. The cortical electromicrophysiology of pathological delta waves in the electroencephalogram of cats. *Electroencephalography and clinical neurophysiology*, 43(3):346–61, September 1977.

[26] HB Barlow. Single units and sensation: a neuron doctrine for perceptual psychology? *Perception*, 1(4):371–94, January 1972.

[27] M Bartos, I Vida, M Frotscher, A Meyer, H Monyer, JRP Geiger, and P Jonas. Fast synaptic inhibition promotes synchronized gamma oscillations in hippocampal interneuron networks. *Proceedings of the National Academy of Sciences of the United States of America*, 99(20):13222–7, October 2002.

[28] M Bartos, I Vida, and P Jonas. Synaptic mechanisms of synchronized gamma oscillations in inhibitory interneuron networks. *Nature reviews neuroscience*, 8(1):45–56, January 2007.

[29] M Bartos, I Vida, and P Jonas. Synaptic mechanisms of synchronized gamma oscillations in inhibitory interneuron networks. *Nature reviews neuroscience*, 8(January):45–56, 2007.

[30] D Battaglia and D Hansel. Synchronous chaos and broad band gamma rhythm in a minimal multi-layer model of primary visual cortex. *PLoS computational biology*, 7(10):e1002176, October 2011.

[31] M Bazhenov and I Timofeev. Thalamocortical oscillations. *Scholarpedia*, 1(6):1319, June 2006.

[32] M Bazhenov, I Timofeev, M Steriade, and TJ Sejnowski. Model of thalamocortical slow-wave sleep oscillations and transitions to activated states. *Journal of neuroscience*, 22(19):8691–704, October 2002.

[33] C Bédard, H Kroeger, and A Destexhe. Does the 1/f frequency scaling of brain signals reflect self-organized critical states? *Physical review letters*, 97(11):118102, 2006.

[34] JM Beggs. The criticality hypothesis: how local cortical networks might optimize information processing. *Philosophical transactions of the royal society A. Mathematical, physical, and engineering sciences*, 366(1864):329–43, February 2008.

[35] JM Beggs and D Plenz. Neuronal avalanches in neocortical circuits. *Journal of neuroscience*, 23(35):11167–77, December 2003.

[36] JM Beggs and D Plenz. Neuronal avalanches are diverse and precise activity patterns that are stable for many hours in cortical slice cultures. *Journal of neuroscience*, 24(22):5216–29, 2004.

[37] JM Beggs and N Timme. Being critical of criticality in the brain. *Frontiers in fractal physiology*, 3:163, January 2012.

[38] M Benayoun, JD Cowan, W van Drongelen, and E Wallace. Avalanches in a Stochastic Model of Spiking Neurons. *PLoS computational biology*, 6(7):e1000846, July 2010.

[39] CH Bennet. *Logical depth and physical complexity. In: R. Herken (ed.): The Universal Turing Machine. A Half Century Survey.* Oxford University Press, Oxford, 1988.

[40] B Berche, M Henkel, and R Kenna. Critical phenomena: 150 years since Cagniard de la Tour. *Journal of physical studies*, 13:3001–1 – 3001–4, 2009.

[41] H Berger. Uber das Elektroenkephalogram des Menschen. *Archive für Psychiatrie und Nervenheilkrankheiten*, 87:527–570, 1929.

[42] JD Berke, M Okatan, J Skurski, and HB Eichenbaum. Oscillatory entrainment of striatal neurons in freely moving rats. *Neuron*, 43(6):883–96, September 2004.

[43] O Bernander, C Koch, and R J Douglas. Amplification and linearization of distal synaptic input to cortical pyramidal cells. *Journal of neurophysiology*, 72(6):2743–53, December 1994.

[44] N Bertschinger and T Natschläger. Real-time computation at the edge of chaos in recurrent neural networks. *Neural computation*, 16(7):1413–36, July 2004.

[45] GQ Bi and MM Poo. Synaptic modifications in cultured hippocampal neurons: dependence on spike timing, synaptic strength, and postsynaptic cell type. *Journal of neuroscience*, 18(24):10464–72, December 1998.

[46] GQ Bi and MM Poo. Distributed synaptic modification in neural networks induced by patterned stimulation. *Nature*, 401(6755):792–6, October 1999.

[47] E Bienenstock. A model of neocortex. *Network*, 6:179–224, 1995.

[48] E Du Bois-Reymond. *Untersuchungen über thierische Elektricität.* E.G. Reimer, Berlin.

[49] C Börgers, S Epstein, and NJ Kopell. Background gamma rhythmicity and attention in cortical local circuits: a computational study. *Proceedings of the National Academy of Sciences of the United States of America*, 102(19):7002–7, May 2005.

[50] C Börgers and NJ Kopell. Gamma oscillations and stimulus selection. *Neural computation*, 20(2):383–414, February 2008.

[51] V Braitenberg and A Schüz. *Cortex: Statistics and Geometry of Neuronal Connectivity (2nd ed.).* Springer, 1998.

[52] JH Breasted. *The Edwin Smith Surgical Papyrus.* University of Chicago Press, Chicago, 1930.

[53] M Brecht, W Singer, and AK Engel. Correlation analysis of corticotectal interactions in the cat visual system. *Journal of neurophysiology*, 79(5):2394–407, May 1998.

[54] V Bringuier, Y Frégnac, A Baranyi, D Debanne, and DE Shulz. Synaptic origin and stimulus dependency of neuronal oscillatory activity in the primary visual cortex of the cat. *Journal of physiology*, 500 (Pt 3:751–74, May 1997.

[55] P Broca. Sur la siège de la faculté du langage articulé. *Bulletins de la Societé d'Anthropologie (Paris)*, 4:200–300, 1963.

[56] N Brunel. Dynamics of sparsely connected networks of excitatory and inhibitory spiking neurons. *Journal of computational neuroscience*, 8(3):183–208, 2000.

[57] N Brunel and V Hakim. Fast global oscillations in networks of integrate-and-fire neurons with low firing rates. *Neural computation*, 11(7):1621–71, October 1999.

[58] N Brunel and V Hakim. Sparsely synchronized neuronal oscillations. *Chaos*, 18(1):015113, March 2008.

[59] N Brunel and XJ Wang. What determines the frequency of fast network oscillations with irregular neural discharges? I. Synaptic dynamics and excitation-inhibition balance. *Journal of neurophysiology*, 90(1):415–30, July 2003.

[60] S.G. Brush. History of the Lenz-Ising Model. *Reviews of modern physics*, 39(4):883–893, 1967.

[61] A Buehlmann and G Deco. Optimal information transfer in the cortex through synchronization. *PLoS computational biology*, 6(9), January 2010.

[62] EA Buffalo, P Fries, R Landman, TJ Buschman, and R Desimone. Laminar differences in gamma and alpha coherence in the ventral stream. *Proceedings of the National Academy of Sciences of the United States of America*, 108(27):11262–7, July 2011.

[63] EH Buhl, K Halasy, and P Somogyi. Diverse sources of hippocampal unitary inhibitory postsynaptic potentials and the number of synaptic release sites. *Nature*, 368(6474):823–8, April 1994.

[64] EH Buhl, G Tamás, and A Fisahn. Cholinergic activation and tonic excitation induce persistent gamma oscillations in mouse somatosensory cortex in vitro. *Journal of physiology*, 513:117–126, November 1998.

[65] G Buzsáki. Large-scale recording of neuronal ensembles. *Nature neuroscience*, 7(5):446–51, 2004.

[66] G Buzsáki. *Rhythms of the Brain*. Oxford University Press, 2006.

[67] G Buzsáki, CA Anastassiou, and C Koch. The origin of extracellular fields and currents–EEG, ECoG, LFP and spikes. *Nature reviews neuroscience*, 13(6):407–20, June 2012.

[68] G Buzsaki, RG Bickford, G Ponomareff, LJ Thal, R Mandel, and FH Gage. Nucleus basalis and thalamic control of neocortical activity in the freely moving rat. *Journal of neuroscience*, 8(11):4007–26, November 1988.

[69] G Buzsáki, C Geisler, DA Henze, and XJ Wang. Interneuron Diversity series: Circuit complexity and axon wiring economy of cortical interneurons. *Trends in neurosciences*, 27(4):186–93, April 2004.

[70] G Buzsáki and XJ Wang. Mechanisms of gamma oscillations. *Annual review of neuroscience*, 35(March):203–25, July 2012.

[71] R y Cajal. *The structure and connexions of neurons. In Nobel Lectures Physiology or Medicine 1901-1921*. Elsevier, New York, 1906.

[72] JA Cardin, LA Palmer, and D Contreras. Stimulus-dependent gamma (30-50 Hz) oscillations in simple and complex fast rhythmic bursting cells in primary visual cortex. *Journal of neuroscience*, 25(22):5339–50, June 2005.

[73] JQ Cardin, M Carlén, K Meletis, U Knoblich, F Zhang, K Deisseroth, LH Tsai, and CI Moore. Driving fast-spiking cells induces gamma rhythm and controls sensory responses. *Nature*, 459(7247):663–7, June 2009.

[74] S Carnot. *Réflexions sur la puissance motrice du feu*. Blanchard (1953), 1824.

[75] M Castelo-Branco, S Neuenschwander, and W Singer. Synchronization of visual responses between the cortex, lateral geniculate nucleus, and retina in the anesthetized cat. *Journal of neuroscience*, 18(16):6395–410, August 1998.

[76] MA Castro-Alamancos. Absence of rapid sensory adaptation in neocortex during information processing states. *Neuron*, 41(3):455–64, February 2004.

[77] H Câteau and T Fukai. Fokker-Planck approach to the pulse packet propagation in synfire chain. *Neural networks*, 14(6-7):675–85, 2001.

[78] M Chalk, JL Herrero, MA Gieselmann, LS Delicato, S Gotthardt, and A Thiele. Attention reduces stimulus-driven gamma frequency oscillations and spike field coherence in V1. *Neuron*, 66(1):114–25, April 2010.

[79] W Chang and DZ Jin. Spike propagation in driven chain networks with dominant global inhibition. *Physical review. E, Statistical, nonlinear, and soft matter physics*, 79(5 Pt 1):051917, May 2009.

[80] AC Chen and CS Herrmann. Perception of pain coincides with the spatial expansion of electroencephalographic dynamics in human subjects. *Neuroscience letters*, 297(3):183–6, January 2001.

[81] DM Chen, S Wu, A Guo, and ZR Yang. Self-organzied criticality in a cellular automaton model of pulse-coupled integrate-and fire neurons. *Journal of physics A: mathematical and general*, 28:5177, 1995.

[82] DR Chialvo. Emergent complex neural dynamics: the brain at the edge. *Nature physics*, 6(10):744–750, 2010.

[83] DR Chialvo and P Bak. Learning from mistakes. *Neuroscience*, 90(4):1137–48, January 1999.

[84] A Clauset, CR Shalizi, and MEJ Newman. Power-law distributions in empirical data. *SIAM review*, 51(4):661–703, 2009.

[85] EA Clement, A Richard, M Thwaites, J Ailon, S Peters, and CT Dickson. Cyclic and sleep-like spontaneous alternations of brain state under urethane anaesthesia. *PloS one*, 3(4):e2004, January 2008.

[86] SR Cobb, K Halasy, I Vida, G Nyiri, G Tamás, EH Buhl, and P Somogyi. Synaptic effects of identified interneurons innervating both interneurons and pyramidal cells in the rat hippocampus. *Neuroscience*, 79(3):629–48, August 1997.

[87] MR Cohen and A Kohn. Measuring and interpreting neuronal correlations. *Nature neuroscience*, 14(7):811–819, June 2011.

[88] A Compte, MV Sanchez-Vives, DA McCormick, and XJ Wang. Cellular and network mechanisms of slow oscillatory activity (<1 Hz) and wave propagations in a cortical network model. *Journal of neurophysiology*, 89(5):2707–25, May 2003.

[89] CM Constantinople and RM Bruno. Effects and mechanisms of wakefulness on local cortical networks. *Neuron*, 69(6):1061–8, March 2011.

[90] Á Corral, CJ Pérez, A Díaz-Guilera, and A Arenas. Synchronization in a lattice model of pulse-coupled oscillators. *Physical review letters*, 75(20):3697–3700, November 1995.

[91] S Crochet and CCH Petersen. Correlating whisker behavior with membrane potential in barrel cortex of awake mice. *Nature neuroscience*, 9(5):608–10, May 2006.

[92] NE Crone, DL Miglioretti, B Gordon, and RP Lesser. Functional mapping of human sensorimotor cortex with electrocorticographic spectral analysis. II. Event-related synchronization in the gamma band. *Brain*, 121 (Pt 1:2301–15, December 1998.

[93] JP Crutchfield and CR Shalizi. Thermodynamic depth of causal states: Objective complexity via minimal representations. *Physical review E*, 59:275–283, 1999.

[94] C Curto, S Sakata, S Marguet, Vladimir Itskov, and KD Harris. A simple model of cortical dynamics explains variability and state dependence of sensory responses in urethane-anesthetized auditory cortex. *Journal of neuroscience*, 29(34):10600–12, August 2009.

[95] Peter Dayan and LF Abbott. *Theoretical Neuroscience*. MIT Press, Cambridge, 2005.

[96] G Deco, A Buehlmann, T Masquelier, and E Hugues. The role of rhythmic neural synchronization in rest and task conditions. *Frontiers in human neuroscience*, 5(February):4, January 2011.

[97] N Dehghani, NG Hatsopoulos, ZD Haga, RA Parker, B Greger, E Halgren, SS Cash, and A Destexhe. Avalanche Analysis from Multielectrode Ensemble Recordings in Cat, Monkey, and Human Cerebral Cortex during Wakefulness and Sleep. *Frontiers in fractal physiology*, 3:302, January 2012.

[98] A Destexhe. Self-sustained asynchronous irregular states and Up-Down states in thalamic, cortical and thalamocortical networks of nonlinear integrate-and-fire neurons. *Journal of computational neuroscience*, 27(3):493–506, December 2009.

[99] A Destexhe, SW Hughes, M Rudolph, and V Crunelli. Are corticothalamic 'up' states fragments of wakefulness? *Trends in neurosciences*, 30(7):334–42, July 2007.

[100] M Diesmann, MO Gewaltig, and A Aertsen. Stable propagation of synchronous spiking in cortical neural networks. *Nature*, 402:529–533, 1999.

[101] R Doursat. *Contribution à l'étude des représentations dans le système nerveux et dans les réseaux de neurones formels. Ph.D. Thesis, Université Pierre et Marie Curie*. 1991.

[102] B Drossel and F Schwabl. Self-organized critical forest-fire model. *Physical review letters*, 69:1629–1632, 1992.

[103] JC Dunn. A Fuzzy Relative of the ISODATA Process and Its Use in Detecting Compact Well-Separated Clusters. *Journal of cybernetics*, 3(3):32–57, 1973.

[104] AS Ecker, P Berens, GA Keliris, M Bethge, NK Logothetis, and AS Tolias. Decorrelated neuronal firing in cortical microcircuits. *Science*, 327(5965):584–7, January 2010.

[105] R Eckhorn, R Bauer, W Jordan, M Brosch, W Kruse, M Munk, and H J Reitboeck. Coherent oscillations: a mechanism of feature linking in the visual cortex? Multiple electrode and correlation analyses in the cat. *Biological cybernetics*, 60(2):121–30, January 1988.

[106] S El Boustani, O Marre, S Béhuret, P Baudot, P Yger, T Bal, A Destexhe, and Y Frégnac. Network-state modulation of power-law frequency-scaling in visual cortical neurons. *PLoS computational biology*, 5(9):e1000519, September 2009.

[107] S El Boustani, M Pospischil, M Rudolph-Lilith, and A Destexhe. Activated cortical states: experiments, analyses and models. *Journal of physiology, Paris*, 101(1-3):99–109, 2007.

[108] A Engel, P Konig, A Kreiter, and W Singer. Interhemispheric synchronization of oscillatory neuronal responses in cat visual cortex. *Science*, 252(5009):1177–9, May 1991.

[109] AK Engel and P Fries. Beta-band oscillations–signalling the status quo? *Current opinion in neurobiology*, 20(2):156–65, April 2010.

[110] AK Engel and W Singer. Temporal binding and the neural correlates of sensory awareness. *Trends in cognitive sciences*, 5(1):16–25, January 2001.

[111] CW Eurich, JM Herrmann, and UA Ernst. Finite-size effects of avalanche dynamics. *Physical review E*, 66(6):66137, 2002.

[112] M Fabre-Thorpe. The characteristics and limits of rapid visual categorization. *Frontiers in psychology*, 2(October):243, January 2011.

[113] EE Fanselow and MA Nicolelis. Behavioral modulation of tactile responses in the rat somatosensory system. *Journal of neuroscience*, 19(17):7603–16, September 1999.

[114] J Feder. *Fractals*. Plenum, New York, 1988.

[115] J Fell and N Axmacher. The role of phase synchronization in memory processes. *Nature reviews neuroscience*, 12:105–118, 2011.

[116] W Feng, MN Havenith, P Wang, W Singer, and D Nikolić. Frequencies of gamma/beta oscillations are stably tuned to stimulus properties. *Neuroreport*, 21(10):680–4, July 2010.

[117] I Ferezou, S Bolea, and CCH Petersen. Visualizing the cortical representation of whisker touch: voltage-sensitive dye imaging in freely moving mice. *Neuron*, 50(4):617–29, May 2006.

[118] D Ferrier. Experiments on the brain of monkeys. *Philosophical transactions*, 165:433–488, 1875.

[119] A Fisahn, FG Pike, EH Buhl, and O Paulsen. Cholinergic induction of network oscillations at 40 Hz in the hippocampus in vitro. *Nature*, 394(6689):186–9, July 1998.

[120] WJ Freeman. *Mass Action in the Nervous System*. Academic, New York, 1975.

[121] Y Frégnac and E Bienenstock. *Coorelational Models of Synaptic Plasticity: Development, Learning and Cortical Dynamics of Mental Representations*. John Wiley & Sons, Ltd, 1998.

[122] Y Frégnac, V Bringuier, and A Baranyi. *Oscillatory Neural Activity in Visuak Cortex: A Critical Re-Evaluation*. Springer, 1994.

[123] Y Frégnac, M Rudolph, A Davison, and A Destexhe. *Complexity in Neuronal Networks. In: Biological Networks*. World Scientific, 2006.

[124] N Friedman, S Ito, BAW Brinkman, M Shimono, REL Deville, KA Dahmen, JM Beggs, and TC Butler. Universal critical dynamics in high resolution neuronal avalanche data. *Physical review letters*, 108(20):208102, May 2012.

[125] A Frien, R Eckhorn, R Bauer, T Woelbern, and A Gabriel. Fast oscillations display sharper orientation tuning than slower components of the same recordings in striate cortex of the awake monkey. *The European journal of neuroscience*, 12(4):1453–65, April 2000.

[126] P Fries. A mechanism for cognitive dynamics: neuronal communication through neuronal coherence. *Trends in cognitive sciences*, 9(10):474–80, October 2005.

[127] P Fries. Neuronal gamma-band synchronization as a fundamental process in cortical computation. *Annual review of neuroscience*, 32:209–24, January 2009.

[128] P Fries, JH Reynolds, AE Rorie, and R Desimone. Modulation of oscillatory neuronal synchronization by selective visual attention. *Science*, 291(5508):1560–3, February 2001.

[129] P Fries, PR Roelfsema, AK Engel, P König, and W Singer. Synchronization of oscillatory responses in visual cortex correlates with perception in interocular rivalry. *Proceedings of the National Academy of Sciences of the United States of America*, 94(23):12699–704, November 1997.

[130] G Fritsch and E Hietzig. Über die elektrische Erregbarkeit des Grosshirns. *Archiv für Anatomie and Physiologie*, pages 300–332, 1870.

[131] M Galarreta and S Hestrin. A network of fast-spiking cells in the neocortex connected by electrical synapses. *Nature*, 402(6757):72–5, November 1999.

[132] FJ Gall and J Spurzheim. *Anatomie et Physiology du Système Nerveux en Général, et du Cerveau en Particulier*. F. Schoell, Paris.

[133] M Gell-Mann. What is complexity? *Complexity*, 1:16–19, 1995.

[134] GL Gerstein, ER Williams, M Diesmann, S Grün, and C Trengove. Detecting synfire chains in parallel spike data. *Journal of neuroscience methods*, 206(1):54–64, April 2012.

[135] W Gerstner, R Kempter, JL van Hemmen, and H Wagner. A neuronal learning rule for sub-millisecond temporal coding. *Nature*, 383(6595):76–81, September 1996.

[136] MO Gewaltig, M Diesmann, and A Aertsen. Propagation of cortical synfire activity: survival probability in single trials and stability in the mean. *Neural networks*, 14(6-7):657–73, 2001.

[137] ED Gireesh and D Plenz. Neuronal avalanches organize as nested theta- and beta/gamma-oscillations during development of cortical layer 2/3. *Proceedings of the National Academy of Sciences of the United States of America*, 105(21):7576–81, May 2008.

[138] T Gisiger. Scale invariance in biology: coincidence or footprint of a universal mechanism? *Biol Rev Camb Philos Soc*, 76(2):161–209, 2001.

[139] M Goard and Y Dan. Basal forebrain activation enhances cortical coding of natural scenes. *Nature neuroscience*, 12(11):1444–9, November 2009.

[140] M Goard and Y Dan. Basal forebrain activation enhances cortical coding of natural scenes. *Nature neuroscience*, 12(11):1444–9, November 2009.

[141] K Goldstein. *Aftereffects of Brain Injuries in War: Their Evaluation and Treatment*. Heinemann, London, 1942.

[142] CM Gray and DA McCormick. Chattering cells: superficial pyramidal neurons contributing to the generation of synchronous oscillations in the visual cortex. *Science*, 274(5284):109–13, October 1996.

[143] CM Gray and W Singer. Stimulus-specific neuronal oscillations in orientation columns of cat visual cortex. *Proceedings of the National Academy of Sciences of the United States of America*, 86(5):1698–702, March 1989.

[144] CM Gray and G Viana Di Prisco. Stimulus-dependent neuronal oscillations and local synchronization in striate cortex of the alert cat. *Journal of neuroscience*, 17(9):3239–53, May 1997.

[145] JS Griffith. On the stability of brain-like structures. *Biophysical journal*, 3:299–308, July 1963.

[146] J Gross, A Schnitzler, L Timmermann, and M Ploner. Gamma oscillations in human primary somatosensory cortex reflect pain perception. *PLoS biology*, 5(5):e133, May 2007.

[147] B Gutenberg and CF Richter. *Seicmicity of the earth*. Princeton University Press, Princeton, 1956.

[148] G Hahn, C Monier, and Y Frégnac. Revisiting power law in vivo as a function of the global brain state, using multiple recordings in anesthetized cat. *Soc. neurosci. abstracts*, 2011.

[149] G Hahn, T Petermann, MN Havenith, S Yu, W Singer, D Plenz, and D Nikolić. Neuronal avalanches in spontaneous activity in vivo. *Journal of neurophysiology*, 104(6):3312, July 2010.

[150] RHR Hahnloser, AA Kozhevnikov, and MS Fee. An ultra-sparse code underlies the generation of neural sequences in a songbird. *Nature*, 419(6902):65–70, September 2002.

[151] B Haider, M Häusser, and M Carandini. Inhibition dominates sensory responses in the awake cortex. *Nature*, 493(7430):97–100, January 2013.

[152] B Haider, MR Krause, A Duque, Y Yu, J Touryan, JA Mazer, and DA McCormick. Synaptic and network mechanisms of sparse and reliable visual cortical activity during nonclassical receptive field stimulation. *Neuron*, 65(1):107–21, January 2010.

[153] H Haken. *Synergetics. Introduction and Advanced Topics*. Springer, Berlin, 2004.

[154] C Haldeman and JM Beggs. Critical branching captures activity in living neural networks and maximizes the number of metastable States. *Physical review letters*, 94(5):058101, February 2005.

[155] E Halgren, TL Babb, and PH Crandall. Responses of human limbic neurons to induced changes in blood gases. *Brain research*, 132(1):43–63, August 1977.

[156] A Hanuschkin, JM Herrmann, A Morrison, and M Diesmann. Compositionality of arm movements can be realized by propagating synchrony. *Journal of computational neuroscience*, 30(3):675–97, June 2011.

[157] KD Harris and A Thiele. Cortical state and attention. *Nature reviews neuroscience*, 12(9):509–23, September 2011.

[158] T Harris. *The theory of branching processes*. Springer, 1963.

[159] J Hass, S Blaschke, T Rammsayer, and JM Herrmann. A neurocomputational model for optimal temporal processing. *Journal of computational neuroscience*, 25(3):449–64, December 2008.

[160] ME Hasselmo. What is the function of hippocampal theta rhythm?–Linking behavioral data to phasic properties of field potential and unit recording data. *Hippocampus*, 15(7):936–49, January 2005.

[161] MN Havenith, S Yu, J Biederlack, NH Chen, W Singer, and D Nikolić. Synchrony makes neurons fire in sequence, and stimulus properties determine who is ahead. *Journal of neuroscience*, 31(23):8570–84, June 2011.

[162] S Havlin, SV Buldyrev, AL Goldberger, RN Mantegna, SM Ossadnik, CK Peng, M Simons, and HE Stanley. Fractals in Biology and Medicine. *Chaos, solitons and fractals*, 6:171–201, 1995.

[163] G Hayon, M Abeles, and D Lehmann. A model for representing the dynamics of a system of synfire chains. *Journal of computational neuroscience*, 18(1):41–53, 2005.

[164] DO Hebb. *The Organization of Behavior*. Wiley, 1949.

[165] HR Heekeren, S Marrett, and LG Ungerleider. The neural systems that mediate human perceptual decision making. *Nature reviews neuroscience*, 9(6):467–79, June 2008.

[166] S Herculano-Houzel, MH Munk, S Neuenschwander, and W Singer. Precisely synchronized oscillatory firing patterns require electroencephalographic activation. *Journal of neuroscience*, 19(10):3992–4010, May 1999.

[167] A Hernández, V Nácher, R Luna, A Zainos, L Lemus, M Alvarez, Y Vázquez, L Camarillo, and R Romo. Decoding a perceptual decision process across cortex. *Neuron*, 66(2):300–14, April 2010.

[168] J Hertz and A Prügel-Bennett. Learning short synfire chains by self-organization. *Network*, 7(2):357–63, May 1996.

[169] J Hertz and A Prügel-Bennett. Learning synfire chains: turning noise into signal. *International journal of neural systems*, 7(4):445–50, September 1996.

[170] AV Herz and JJ Hopfield. Earthquake cycles and neural reverberations: Collective oscillations in systems with pulse-coupled threshold elements. *Physical review letters*, 75(6):1222–1225, August 1995.

[171] Hippocrates. *On the Sacred Disease. In Hippocrates and Galen. Great Books of the Western World*. William. Benton, Chicago, 1952.

[172] JJ Hopfield. Neural networks and physical systems with emergent collective computational abilities. *Proceedings of the National Academy of Sciences of the United States of America*, 79(8):2554–8, April 1982.

[173] DH Hubel and TN Wiesel. Receptive fields of single neurones in the cat's striate cortex. *The Journal of physiology*, 148:574–91, October 1959.

[174] HE Hurst. Long-term storage capacity of reservoirs. *Transactions of the American society of civil engineers*, 116:770–808, 1951.

[175] Y Ikegaya, G Aaron, R Cossart, D Aronov, I Lampl, D Ferster, and R Yuste. Synfire chains and cortical songs: temporal modules of cortical activity. *Science*, 304(5670):559–64, April 2004.

[176] Y Ikegaya, W Matsumoto, HY Chiou, R Yuste, and G Aaron. Statistical significance of precisely repeated intracellular synaptic patterns. *PloS one*, 3(12):e3983, January 2008.

[177] EM Izhikevich. Polychronization: computation with spikes. *Neural computation*, 18(2):245–82, March 2006.

[178] G Jaeger. The Ehrenfest Classification of Phase Transitions: Introduction and Evolution. *Archive for history of exact sciences*, 53:51–81, 1998.

[179] HJ Jensen. *Self-Organized Criticality: Emergent Complex Behavior in Physical and Biological Systems (Cambridge Lecture Notes in Physics)*. Cambridge University Press, 1998.

[180] O Jensen, J Kaiser, and JP Lachaux. Human gamma-frequency oscillations associated with attention and memory. *Trends in neurosciences*, 30(7):317–24, July 2007.

[181] DZ Jin. Spiking neural network for recognizing spatiotemporal sequences of spikes. *Physical review. E, statistical, nonlinear, and soft matter physics*, 69(2 Pt 1):021905, February 2004.

[182] DZ Jin. Generating variable birdsong syllable sequences with branching chain networks in avian premotor nucleus HVC. *Physical review. E, statistical, nonlinear, and soft matter physics*, 80(5 Pt 1):051902, November 2009.

[183] DZ Jin, FM Ramazanolu, and HS Seung. Intrinsic bursting enhances the robustness of a neural network model of sequence generation by avian brain area HVC. *Journal of computational neuroscience*, 23(3):283–99, December 2007.

[184] MJ Jutras and EA Buffalo. Synchronous neural activity and memory formation. *Current opinion in neurobiology*, 20(2):150–5, April 2010.

[185] Y Kajikawa and CE Schroeder. How local is the local field potential? *Neuron*, 72(5):847–58, December 2011.

[186] S Katzner, I Nauhaus, A Benucci, V Bonin, DL Ringach, and M Carandini. Local origin of field potentials in visual cortex. *Neuron*, 61(1):35–41, January 2009.

[187] S Kauffman. *Origins of Order: Self-Organization and Selection in Evolution*. Oxford University Press, Oxford, 1993.

[188] Paul S Khayat, Robert Niebergall, and Julio C Martinez-Trujillo. Frequency-dependent attentional modulation of local field potential signals in macaque area MT. *Journal of neuroscience*, 30(20):7037–48, May 2010.

[189] O Kinouchi and M Copelli. Optimal dynamical range of excitable networks at criticality. *Nature physics*, 2(5):348–351, 2006.

[190] Z F Kisvárday, C Beaulieu, and U T Eysel. Network of GABAergic large basket cells in cat visual cortex (area 18): implication for lateral disinhibition. *Journal of comparative neurology*, 327(3):398–415, January 1993.

[191] K Kitano, H Okamoto, and T Fukai. Time representing cortical activities: two models inspired by prefrontal persistent activity. *Biological cybernetics*, 88(5):387–94, 2003.

[192] A Klaus, S Yu, and D Plenz. Statistical Analyses Support Power Law Distributions Found in Neuronal Avalanches. *PLoS ONE*, 6(5):e19779, May 2011.

[193] KD Kniffki, M Pawla, and M Vahle-Hinz. *Fractal dimension and dendritic branching of neurons in the somatosensory thalamus*. Birkhauser Verlag, Basel, 1994.

[194] Kolmogorov A. Three approaches to the quantitative definition of information. *Problems of information transmission*, 1:1–17, 1965.

[195] N Kopell, GB Ermentrout, MA Whittington, and RD Traub. Gamma rhythms and beta rhythms have different synchronization properties. *Proceedings of the National Academy of Sciences of the United States of America*, 97(4):1867–72, February 2000.

[196] N Kopell, MA Whittington, and MA Kramer. Neuronal assembly dynamics in the beta1 frequency range permits short-term memory. *Proceedings of the National Academy of Sciences of the United States of America*, 108(9):3779–84, March 2011.

[197] AK Kreiter and W Singer. Stimulus-dependent synchronization of neuronal responses in the visual cortex of the awake macaque monkey. *Journal of neuroscience*, 16(7):2381–96, April 1996.

[198] J Kremkow, A Aertsen, and A Kumar. Gating of signal propagation in spiking neural networks by balanced and correlated excitation and inhibition. *Journal of neuroscience*, 30(47):15760–8, November 2010.

[199] A Kumar, S Rotter, and A Aertsen. Conditions for propagating synchronous spiking and asynchronous firing rates in a cortical network model. *Journal of neuroscience*, 28(20):5268–80, 2008.

[200] A Kumar, S Rotter, and A Aertsen. Spiking activity propagation in neuronal networks: reconciling different perspectives on neural coding. *Nature reviews neuroscience*, 11(9):615–627, September 2010.

[201] S Kunkel, M Diesmann, and A Morrison. Limits to the development of feed-forward structures in large recurrent neuronal networks. *Frontiers in computational neuroscience*, 4:160, January 2011.

[202] VA Lamme and H Spekreijse. Neuronal synchrony does not represent texture segregation. *Nature*, 396(6709):362–6, November 1998.

[203] G Laurent. Olfactory network dynamics and the coding of multidimensional signals. *Nature reviews neuroscience*, 3(11):884–95, November 2002.

[204] JF Léger, EA Stern, A Aertsen, and D Heck. Synaptic integration in rat frontal cortex shaped by network activity. *Journal of neurophysiology*, 93(1):281–93, January 2005.

[205] A Levina, JM Herrmann, and T Geisel. Dynamical synapses causing self-organized criticality in neural networks. *Nature physics*, 3(12):857–860, 2007.

[206] N Levy, D Horn, I Meilijson, and E Ruppin. Distributed synchrony in a cell assembly of spiking neurons. *Neural networks*, 14(6-7):815–24, 2001.

[207] MS Lewicki. A review of methods for spike sorting: the detection and classification of neural action potentials. *Network*, 9(4):R53–78, November 1998.

[208] LS Liebovitch, D Scheurle, M Rusek, and M Zochowsku. No Title. *Methods*, 24:359–375, 2001.

[209] B Lima, W Singer, NH Chen, and S Neuenschwander. Synchronization dynamics in response to plaid stimuli in monkey V1. *Cerebral cortex*, 20(7):1556–73, July 2010.

[210] B Lima, W Singer, and S Neuenschwander. Gamma responses correlate with temporal expectation in monkey primary visual cortex. *Journal of neuroscience*, 31(44):15919–31, November 2011.

[211] V Litvak, H Sompolinsky, I Segev, and M Abeles. On the transmission of rate code in long feedforward networks with excitatory-inhibitory balance. *Journal of neuroscience*, 23(7):3006–15, April 2003.

[212] R Llinas and D Pare. *Coherent oscillations in specific and nonspecific thalamocortical networks and their role in cognition. In: Thalamus*. Elsevier, Amsterdam, 1998.

[213] RR Llinás, AA Grace, and Y Yarom. In vitro neurons in mammalian cortical layer 4 exhibit intrinsic oscillatory activity in the 10- to 50-Hz frequency range. *Proceedings of the National Academy of Sciences of the United States of America*, 88(3):897–901, February 1991.

[214] S Lloyd and H Pagels. Complexity as thermodynamic depth. *Annals of physics*, 188:186–213, 1988.

[215] J Loeb. *Comparative Physiology of the Brain and Comparative Psychology*. G.P. Putnam's Sons, New York, 1902.

[216] MA Long, DZ Jin, and MS Fee. Support for a synaptic chain model of neuronal sequence generation. *Nature*, 468(7322):394–9, November 2010.

[217] SB Lowen, SS Cash, M Poo, and MC Teich. Quantal neurotransmitter secretion rate exhibits fractal behavior. *Journal of neuroscience*, 17(15):5666, 1997.

[218] SB Lowen and MC Teich. *Fractal-Based Point Processes*. Wiley-Intersience, 2005.

[219] ET Lu and RJ Hamilton. Avalanches of the distribution of solar flares. *Astrophysical journal*, 380:89–92, 1991.

[220] E Lucas-Meunier, C Monier, M Amar, G Baux, Y Frégnac, and P Fossier. Involvement of nicotinic and muscarinic receptors in the endogenous cholinergic modulation of the balance between excitation and inhibition in the young rat visual cortex. *Cerebral cortex*, 19(10):2411–27, October 2009.

[221] A Luczak, P Barthó, and KD Harris. Spontaneous events outline the realm of possible sensory responses in neocortical populations. *Neuron*, 62(3):413–25, May 2009.

[222] A Luczak, P Barthó, SL Marguet, G Buzsáki, and KD Harris. Sequential structure of neocortical spontaneous activity in vivo. *Proceedings of the National Academy of Sciences*, 104(1):347, 2007.

[223] W Lutzenberger and B Ripper. Dynamics of gamma-band activity during an audiospatial working memory task in humans. *Journal of neuroscience*, 22(13):5630–8, July 2002.

[224] W Maass, T Natschläger, and H Markram. Real-time computing without stable states: a new framework for neural computation based on perturbations. *Neural computation*, 14(11):2531–60, November 2002.

[225] BD Malamud and DL Turcotte. Natural Hazards. *Advances in geophysics*, 40:1–90, 1999.

[226] BB Mandelbrot. *The Fractal Geometry of Nature*. W.H. Freeman and Company, 1982.

[227] BB Mandelbrot and RL Hudson. *The Misbehavior of Markets: A Fractal View of Financial Turbulence*. Basic Books, 2006.

[228] EO Mann, JM Suckling, N Hajos, SA Greenfield, and O Paulsen. Perisomatic feedback inhibition underlies cholinergically induced fast network oscillations in the rat hippocampus in vitro. *Neuron*, 45(1):105–17, January 2005.

[229] ID Manns, A Alonso, and BE Jones. Discharge properties of juxtacellularly labeled and immunohistochemically identified cholinergic basal forebrain neurons recorded in association with the electroencephalogram in anesthetized rats. *Journal of neuroscience*, 20(4):1505–18, February 2000.

[230] H Markram, J Lübke, M Frotscher, and B Sakmann. Regulation of synaptic efficacy by coincidence of postsynaptic APs and EPSPs. *Science*, 275(5297):213–5, January 1997.

[231] O Marre, P Yger, AP Davison, and Y Frégnac. Reliable recall of spontaneous activity patterns in cortical networks. *Journal of neuroscience*, 29(46):14596–606, November 2009.

[232] A Mazzoni, FD Broccard, E Garcia-Perez, P Bonifazi, ME Ruaro, and V Torre. On the dynamics of the spontaneous activity in neuronal networks. *PloS one*, 2(5):e439, 2007.

[233] DA McCormick and HC Pape. Noradrenergic and serotonergic modulation of a hyperpolarization-activated cation current in thalamic relay neurones. *Journal of physiology*, 431:319–42, December 1990.

[234] C Mehring, U Hehl, M Kubo, M Diesmann, and A Aertsen. Activity dynamics and propagation of synchronous spiking in locally connected random networks. *Biological cybernetics*, 88(5):395–408, 2003.

[235] L Melloni, C Molina, M Pena, D Torres, W Singer, and E Rodriguez. Synchronization of neural activity across cortical areas correlates with conscious perception. *Journal of neuroscience*, 27(11):2858–65, March 2007.

[236] SJ Middleton, C Racca, MO Cunningham, RD Traub, H Monyer, T Knöpfel, IS Schofield, A Jenkins, and MA Whittington. High-frequency network oscillations in cerebellar cortex. *Neuron*, 58(5):763–74, June 2008.

[237] D Millman, S Mihalas, A Kirkwood, and E Niebur. Self-organized criticality occurs in non-conservative neuronal networks during Up states. *Nature physics*, 6(10):801–805, October 2010.

[238] VV Moca, D Nikolic, W Singer, and RC Muresan. Membrane Resonance Enables Stable and Robust Gamma Oscillations. *Cerebral cortex*, October 2012.

[239] A Mokeichev, M Okun, O Barak, Y Katz, O Ben-Shahar, and I Lampl. Stochastic emergence of repeating cortical motifs in spontaneous membrane potential fluctuations in vivo. *Neuron*, 53(3):413–25, February 2007.

[240] H Munk. Weiteres zur Physiologie der Sehsphäre der Grosshirnrinde. *Centralblatt für praktische Augenheilkunde*, 3:255–266, 1879.

[241] H Munk. *Über die Funktionen der Grosshirnrinde*. A. Hirschwald, Berlin, 1890.

[242] MH Munk, PR Roelfsema, P König, AK Engel, and W Singer. Role of reticular activation in the modulation of intracortical synchronization. *Science*, 272(5259):271–4, April 1996.

[243] I Nauhaus, L Busse, M Carandini, and DL Ringach. Stimulus contrast modulates functional connectivity in visual cortex. *Nature neuroscience*, 12(1):70–6, January 2009.

[244] S Neuenschwander, M Castelo-Branco, and W Singer. Synchronous oscillations in the cat retina. *Vision research*, 39(15):2485–97, July 1999.

[245] S Neuenschwander and W Singer. Long-range synchronization of oscillatory light responses in the cat retina and lateral geniculate nucleus. *Nature*, 379(6567):728–32, February 1996.

[246] G Nicolis and GR Nicolis. Complex systems. *Scholarpedia*, 2007.

[247] CM Niell and MP Stryker. Modulation of visual responses by behavioral state in mouse visual cortex. *Neuron*, 65(4):472–9, February 2010.

[248] D Nikolić, P Fries, and W Singer. Gamma oscillations: precise temporal coordination without a metronome. *Trends in cognitive sciences*, 17(2):54–5, February 2013.

[249] Y Nir, RJ Staba, T Andrillon, VV Vyazovskiy, C Cirelli, I Fried, and G Tononi. Regional slow waves and spindles in human sleep. *Neuron*, 70(1):153–69, April 2011.

[250] M Okun, A Naim, and I Lampl. The subthreshold relation between cortical local field potential and neuronal firing unveiled by intracellular recordings in awake rats. *Journal of neuroscience*, 30(12):4440–8, March 2010.

[251] MW Oram, MC Wiener, R Lestienne, and BJ Richmond. Stochastic nature of precisely timed spike patterns in visual system neuronal responses. *Journal of neurophysiology*, 81(6):3021–33, June 1999.

[252] S Pajevic and D Plenz. Efficient network reconstruction from dynamical cascades identifies small-world topology of neuronal avalanches. *PLoS computational biology*, 5(1):e1000271, 2009.

[253] S Palva and JM Palva. New vistas for alpha-frequency band oscillations. *Trends in neurosciences*, 30(4):150–8, April 2007.

[254] S Palva, JM Palva, Y Shtyrov, T Kujala, RJ Ilmoniemi, K Kaila, and R Näätänen. Distinct gamma-band evoked responses to speech and non-speech sounds in humans. *Journal of neuroscience*, 22(4):RC211, February 2002.

[255] V Pasquale, P Massobrio, LL Bologna, M Chiappalone, and S Martinoia. Self-organization and neuronal avalanches in networks of dissociated cortical neurons. *Neuroscience*, 153(4):1354–69, 2008.

[256] A Pazienti and S Grün. Robustness of the significance of spike synchrony with respect to sorting errors. *Journal of computational neuroscience*, 21(3):329–42, 2006.

[257] T Petermann, TC Thiagarajan, MA Lebedev, MAL Nicolelis, DR Chialvo, and D Plenz. Spontaneous cortical activity in awake monkeys composed of neuronal avalanches. *Proceedings of the National Academy of Sciences of the United States of America*, 106(37):15921–6, September 2009.

[258] CCH Petersen, A Grinvald, and B Sakmann. Spatiotemporal dynamics of sensory responses in layer 2/3 of rat barrel cortex measured in vivo by voltage-sensitive dye

imaging combined with whole-cell voltage recordings and neuron reconstructions. *Journal of neuroscience*, 23(4):1298–309, February 2003.

[259] CCH Petersen, TTG Hahn, M Mehta, A Grinvald, and B Sakmann. Interaction of sensory responses with spontaneous depolarization in layer 2/3 barrel cortex. *Proceedings of the National Academy of Sciences of the United States of America*, 100(23):13638–43, November 2003.

[260] G Pfurtscheller, B Graimann, JE Huggins, SP Levine, and LA Schuh. Spatiotemporal patterns of beta desynchronization and gamma synchronization in corticographic data during self-paced movement. *Clinical neurophysiology*, 114(7):1226–36, July 2003.

[261] D Pinault and M Deschênes. Voltage-dependent 40-Hz oscillations in rat reticular thalamic neurons in vivo. *Neuroscience*, 51(2):245–58, November 1992.

[262] D Plenz and A Aertsen. Neural dynamics in cortex-striatum co-cultures–II. Spatiotemporal characteristics of neuronal activity. *Neuroscience*, 70(4):893–924, February 1996.

[263] D Plenz and DR Chialvo. Scaling properties of neuronal avalanches are consistent with critical dynamics. December 2009.

[264] D Plenz and TC Thiagarajan. The organizing principles of neuronal avalanches: cell assemblies in the cortex? *Trends in neurosciences*, 30(3):101–10, 2007.

[265] JFA Poulet, LMJ Fernandez, S Crochet, and CCH Petersen. Thalamic control of cortical states. *Nature neuroscience*, 15(3):370–2, March 2012.

[266] JFA Poulet and CCH Petersen. Internal brain state regulates membrane potential synchrony in barrel cortex of behaving mice. *Nature*, 454(7206):881–5, August 2008.

[267] V Priesemann, MHJ Munk, and M Wibral.

[268] N Prigogine and G Nicolis. On symmetry-breaking instabilities in dissipative systems. *Journal of chemical physics*, 46:3542–3550.

[269] Y Prut, E Vaadia, H Bergman, I Haalman, H Slovin, and M Abeles. Spatiotemporal structure of cortical activity: properties and behavioral relevance. *Journal of neurophysiology*, 79(6):2857–74, June 1998.

[270] MV Puig, A Watakabe, M Ushimaru, T Yamamori, and Y Kawaguchi. Serotonin modulates fast-spiking interneuron and synchronous activity in the rat prefrontal cortex through 5-HT1A and 5-HT2A receptors. *Journal of neuroscience*, 30(6):2211–22, February 2010.

[271] F Pulvermüller. A brain perspective on language mechanisms: from discrete neuronal ensembles to serial order. *Progress in neurobiology*, 67(2):85–111, June 2002.

[272] RQ Quiroga. Spike Sorting. *Scholarpedia*, 2007.

[273] A Renart, J De la Rocha, P Bartho, L Hollender, N Parga, A Reyes, and KD Harris. The asynchronous state in cortical circuits. *Science*, 327(5965):587, 2010.

[274] AD Reyes. Synchrony-dependent propagation of firing rate in iteratively constructed networks in vitro. *Nature neuroscience*, 6(6):593–9, June 2003.

[275] TL Ribeiro, M Copelli, F Caixeta, H Belchior, DR Chialvo, ML Nicolelis, and S Ribeiro. Spike Avalanches Exhibit Universal Dynamics across the Sleep-Wake Cycle. *PLoS one*, 5(11):e14129, November 2010.

[276] E Rodriguez, N George, JP Lachaux, J Martinerie, B Renault, and FJ Varela. Perception's shadow: long-distance synchronization of human brain activity. *Nature*, 397(6718):430–3, February 1999.

[277] R Rodriguez, U Kallenbach, W Singer, and MHJ Munk. Stabilization of visual responses through cholinergic activation. *Neuroscience*, 165(3):944–54, February 2010.

[278] ViM Rodriguez-Molina, A Aertsen, and DH Heck. Spike timing and reliability in cortical pyramidal neurons: effects of EPSC kinetics, input synchronization and background noise on spike timing. *PloS one*, 2(3):e319, January 2007.

[279] PR Roelfsema, AK Engel, P König, and W Singer. Visuomotor integration is associated with zero time-lag synchronization among cortical areas. *Nature*, 385(6612):157–61, January 1997.

[280] PR Roelfsema, VAF Lamme, and H Spekreijse. Synchrony and covariation of firing rates in the primary visual cortex during contour grouping. *Nature neuroscience*, 7(9):982–91, September 2004.

[281] PR Roelfsema, M Self, J Poort, B Dagnino, MA Gariel-Mathis, C Van der Togt, and T Van Kerkoele. Alpha and gamma oscillations as markers of feedforward and feedbakc processing in areas V1 and V4 of monkey visual cortex. *Soc. neurosci. abstracts*, 2012.

[282] AK Roopun, SJ Middleton, MO Cunningham, FEN LeBeau, A Bibbig, MA Whittington, and RD Traub. A beta2-frequency (20-30 Hz) oscillation in nonsynaptic networks of somatosensory cortex. *Proceedings of the National Academy of Sciences of the United States of America*, 103(42):15646–50, October 2006.

[283] RJ Rosenbaum, J Trousdale, and K Josić. Pooling and correlated neural activity. *Frontiers in computational neuroscience*, 4(April):9, January 2010.

[284] C Rossant, S Leijon, AK Magnusson, and R Brette. Sensitivity of noisy neurons to coincident inputs. *Journal of neuroscience*, 31(47):17193–206, November 2011.

[285] A Roxin, V Hakim, and N Brunel. The statistics of repeating patterns of cortical activity can be reproduced by a model network of stochastic binary neurons. *Journal of neuroscience*, 28(42):10734–45, October 2008.

[286] M Rubinov, O Sporns, JP Thivierge, and M Breakspear. Neurobiologically Realistic Determinants of Self-Organized Criticality in Networks of Spiking Neurons. *PLoS computational biology*, 7(6):e1002038, June 2011.

[287] M Rudolph, M Pospischil, I Timofeev, and A Destexhe. Inhibition determines membrane potential dynamics and controls action potential generation in awake and sleeping cat cortex. *Journal of neuroscience*, 27(20):5280–90, May 2007.

[288] LA Safonov, Y Isomura, S Kang, ZR Struzik, T Fukai, and H Câteau. Near scale-free dynamics in neural population activity of waking/sleeping rats revealed by multiscale analysis. *PloS one*, 5(9), January 2010.

[289] S Sakata and KD Harris. Laminar structure of spontaneous and sensory-evoked population activity in auditory cortex. *Neuron*, 64(3):404–18, November 2009.

[290] E Salinas and TJ Sejnowski. Impact of correlated synaptic input on output firing rate and variability in simple neuronal models. *Journal of neuroscience*, 20(16):6193–209, August 2000.

[291] E Salinas and TJ Sejnowski. Correlated neuronal activity and the flow of neural information. *Nature reviews neuroscience*, 2(August):539–550, 2001.

[292] MV Sanchez-Vives and DA McCormick. Cellular and network mechanisms of rhythmic recurrent activity in neocortex. *Nature neuroscience*, 3(10):1027–34, October 2000.

[293] G Schneider, MN Havenith, and D Nikolić. Spatiotemporal structure in large neuronal networks detected from cross-correlation. *Neural computation*, 18(10):2387–413, October 2006.

[294] S Schrader, M Diesmann, and A Morrison. A compositionality machine realized by a hierarchic architecture of synfire chains. *Frontiers in computational neuroscience*, 4:154, January 2011.

[295] S Schrader, S Grün, M Diesmann, and GL Gerstein. Detecting synfire chain activity using massively parallel spike train recording. *Journal of neurophysiology*, 100(4):2165–76, October 2008.

[296] R Segev, M Benveniste, E Hulata, N Cohen, A Palevski, E Kapon, Y Shapira, and E Ben-Jacob. Long term behavior of lithographically prepared in vitro neuronal networks. *Physical review letters*, 88(11):118102, March 2002.

[297] MN Shadlen and WT Newsome. The variable discharge of cortical neurons: implications for connectivity, computation, and information coding. *Journal of neuroscience*, 18(10):3870–96, May 1998.

[298] WL Shew and D Plenz. The Functional Benefits of Criticality in the Cortex. *The neuroscientist*, May 2012.

[299] WL Shew, H Yang, T Petermann, R Roy, and D Plenz. Neuronal avalanches imply maximum dynamic range in cortical networks at criticality. *Journal of neuroscience*, 29(49):15595–600, December 2009.

[300] WL Shew, H Yang, S Yu, R Roy, and D Plenz. Information capacity and transmission are maximized in balanced cortical networks with neuronal avalanches. *Journal of neuroscience*, 31(1):55–63, January 2011.

[301] T Shmiel, R Drori, O Shmiel, Y Ben-Shaul, Z Nadasdy, M Shemesh, M Teicher, and M Abeles. Neurons of the cerebral cortex exhibit precise interspike timing in correspondence to behavior. *Proceedings of the National Academy of Sciences of the United States of America*, 102(51):18655–7, December 2005.

[302] T Shmiel, R Drori, O Shmiel, Y Ben-Shaul, Z Nadasdy, M Shemesh, M Teicher, and M Abeles. Temporally precise cortical firing patterns are associated with distinct action segments. *Journal of neurophysiology*, 96(5):2645–52, November 2006.

[303] M Siegel, AK Engel, and TH Donner. Cortical network dynamics of perceptual decision-making in the human brain. *Frontiers in human neuroscience*, 5(February):21, January 2011.

[304] HA Simon. The architecture of complexity. *Proceedings of the American Philosophical Society*, 106(6):467–482, 1962.

[305] HA Simon. *The Sciences of the Artificial*. MIT Press, Cambridge, 1981.

[306] W Singer. Neuronal synchrony: a versatile code for the definition of relations? *Neuron*, 24(1):49–65, 111–25, September 1999.

[307] VS Sohal. Insights into cortical oscillations arising from optogenetic studies. *Biological psychiatry*, 71(12):1039–45, June 2012.

[308] VS Sohal, F Zhang, O Yizhar, and K Deisseroth. Parvalbumin neurons and gamma rhythms enhance cortical circuit performance. *Nature*, 459(7247):698–702, June 2009.

[309] S Song, KD Miller, and LF Abbott. Competitive Hebbian learning through spike-timing-dependent synaptic plasticity. *Nature neuroscience*, 3(9):919–26, September 2000.

[310] D Sornette. *Critical Phenomena in Natural Sciences (Second ed.)*. Springer, Berlin, 2004.

[311] O Sporns. Complexity, 2007.

[312] M Steriade, A Nuñez, and F Amzica. A novel slow ($<$ 1 Hz) oscillation of neocortical neurons in vivo: depolarizing and hyperpolarizing components. *Journal of neuroscience*, 13(8):3252–65, August 1993.

[313] M Steriade and I Timofeev. Neuronal plasticity in thalamocortical networks during sleep and waking oscillations. *Neuron*, 37(4):563–76, February 2003.

[314] CV Stewart and D Plenz. Inverted-U profile of dopamine-NMDA-mediated spontaneous avalanche recurrence in superficial layers of rat prefrontal cortex. *Journal of neuroscience*, 26:8148–8159, 2006.

[315] CV Stewart and D Plenz. Homeostasis of neuronal avalanches during postnatal cortex development in vitro. *Journal of neuroscience methods*, 169(2):405–16, 2008.

[316] MP Stryker. Cortical physiology. Is grandmother an oscillation? *Nature*, 338(6213):297–8, March 1989.

[317] E Tagliazucchi, P Balenzuela, D Fraiman, and DR Chialvo. Criticality in large-scale brain FMRI dynamics unveiled by a novel point process analysis. *Frontiers in fractal physiology*, 3:15, January 2012.

[318] C Tallon-Baudry. Oscillatory synchrony and human visual cognition. *Journal of physiology, Paris*, 97(2-3):355–63, 2003.

[319] C Tallon-Baudry. The roles of gamma-band oscillatory synchrony in human visual cognition. *Frontiers in bioscience*, 14:321–32, January 2009.

[320] G Tamás, EH Buhl, A Lörincz, and P Somogyi. Proximally targeted GABAergic synapses and gap junctions synchronize cortical interneurons. *Nature neuroscience*, 3(4):366–71, April 2000.

[321] G Tamás, P Somogyi, and EH Buhl. Differentially interconnected networks of GABAergic interneurons in the visual cortex of the cat. *Journal of neuroscience*, 18(11):4255–70, June 1998.

[322] T Tanaka, T Kaneko, and T Aoyagi. Recurrent infomax generates cell assemblies, neuronal avalanches, and simple cell-like selectivity. *Neural Computation*, 21(4):1038–1067, 2009.

[323] MC Teich, C Heneghan, SB Lowen, B Ozaki, and E Kaplan. Fractal character of the neural spike train in the visual system of the cat. *Journal of the optical society of America*, 14(3):529–46, March 1997.

[324] MC Teich, DH Johnson, AR Kumar, and RG Turcott. Rate fluctuations and fractional power-law noise recorded in the lower auditory pathway of the cat. *Hearing research*, 46:41–52, 1990.

[325] T Tetzlaff, M Helias, GT Einevoll, and M Diesmann. Decorrelation of Neural-Network Activity by Inhibitory Feedback. *PLoS computational biology*, 8(8):e1002596, August 2012.

[326] A Thiele and G Stoner. Neuronal synchrony does not correlate with motion coherence in cortical area MT. *Nature*, 421(6921):366–70, January 2003.

[327] S Thorpe, D Fize, and C Marlot. Speed of processing in the human visual system. *Nature*, 381(6582):520–2, June 1996.

[328] SJ Thorpe and M Fabre-Thorpe. Neuroscience. Seeking categories in the brain. *Science*, 291(5502):260–3, January 2001.

[329] P Tiesinga, JM Fellous, and TJ Sejnowski. Regulation of spike timing in visual cortical circuits. *Nature reviews neuroscience*, 9(2):97–107, March 2008.

[330] P Tiesinga and TJ Sejnowski. Cortical enlightenment: are attentional gamma oscillations driven by ING or PING? *Neuron*, 63(6):727–32, September 2009.

[331] PH Tiesinga, JM Fellous, E Salinas, JV José, and TJ Sejnowski. Inhibitory synchrony as a mechanism for attentional gain modulation. *Journal of physiology, Paris*, 98(4-6):296–314.

[332] J Touboul and A Destexhe. Can power-law scaling and neuronal avalanches arise from stochastic dynamics? *PloS one*, 5(2):e8982, 2010.

[333] RD Traub. Model of synchronized population bursts in electrically coupled interneurons containing active dendritic conductances. *Journal of computational neuroscience*, 2(4):283–9, December 1995.

[334] RD Traub and MA Whittington. *Cortical Oscillations in Health and Disease*. Oxford University Press, 2010.

[335] RD Traub, MA Whittington, SB Colling, G Buzsáki, and JG Jefferys. Analysis of gamma rhythms in the rat hippocampus in vitro and in vivo. *Journal of physiology*, 493 (Pt 2:471–84, June 1996.

[336] RD Traub, MA Whittington, IM Stanford, and JG Jefferys. A mechanism for generation of long-range synchronous fast oscillations in the cortex. *Nature*, 383(6601):621–4, October 1996.

[337] C Trengove, C van Leeuwen, and M Diesmann. High-capacity embedding of synfire chains in a cortical network model. *Journal of computational neuroscience*, August 2012.

[338] HC Tuckwell. *Introduction to theoretical neurobiology*. Cambridge University Press, Cambridge, UK, 1988.

[339] DL Turcotte. *Fractals and Chaos in Geology and Geophysics (Second ed.)*. Cambridge University Press, Cambridge, UK, 1997.

[340] DL Turcotte. Self-organized criticality. *Rep. Prog. Physics*, 62:1377–1429, 1999.

[341] AM Turing. Computing machinery and intelligence. *Mind*, 59:433–460, 1950.

[342] PJ Uhlhaas and W Singer. Neural synchrony in brain disorders: relevance for cognitive dysfunctions and pathophysiology. *Neuron*, 52(1):155–68, October 2006.

[343] PJ Uhlhaas and W Singer. Abnormal neural oscillations and synchrony in schizophrenia. *Nature reviews neuroscience*, 11(2):100–13, March 2010.

[344] PJ Uhlhaas and W Singer. Neuronal dynamics and neuropsychiatric disorders: toward a translational paradigm for dysfunctional large-scale networks. *Neuron*, 75(6):963–80, September 2012.

[345] MCW van Rossum, GG Turrigiano, and SB Nelson. Fast propagation of firing rates through layered networks of noisy neurons. *Journal of neuroscience*, 22(5):1956–66, March 2002.

[346] C van Vreeswijk and H Sompolinsky. Chaos in neuronal networks with balanced excitatory and inhibitory activity. *Science*, 274(5293):1724–6, December 1996.

[347] BCM van Wijk, PJ Beek, and A Daffertshofer. Neural synchrony within the motor system: what have we learned so far? *Frontiers in human neuroscience*, 6(September):1–15, 2012.

[348] CH Vanderwolf. Hippocampal electrical activity and voluntary movement in the rat. *Electroencephalography and clinical neurophysiology*, 26(4):407–18, April 1969.

[349] CH Vanderwolf and GB Baker. Evidence that serotonin mediates non-cholinergic neocortical low voltage fast activity, non-cholinergic hippocampal rhythmical slow activity and contributes to intelligent behavior. *Brain research*, 374(2):342–56, May 1986.

[350] F Varela, JP Lachaux, E Rodriguez, and J Martinerie. The brainweb: phase synchronization and large-scale integration. *Nature reviews neuroscience*, 2(4):229–39, April 2001.

[351] R Vicente, LL Gollo, CR Mirasso, I Fischer, and G Pipa. Dynamical relaying can yield zero time lag neuronal synchrony despite long conduction delays. *Proceedings of the National Academy of Sciences of the United States of America*, 105(44):17157–62, November 2008.

[352] I Vida, M Bartos, and P Jonas. Shunting inhibition improves robustness of gamma oscillations in hippocampal interneuron networks by homogenizing firing rates. *Neuron*, 49(1):107–17, January 2006.

[353] TP Vogels and LF Abbott. Signal propagation and logic gating in networks of integrate-and-fire neurons. *Journal of neuroscience*, 25(46):10786–95, 2005.

[354] TP Vogels, K Rajan, and LF Abbott. Neural network dynamics. *Annual review of neuroscience*, 28(c):357–76, 2005.

[355] L von Bertalanffy. *General System Theory*. George Braziller, New York, 1969.

[356] C Von der Malsburg. The correlation theory of brain function. *Internal report, Max Planck Institute for Biophysical Chemistry, Göttingen, Federal Republik of Germany*, 1981.

[357] C von der Malsburg and W Schneider. A neural cocktail-party processor. *Biological cybernetics*, 54(1):29–40, January 1986.

[358] C von Ehrenfels. Über Gestaltqualitäten. *Vierteljahrschrift fur wissenschaftliche Philosophie*, 14:249–292, 1890.

[359] A Waddington, PA Appleby, M De Kamps, and N Cohen. Triphasic spike-timing-dependent plasticity organizes networks to produce robust sequences of neural activity. *Frontiers in computational neuroscience*, 6:88, January 2012.

[360] XJ Wang. Neurophysiological and computational principles of cortical rhythms in cognition. *Physiological reviews*, pages 1195–1268, 2010.

[361] XJ Wang and G Buzsáki. Gamma oscillation by synaptic inhibition in a hippocampal interneuronal network model. *Journal of neuroscience*, 16(20):6402–13, October 1996.

[362] LM Ward and PE Greenwood. 1/f noise. *Scholarpedia*, 2007.

[363] T Wennekers, M Garagnani, and F Pulvermüller. Language models based on Hebbian cell assemblies. *Journal of physiology, Paris*, 100(1-3):16–30, 2006.

[364] G Werner. Fractals in the nervous system: conceptual implications for theoretical neuroscience. *Frontiers in fractal physiology*, 1:15, January 2010.

[365] MA Whittington, IM Stanford, SB Colling, JG Jefferys, and RD Traub. Spatiotemporal patterns of gamma frequency oscillations tetanically induced in the rat hippocampal slice. *Journal of physiology*, 502 (Pt 3:591–607, August 1997.

[366] MA Whittington, RD Traub, and JG Jefferys. Synchronized oscillations in interneuron networks driven by metabotropic glutamate receptor activation. *Nature*, 373(6515):612–5, February 1995.

[367] MA Whittington, RD Traub, N Kopell, B Ermentrout, and EH Buhl. Inhibition-based rhythms: experimental and mathematical observations on network dynamics. *International journal of psychophysiology*, 38(3):315–36, December 2000.

[368] N Wiener. *Cybernetics: Or Control and Communication in the Animal and the Machine*. MIT Press, Cambridge, 1948.

[369] TJ Wills, C Lever, F Cacucci, N Burgess, and J O'Keefe. Attractor dynamics in the hippocampal representation of the local environment. *Science*, 308(5723):873–6, May 2005.

[370] HR Wilson and JD Cowan. Excitatory and inhibitory interactions in localized populations of model neurons. *Biophysical journal*, 12(1):1–24, January 1972.

[371] T Womelsdorf, JM Schoffelen, R Oostenveld, W Singer, R Desimone, AK Engel, and P Fries. Modulation of neuronal interactions through neuronal synchronization. *Science*, 316(5831):1609–12, June 2007.

[372] D Xing, CI Yeh, and RM Shapley. Spatial spread of the local field potential and its laminar variation in visual cortex. *Journal of neuroscience*, 29(37):11540–9, September 2009.

[373] H Yang, WL Shew, R Roy, and D Plenz. Maximal variability of phase synchrony in cortical networks with neuronal avalanches. *Journal of neuroscience*, 32(3):1061–72, January 2012.

[374] S Yu, D Huang, W Singer, and D Nikolic. A small world of neuronal synchrony. *Cerebral cortex*, 18(12):2891–901, December 2008.

[375] S Yu, H Yang, H Nakahara, GS Santos, D Nikolić, and D Plenz. Higher-order interactions characterized in cortical activity. *Journal of neuroscience*, 31(48):17514–26, November 2011.

[376] S Zapperi, KB Lauritsen, and HE Stanley. Self-organized branching processes: mean-field theory for avalanches. *Physical review letters*, 75(22):4071–4074, 1995.

[377] LI Zhang, HW Tao, CE Holt, WA Harris, and M Poo. A critical window for cooperation and competition among developing retinotectal synapses. *Nature*, 395(6697):37–44, September 1998.

[378] K Ziemelis. Complex systems. *Nature*, 410:242–258, 2001.

[379] GK Zipf. *Human Behavior and the Principle of Least Effort*. Addison-Wesley, Reading, 1949.

[380] E Zohary, MN Shadlen, and WT Newsome. Correlated neuronal discharge rate and its implications for psychophysical performance. *Nature*, 370(6485):140–3, July 1994.